

Determination of structural parameters of single plants and canopies using 3D techniques

Kumulative Dissertation

zur

Erlangung des Doktorgrades der
Mathematisch-Naturwissenschaftlichen Fakultät
der Heinrich-Heine-Universität Düsseldorf

vorgelegt von

Dipl.-Biol.

Bernhard Biskup
aus Bergisch Gladbach

März 2009

Aus dem

Institut für Chemie und Dynamik der Geosphäre (ICG-III): Phytosphäre

Forschungszentrum Jülich GmbH

Referent: Prof. Dr. Ulrich Schurr

Korreferent: Prof. Dr. Martin Lercher

Tag der mündlichen Prüfung: 29.06.2009

Selbständigkeitserklärung

Hiermit erkläre ich, dass ich die vorliegende Dissertation eigenständig und ohne fremde Hilfe angefertigt habe. Arbeiten Dritter wurden entsprechend zitiert. Diese Dissertation wurde bisher in dieser oder ähnlicher Form noch bei keiner anderen Institution eingereicht. Ich habe bisher keine erfolglosen Promotionsversuche unternommen.

Statement of authorship

I hereby certify that this dissertation is the result of my own work. No other person's work has been used without due acknowledgement. This dissertation has not been submitted in the same or similar form to other institutions. I have not previously failed a doctoral examination procedure.

To Annika, Lilith and Jutta

Zusammenfassung

Bildverarbeitungsverfahren sind essenzieller Bestandteil vieler lebenswissenschaftlicher Analyseverfahren. In zunehmendem Maße leisten sie als digitale Messwerkzeuge wesentliche Beiträge zur Beantwortung zentraler biologischer Fragen. Um quantitative Aussagen zu ermöglichen, müssen genaue und robuste Verfahren entwickelt werden, die auf die besonderen Belange der zu untersuchenden biologischen Systeme eingehen.

Die quantitative Erfassung von 3D-Strukturen auf verschiedenen Skalenebenen ist ein für viele pflanzenwissenschaftliche Fragestellungen wichtiges Thema: so spielt die kurz- und langfristige Anpassung der räumlichen Verteilung und Ausrichtung der Blätter in einem Kronendach eine wichtige Rolle für die Lichtnutzungseffizienz in komplexen Beständen. Die aktive Ausrichtung der Blätter zur Sonne ermöglicht dabei die optimale Ausnutzung (Diaheliotropismus) bzw. Limitierung (Paraheliotropismus) der verfügbaren Strahlungsenergie. Die Pflanzenarchitektur hat einen entscheidenden Einfluss auf die Ressourcen-Nutzungseffizienz. Ihre Optimierung mittels Züchtung gewinnt aufgrund der zunehmenden Notwendigkeit, mehr Nahrung, Futter und Treibstoff (Biomasse) auf tendenziell schwindender Anbaufläche zu produzieren, immer stärker an Bedeutung. Bislang war es schwierig, derartige Untersuchungen quantitativ durchzuführen, weil entsprechende Methoden fehlen.

Mittels Fernerkundung wird versucht, die Produktivität von Pflanzenbeständen auf großer Fläche verlässlich und schnell zu messen, um z. B. Vorhersagen über Erträge landwirtschaftlicher Nutzflächen und Wälder zu treffen oder zur Modellierung des Klimawandels die CO₂-Fixierung abzuschätzen. Die komplexe 3D-Struktur von Pflanzen stellt dabei eine besondere Herausforderung dar, da sie das spektrale Signal in vielfältiger Weise beeinflussen und auf diese Weise die Schätzung vegetationsbezogener Parameter (z. B. Photosyntheseleistung) verfälschen kann.

Zur hochpräzisen Erfassung pflanzlicher Wachstumsprozesse sind verbesserte technologische Ansätze notwendig, die über bereits für andere Zwecke etablierte Stereoverfahren hinausgehen. An Bedeutung gewinnt neben dem Anspruch erhöhter Präzision auch der Anspruch, pflanzliche Eigenschaften im Hochdurchsatz zu vermessen (sogenannte morphometrische und physiologische Phänotypisierung).

Ziel dieser Arbeit war es, verschiedene optische 3D-Rekonstruktionsverfahren zur Bestimmung von Strukturparametern pflanzlicher Oberflächen bis hin zu Kronendächern zu entwickeln und diese auf biologische Fragestellungen anzuwenden. Dabei bieten optische Verfahren gegenüber alternativen Methoden zur Strukturbestimmung (z. B. Gap Fraction-Analyse, Stratified clipping, Point-Quadrat-Methoden, Digitizer) häufig Vorteile: sie sind nichtinvasiv, erlauben eine schnelle, wenig arbeitsintensive Aufnahme, bieten z. T. eine hohe räumliche und zeitliche Auflösung und sind potentiell zur Fernerkundung geeignet. In dieser Arbeit wurden verschiedene prototypische Anwendungen zur 3D-Vermessung von Pflanzen entwickelt, die den verschiedenen Anforderungen der biologischen Datenerfassung gerecht werden mussten.

Um dynamische Veränderungen von Blattstellungen quantitativ analysieren zu können, wurde ein korrelationsbasiertes Zwei-Kamera-Stereosystem entwickelt. Das Verfahren umfasst folgende wesentliche Schritte: (1) Kalibrierung des Stereosystems, (2) Rektifizierung und Vorbehandlung der Eingabebilder, (3) Korrespondenzsuche, (4) 3D-Rekonstruktion, (5) Segmentierung von Blattflächen, (6) Bestimmung der Blattwinkel. Das Verfahren wurde prototypisch auf unterschiedliche biologische Problemstellungen angewendet: (1) Anhand der Verteilung der Blattneigungswinkel wurde moderater Trockenstress diagnostiziert. (2) Nyctinastische Bewegungen einzelner Blätter von *Glycine max* wurden gemessen, wobei mit dem Sonnenaufgang eine Erhöhung der Oszillationsfrequenz bei gleichzeitig gesenkter Amplitude festgestellt wurde. (3) Tagesgänge der Blattwinkelverteilung eines geschlossenen Bestandes von *Glycine max* (cv. Pioneer 93B15) und die paraheliotrope Blattbewegung wurden quantifiziert. In einer zweiten Studie konnte mittels des Stereosystems in Verbindung mit Gaswechsel- und Chlorophyllfluoreszenzmessungen gezeigt werden, dass Ertragssteigerungen unter erhöhter atmosphärischer CO₂-Konzentration durch eine gesteigerte maximale Elektronentransportrate ETR_{max} und nicht durch Strukturunterschiede der äußeren Blattschichten verursacht werden.

Zur Untersuchung von Wachstumsprozessen auf komplexen 3D-Strukturen wurde ein weiteres Stereoverfahren entwickelt, das auf dem Prinzip des optischen Flusses basiert. Beispielhaft wurden unterschiedliche pflanzliche Oberflächen auf unterschiedlichen Größenskalen (Früchte, Wurzelknollen, Blätter, Moose, Kronendächer) und unter unterschiedlichen Lichtverhältnissen rekonstruiert. Das Verfahren verwendet eine größere Anzahl von Kamerapositionen zur 3D-Rekonstruktion und erlaubt auf diese Weise eine genaue Tiefenschätzung.

Auch in Screening-Verfahren mit hohen Durchsätzen sind 3D-Verfahren von großem Nutzen, müssen aber den Rahmenbedingungen der Online-Analyse zumindest nahekommen, um relevant eingesetzt werden zu können. Ein Hochdurchsatz-Screeningsystem (GROWSCREEN 3D) wurde entwickelt, das mittels 3D-Vermessung die hochgenaue Bestimmung von Wachstumstagesgängen von Blattscheiben erlaubt und so zur Phänotypisierung von Wachstumsdynamiken geeignet ist. Darüber hinaus erlaubt es, die Wirkung wachstumsbeeinflussender Substanzen zu quantifizieren. Die Verwendung von 3D-Oberflächeninformationen ermöglichte die akkurate Bestimmung der Oberfläche, die durch Messung der projizierten Fläche nicht möglich gewesen wäre (Absinken des Flüssigkeitsspiegels und gewölbte Oberflächen durch differentielles Wachstum). Mit GROWSCREEN 3D konnten selbst solche Wuchsraten quantitativ bestimmt werden, die unter dem Einfluss des Herbizids Glyphosat auf den Shikimat-Stoffwechselweg stark verringert waren. Änderungen der Wachstumsdynamik, die durch ein Fehlen der Stärke-Biosynthese in der *Arabidopsis thaliana* Mutante starch-free 1 (*stf-1*) hervorgerufen werden, konnten mit dem System aufgelöst werden. Isolierte Blattscheiben zeigten die gleichen charakteristischen Änderungen in der Wachstumsdynamik des Phänotyps, die von ganzen Pflanzen bekannt waren. Ein weiteres Hochdurchsatz-Screeningsystem (GROWSCREEN FLUORO; nicht Teil dieser Dissertation) wurde entwickelt: Es erlaubt die nicht-invasive, simultane Untersuchung von Wachstum und Photosynthese.

Summary

Image processing is essential to many biological analysis techniques. To an increasing degree, image processing contributes to finding answers to central biological questions. Exact and robust methods, tailored to the particular biological system in question, are needed to allow quantitative measurements.

Quantitative 3D measurements of structures at different scales are relevant to the investigation of various biological problems. E.g., short- and long-term adaptations of the spatial distribution and orientation of leaves in a canopy greatly determine light use efficiency in complex stands. Active re-orientation with respect to the sun enables optimal use (dielheliotropism) or limitation of the available radiation energy. Plant architecture strongly influences resource use efficiency. Optimization of architecture by means of breeding is continuously gaining importance, driven by the necessity to produce more food, feed and fuel (biomass) while the amount of cultivable land is decreasing. To date, it has been difficult to study plant architecture in a quantitative manner due to the lack of appropriate methods.

Remote sensing is an important approach to measuring plant productivity on large areas quickly and reliably. It is used e.g. to predict yield of agricultural area or forests or to estimate CO₂ fixation for modelling climate change. The complex 3D structure of plants poses a particular challenge to remote sensing, because it alters the spectral signal in a complex fashion, distorting estimation of vegetation parameters (e.g. photosynthetic performance).

Attempting to make highly precise measurements of plant growth requires enhanced technological approaches, going beyond stereo approaches established for different applications. Along with the pursuit for higher precision, there is an increasing demand for high-throughput measurements of plant properties (so-called morphometric and physiological phenotyping).

A primary goal of this dissertation was the development of optical 3D reconstruction techniques for determining structural parameters of plant surfaces on different scales (up to canopies), and to apply the techniques to biological problems. Oftentimes, optical techniques have advantages over alternative techniques (e.g. gap fraction analysis, stratified clipping, point-quadrat, digitizers): they are non-invasive, may provide high spatial and temporal resolution may be suitable for remote sensing. In this dissertation, several prototypical applications for 3D measurements of plants were developed, meeting the particular needs of collection of biological data.

To analyse dynamic changes of leaf orientation, a correlation-based 2-camera stereo system was developed. The processing comprises the following essential steps: (1) calibration of stereo system, (2) rectification and preprocessing of input images, (3) correspondence search, (4) 3D reconstruction, (5) segmentation of leaf areas, (6) measurement of leaf angles. The technique was applied to different biological problems: (1) drought stress was diagnosed by analyzing the distribution of leaf inclination angles. (2) nyctinastic leaf movements of *Glycine max* were

measured, revealing an increase in oscillation frequency and a concomitant decrease in amplitude. (3) the diurnal course of inclination angle of *Glycine max* (var. Pioneer 93B15) and paraheliotropic leaf movements were quantified. A second study using the same stereo system in conjunction with gas exchange and chlorophyll fluorescence measurement revealed that yield increases under elevated [CO₂] are caused by an increase in maximum electron transport rate ETR_{max} rather than by structural differences in the outer canopy.

To investigate growth processes on complex 3D structures, another stereo technique based on the principle of optical flow was developed. Plant surfaces were reconstructed on different scales (fruit, tubers, leaves, mosses, canopies) and under varying illumination. The technique makes use of a higher number of camera positions, thereby enabling high precision depth measurements.

Three-dimensional reconstruction are also useful in high-throughput screening. However, they must allow for online analysis to be of any practical relevance. In the scope of this dissertation, a high-throughput screening system (GROWSCREEN 3D) was developed, which allows measuring diel growth dynamics of floating leaf discs with high precision. Thus, it is useful for phenotyping of growth dynamics. Moreover, it allows quantification of the effects of substances on growth. Making use of 3D information allows accurate determination of surface area, which would not be possible with only the projected area available (sinking level of nutrient solution and convex surfaces due to differential growth). GROWSCREEN 3D was able to measure even growth rates that were strongly reduced under the influence of the herbicide glyphosate on the shikimate pathway. Changes in growth dynamics caused by missing starch biosynthesis in the *Arabidopsis thaliana* mutant starch-free 1 (*stf-1*) could be resolved by GROWSCREEN 3D. Isolated leaf discs exhibited the same characteristics in growth dynamics of the phenotype that was known from whole plants. Another high-throughput system (GROWSCREEN FLUORO; not in the scope of this dissertation) was developed that is suitable for non-invasive, simultaneous investigation of growth and photosynthesis.

Table of Contents

1	Introduction	16
1.1	Motivation	16
1.2	Stereo Vision and 3D reconstruction	16
1.2.1	Perspective (pinhole) camera	17
1.2.2	Camera & stereo calibration	17
1.2.3	The correspondence problem	19
1.2.4	3D reconstruction	20
1.2.5	Applications of 3D reconstruction	21
1.3	Canopy structure	22
1.3.1	Importance of canopy structure	22
1.3.2	Abiotic factors influenced by canopy structure	22
1.3.3	Direct vs. indirect methods of measuring structural parameters of canopies	23
1.3.4	Existing 3D approaches to measuring structural parameters of canopies	24
1.3.5	New approaches to measuring structural parameters	24
1.3.6	Possible applications of the newly developed 3D techniques	25
1.4	Application: elevated atmospheric CO ₂ concentrations	28
1.4.1	Future atmospheric gas concentrations	28
1.4.2	Free air carbon enrichment (FACE)	29
1.4.3	Effects of elevated atmospheric [CO ₂] concentrations on plants	30
1.4.4	Measurements at SoyFACE	31
1.5	Plant growth	31
1.5.1	Spatial and temporal patterns of leaf growth in dicots	32
1.5.2	Classical measurement methods	33
1.5.3	Measuring growth at sub-leaf resolution	33
1.5.4	High-throughput leaf growth measurements	33
1.5.5	Leaf disc growth measurements	34
1.5.6	Growth as a phenotypic characteristic	34
2	Synopsis	34
3	Personal bibliography	35
3.1	Publications of dissertation	35
3.2	Other publications	35
4	References	36
5	Publications	53
5.1	First publication: Stereo imaging system	53
	Abstract	55
	Introduction	55
	Stereo camera system	56

Case studies	60
Discussion	61
Acknowledgements	62
References	62
5.2 Second publication: Quantification of plant surface structures	63
Abstract	65
Zusammenfassung	66
Introduction	67
Small baseline approach to quantify three-dimensional surfaces	68
Surface reconstruction of single leaves and small plants	72
Surface reconstruction of rainforest canopy	72
Discussion	74
Acknowledgements	75
References	75
Figures	79
5.3 Third publication: Photosynthesis of soybean cultivars	85
Title	86
Abstract	89
Introduction	90
Material and Methods	92
Results	100
Discussion	104
Acknowledgements	107
References	108
Table	114
Figure legends	115
Figures	117
5.4 Fourth publication: Imaging leaf disc diel growth dynamics	123
Title	124
Abstract	124
Introduction	124
Results	126
Discussion	128
Conclusion	131
Materials and methods	131
Acknowledgements	132
Literature cited	132
Supplemental data	134

Abbreviations

93B15	Soybean variety produced by Pioneer Hi-Bred International, Inc.
2D, 2-D	Two-dimensional
3D, 3-D	Three-dimensional
ANOVA	Analysis of variance
ATP	Adenosine triphosphate
B	Base (of leaf)
BCCE	Brightness change constraint equation
BLAS	Basic Linear Algebra Subprograms
BRDF	Bidirectional reflectance distribution function
CCD	Charge-coupled device
CDT	Central Daylight Time
CIFS	Common Internet File System
COV	Coefficient of variation
DDR	double data rate
DISP	Digital image sequence processing
DOY	Day of year
dpi	Dots per inch
ETR	Electron transport rate
FACE	Free air concentration enrichment
FR	Far-red light
FWHM	Full width at half maximum
GB	Gigabytes
HK	Hakaphos
GLY_HI	Glyphosate, high concentration
GLY_LO	Glyphosate, low concentration
GROWSCREEN	Phenotyping platform (Walter <i>et al.</i> 2007)
GROWSCREEN 3D	Phenotyping platform (Biskup <i>et al.</i> 2009)
GROWSCREEN FLUORO	Phenotyping platform (Jansen <i>et al.</i> [FunctPlantBiol])
HSV	Hue, saturation & (brightness) value
IEEE	Institute of Electrical and Electronics Engineers
IPCC	Intergovernmental Panel on Climate Change
IR	Infrared
LAI	Leaf area index
LAPACK	Linear algebra package
LED	Light emitting diode
LIDAR	Light Detection and Ranging
L/R	Left/right
M	Middle (of leaf)
MTA	Mean tilt angle

NPK	Nitrogen, phosphorus, potassium (fertilizer)
NPQ	Non-photochemical quenching
PAR	Photosynthetically active radiation
PFD	Photon flux density
PPFD	Photosynthetic PFD
<i>pgm</i>	Phosphoglucomutase gene
PS	Photosystem
PRI	Photochemical reflectance index
R	Red light
RAID	Redundant array of inexpensive discs
RAM	Random access memory
RANSAC	Random sample consensus
RGR	Relative growth rate
ROI	Region of interest
Rubisco	Ribulose-1,5-bisphosphate carboxylase/oxygenase
SEM	Standard error of mean; scanning electron microscope
SLW	Specific leaf weight
SoyFACE	Soybean Free Air Concentration Enrichment (facility)
SQL	Structured Query Language
<i>stf1</i>	starch-free 1 (mutant of <i>Arabidopsis thaliana</i>)
SWIG	Simplified wrapper and interface generator
T	Tip (of leaf)
TIFF	Tagged Image File Format
TLS	Total least squares
TW	Tap water
UML	Unified Modeling Language
USB	Universal Serial Bus
USDA	United States Department of Agriculture
UPS	Uninterruptible power supply
VPD	Atmospheric vapor pressure deficit
[X]	Concentration of substance X

Citations of publications of this dissertation

The publications belonging to this cumulative dissertation are cited in the following way. For submitted manuscripts, abbreviated journal names are given instead of years. See section 3.1 for complete references.

#	Citation	Journal	Status
1	Biskup <i>et al.</i> (2007)	Plant, Cell and Environment	published
2	Biskup <i>et al.</i> (2009)	Nova Acta Leopoldina	in press
3	Rascher <i>et al.</i> ([AgrForestMeteorol])	Agricultural and Forest Meteorology	submitted
4	Biskup <i>et al.</i> (2009)	Plant Physiology	published

1 Introduction

The determination of plant structure and plant growth dynamics in an automated and quantitative manner is an important and timely task of plant biology. Towards a quantitative understanding, this doctoral dissertation is concerned with the development and establishment of stereo vision systems and techniques for measuring structural parameters of plants. The proposed systems are applicable on different scales, from single leaf discs to canopies to the ecosystem level. The biological problems addressed encompass diurnal growth rates of leaves, leaf movements, and leaf orientation under drought stress and under elevated atmospheric CO₂ concentration.

1.1 Motivation

Plant development is governed by a multitude of abiotic and biotic factors, oftentimes causing feedback (e.g. self-shading). Efficient use of available sunlight can be viewed as the primary objective a plant needs to fulfill. Secondary objectives are, among others, to withstand wind and to minimize transpiration. In an evolving plant community, light conditions may change rapidly, as competing plants grow higher and increase their leaf area. On the other hand, diel variations in light intensity and direction mean sub-optimal light intensities in the morning and late afternoon, but saturating intensities at noon. Depending on the latitude and time of year, such effects may become so severe that a plant must regulate the intensity of incident light. Diaheliotropic leaf movements (Jurik *et al.* 1990) increase intensity, while paraheliotropic leaf movements decrease intensity, thus avoiding photoinhibition, reducing leaf temperature and increasing water use efficiency (Ludlow & Björkman 1984; Forseth & Teramura; Gamon & Pearcy 1989; Jurik *et al.* 1990; Kao & Forseth 1991; 1992; Muraoka *et al.* 1998; King 1997; Falster & Westoby 2003). Flexible leaf orientation can be viewed as a means to maximize carbon gain under highly variable conditions (Muraoka *et al.* 1998). Assessing the structure and the dynamics of structural changes of plant canopies is of vital interest to ecophysiology. Because most plants develop in three-dimensional space, being able to measure structural parameters in three dimensions seems desirable.

1.2 Stereo Vision and 3D reconstruction

Stereopsis, i.e. the fusion of different projections of a scene on the retinae of the eyes of humans and some animal species, was studied as early as 1838 (Wheatstone 1838), who found that the difference between the two eyes' images (binocular disparity) is perceived as depth. Today, an analogous problem, the reconstruction of surfaces in three-dimensional (3D, Euclidean) space from images, is dealt with in the science computer stereo vision (Trucco & Verri 1998; Hartley & Zisserman 2004). The principal steps required are: (1) Camera & stereo calibration; (2) Finding correspondences; (3) 3D reconstruction.

1.2.1 Perspective (pinhole) camera

When a point in 3D space is projected through a camera lens onto a camera sensor array, one dimension (depth) is lost. That is, multiple points lying on the same ray of sight will be projected to the same point in an image. The mapping of a point in Euclidean 3-space (\mathbb{R}^3) to an image (\mathbb{R}^2) (*perspective projection*) occurs as follows:

$$\begin{pmatrix} x \\ y \\ z \end{pmatrix} = \frac{f}{Z} \begin{pmatrix} X \\ Y \\ Z \end{pmatrix}$$

with the focal length f , the world point $(X, Y, Z)^T$ and the image point $(x, y, z)^T$ (in world coordinates).

As in human vision, at least two views (images) are required to recover depth, because only the intersection of two rays uniquely identifies the point in space. Using more than two views increases accuracy and is well-suited e.g. for laboratories where cameras may be mounted permanently. However, such an approach is more expensive and practical handling may be more cumbersome in outdoor situations. Therefore, the techniques presented in this dissertation (with the exception of Biskup *et al.* 2009) are based on two-view configurations.

1.2.2 Camera & stereo calibration

Camera calibration

Camera calibration is a prerequisite for determining metric information from images. In the context of this work, it is the act of recovering the *intrinsic parameters* of a camera. Intrinsic parameters encompass the focal length, the principal point (where the optical axis crosses the image plane), the radial and tangential distortion parameters. Given the intrinsic parameters, a camera can be used as a direction sensor, i.e. each pixel is associated with a particular ray of sight. High calibration accuracy is essential for accurate measurements from images.

Camera calibration has long been used in classical, film-based photogrammetry (Conrady 1919), with geographical mapping as the main application. However, the necessity for precise, quantitative photogrammetry arose with World War I and the emergence of aerial reconnaissance (Clarke & Fryer 1998) and early stereoscopic plotting. In general, camera calibration is achieved by observing one or more images of a *calibration target*, i.e. a two- or three-dimensional object of known geometry. Such calibration targets need to be crafted with sufficient precision, or they may cause severe errors in estimating camera parameters. Three-dimensional targets have the advantage of providing sufficient information for camera calibration using a single image (Heikkilä 2000), but are more difficult to manufacture than two-dimensional targets. In more

recent times, interest in calibration was revitalized due to the emergence of computer vision. While digital cameras use a different way of capturing images, the lens systems are equivalent. Since the number of exposures is no longer a cost factor in digital photography, calibration methods are likewise no longer restricted to using few images. Moreover, the availability of computers enables the use of more complex calibration models and non-linear optimization. Closely related to camera calibration is *image undistortion*, the act of removing distortions. In pre-digital times, reprojection of distorted images through the same lens or through special reduction lens systems was one way (Baker 1980) to neutralize distortions. Another way was to build stereographs with distortion correction facilities or to use correction curves (Clarke & Fryer 1998). Using a computer, undistortion can straightforwardly be achieved by resampling the distorted image at the appropriate positions as determined during calibration.

In this dissertation, the calibration method implemented by Bouguet (2005) (based on the work of Zhang 1999; 2000) was used in Biskup *et al.* (2007); Rascher *et al.* ([AgrForestMeteorol]); Biskup *et al.* (2009). The calibration method requires a sufficient number (> 20 image pairs of a planar chessboard pattern (created with an ordinary laser printer). Knowing the size of the chessboard, the above mentioned calibration parameters can be estimated, with focal length and principal point in metric units. The method was chosen because it is well-established in computer vision (e.g. Zelnik-Manor & Irani 2002; Würmlin *et al.* 2002; Mulder *et al.* 2003; Hartley & Zisserman 2004) and practicable under field conditions. Many calibration techniques have been developed solely with indoor laboratory conditions in mind. The emerging field of self-calibration (e.g. Faugeras *et al.* 1992), which deals with obtaining calibration parameters without calibration targets may simplify the calibration task in the future; however, in many cases, self-calibration relies on constraints (e.g. minimum number of different views, limited view configuration) and on information about the scene, e.g. lines pointing to a vanishing point, or orthogonal lines, as oftentimes present in indoor scenes (Hartley 1992). Moreover, self-calibration tends to be less robust than standard calibration procedures. Camera calibration in the context of the measurements discussed here required only limited time and labor. One advantage of a practically usable self-calibration procedure would be an increased working volume (i.e. space volume in which accurate 3D measurements are possible): regardless of the exact method used, calibration only gives information about the volume in which the target is imaged; moving farther away from this volume, calibration quality degrades. A compromise would be to use a calibration target and to increase the working volume with additional point correspondences from the environment (Zhang 1999). One-dimensional targets (e.g. poles with equidistant beads; at the expense of requiring more images) could also increase the working volume while still allowing handling under field conditions (e.g. wind gusts; Zhang 2002).

Stereo Calibration

Having two calibrated cameras is not sufficient for 3D reconstruction. It is also necessary to determine the relative orientation of two cameras that form a *stereo rig*, which is achieved

through *stereo calibration*. Highly accurate stereo calibration is essential to derive accurate 3D models. In general, the calibration parameters are specified as a rotation matrix \mathbf{R} and a translation vector \mathbf{t} (*extrinsic parameters*) that transform the first camera reference frame, \mathbf{C} , to the second camera reference frame, \mathbf{C}' , according to the rigid motion equation:

$$\mathbf{C}' = \mathbf{RC} + \mathbf{t}$$

When two simultaneously triggered cameras are used, the calibration method by Bouguet (2005) (see above) can be extended to stereo calibration. By knowing corresponding projections of many 3D points to both images of a stereo pair, \mathbf{R} and \mathbf{t} can be recovered. This approach was chosen in Biskup *et al.* (2007) and Rascher *et al.* ([AgrForestMeteorol]). In contrast, in Biskup *et al.* (2009) and Biskup *et al.* (2009), a single camera was moved by a highly precise displacement stage. Since both cameras were looking in parallel directions and the stereo baseline b (i.e. the distance between camera centers) was known, calibration was trivial since $\mathbf{R} = \mathbf{I}$ (identity matrix) and $\mathbf{t} = (b, 0, 0)^T$ (*hardware calibration*).

1.2.3 The correspondence problem

The problem of identifying corresponding points, i.e. projections of the same point in 3D space in two or more images, is known as the *correspondence problem* of stereo vision. The task is complicated by noise, occlusions and complex reflective properties of the viewed objects. Finding a high proportion of true correspondences strongly influences the quality of the depth map. There is a multitude of approaches to finding correspondences; some of the more common are described below.

Algorithms less suitable for imaging plants

Several classes of correspondence search algorithms exist, many of which are of limited practical use in solving the problem of reconstructing plants in 3D. E.g., reconstruction from long image sequences (hundreds of images) from different views (Pollefeys *et al.* 2000) has the advantage of not requiring camera and stereo calibration. It was used successfully to reconstruct buildings. However, since acquiring a longer sequence takes time, the method is not applicable in the presence of wind, because stereo matching requires a rigid scene. *Shape from shading* (see e.g. Zhang *et al.* 1999) attempts to recover shape, given the reflection properties of the scene material and the direction of illumination. The strength of this method is the ability to cope with large untextured surfaces, where correlation or feature-based methods fail due to ambiguity. However, since plant leaves have complex reflective properties and outdoor illumination cannot be controlled, the approach seems feasible only under controlled laboratory conditions. *Space carving* (Dyer 2001), a volumetric technique, is most suitable for compact objects. Re-

cently, progress has been made by using an array of *monocular depth cues* (e.g. color, haze, texture gradients, defocus or geometric hints like converging lines) to estimate depth. While requiring only one image would be a practical advantage, it is arguable whether the approach will work on plant scenes, given their complex structure and reflective properties. However, Saxena *et al.* (2008) were able to increase reconstruction accuracy with respect to ground truth by using a combination of monocular and stereo information, similar to human vision (e.g. Stevens & Brookes 1988).

Feature-based algorithms start by identifying salient features like corners or edges. Because such features tend to be sparse, the resulting depth map will also be sparse, requiring interpolation. Feature-based algorithms can be particularly useful if additional knowledge about scene geometry is available, e.g. indoor scenes which are known to be bounded by vertical walls. With real-time requirements such as robot vision and control, operating on a comparably small set of 3D points can be reasonable and sufficient for a task like robot motion planning.

Optical-flow based methods

A different approach is to use the concept of *optical flow* (Lucas & Kanade 1981; Horn & Schunck 1981) for measuring disparities. Optical flow is the distribution of apparent velocities of moving brightness patterns in an image, caused either by moving the camera or objects of the scene (Horn & Schunck 1981). The approach is based on the brightness constancy assumption, which states that the intensity of surface elements projected on the camera sensor is (almost) constant between images. A sequence of images taken by a camera moving along a baseline with small, equidistant displacements is interpreted as a spatio-temporal volume. Because partial derivatives are used for disparity estimation, optical-flow-based methods are also termed *differential*. By using optimal digital filters (convolution kernels; filters that are optimized for measuring orientations; Schar 2004) to compute grey value derivatives, differential techniques are very accurate. However, occlusions pose a problem because the flow field is assumed to be continuous. The image acquisition set-up must account for the limited disparity range that can be detected with optical-flow based methods (determined by the size of the derivative filters), i.e. working volume is more limited than with correlation-based methods (this may be overcome with warping or hierarchical methods; Brox *et al.* 2004; Mémmin & Pérez 1998).

In the frame of this dissertation, an optical-flow-based algorithm was used in Biskup *et al.* (2009). In contrast to Biskup *et al.* (2007) and Rascher *et al.* ([AgrForestMeteorol]), the study did not focus on the leaf level; instead, different fruit and other plant organs were reconstructed on a small scale. With the ultimate goal of measuring growth rates of plant organs (Schar & Küsters 2002), a highly precise algorithm was favored there. On the large scale, a canopy envelope was reconstructed .

1.2.4 3D reconstruction

Once the stereo rig has been calibrated and correspondences have been established, the scene (i.e. the original 3D points) can be reconstructed. In the general case with non-parallel cameras, the following system of equations needs to be solved for a , b and c :

$$a\mathbf{p}_l - b\mathbf{R}^T\mathbf{p}_r + c(\mathbf{p}_l \times \mathbf{R}^T\mathbf{p}_r) = \mathbf{t}$$

where \mathbf{p}_l and \mathbf{p}_r denote corresponding image points in the left and right images, \mathbf{R} and \mathbf{t} are the extrinsic parameters of the stereo rig. ‘ \times ’ denotes the vector cross product. This computation is simplified if both cameras are oriented in parallel (Biskup *et al.* 2007).

Correlation-based methods

Correlation-based (area-based) algorithms determine disparities by computing a cost function over a disparity range and selecting the extremum as the true disparity. Such algorithms assume the scene is locally fronto-parallel. This assumption usually holds if (1) the area in question is small (e.g. a small rectangular window), and (2) if the camera displacement is small enough so perspective distortion is negligible. Area-based algorithms have difficulties with occlusions, i.e. parts of the scene that are only visible in one image but occluded by other parts of the scene in the second image. Several approaches have been taken to cope with the occlusion problem: (1) multiple view stereo vision, in which many different camera positions are used in the attempt to cover the entire surface under investigation (see e.g. Pollefeys *et al.* 2000). (2) Multiple windows: correlation scores of differently-shaped windows are computed, and only the best matching window is used (presumably one which excludes an occlusion boundary; e.g. Fusiello *et al.* 1997). A similar approach is to use color information to determine an appropriate window size and shape (Yoon & Kweon 2006).

An area-based algorithm was used in this dissertation for reconstructing canopies (Biskup *et al.* 2007; Rascher *et al.* [AgrForestMeteorol]) as well as leaf discs (Biskup *et al.* 2009). Since the orientation of individual leaves was under investigation, a sufficiently large image area was available with this method and border effects at which the chosen algorithm was less accurate were not relevant. The good performance of the algorithm made it a good choice for a field system in which it is desirable to get results quickly.

1.2.5 Applications of 3D reconstruction

During the past 10–15 years, 3D reconstruction has found its way into many application areas, like robot vision and robotic navigation (e.g. Olson *et al.* 2007), medical imaging (e.g. Preim & Bartz 2007), quality control and material testing (e.g. Leopold *et al.* 2003), automotive sensors (e.g. van der Mark & Gavrila 2006; Morat *et al.* 2007), Cultural heritage preservation

(e.g. Pollefeys *et al.* 2001) and remote sensing (Omasa *et al.* 2003; 2007), to name the most important areas. The main reason for this is the increasing availability of computing power at decreasing cost, making sophisticated processing and even real-time applications feasible. On the algorithmic side, accuracy improvements have paved the way to high-precision applications (Scharstein *et al.* 2001).

1.3 Canopy structure

1.3.1 Importance of canopy structure

Plant canopy structure and its impact on ecosystem productivity, micro-climate and light availability has been a subject of investigation for a long time (e.g. Monsi & Saeki 1953; Ross 1981). In many cases, thorough knowledge of the orientation and distribution of leaves within a canopy is a prerequisite to scaling leaf-level processes to ecosystem level. A better understanding of canopy structure is required to answer a variety of questions to address problems such as (1) the refinement of photosynthesis models, (2) general clarification of plant functions and (3) distribution of growth within canopies. The biophysical and biochemical details of photosynthesis have been thoroughly studied in many aspects (Hoover 1937; Hill & Scarisbrick 1940; Emerson 1958; Balegh & Biddulph 1970; Mitchell 1961; Deisenhofer *et al.* 1985; Kühlbrandt *et al.* 1994; Frenkel 1995). The impact of light spectrum and intensity, temperature humidity, water availability and other factors could readily be investigated in laboratory settings. However, at the scale of whole plants or canopies, the local set of abiotic parameters becomes highly heterogeneous.

1.3.2 Abiotic factors influenced by canopy structure

Light penetration

The amount of available light decreases deeper into the canopy. The attenuation of available light is mostly governed by the position of the sun, the density of leaf material and the orientation of leaves (e.g. Monsi & Saeki 1953; Hirose 2005; Ort & P. 2003). Often, the outer canopy is exposed to saturating light intensities, while the layers below receive less than saturating light. Permanent or short-term modifications of canopy structure increase the canopy carbon gain (Muraoka *et al.* 1998; Ort & P. 2003; Roden 2003). Vertical gradients in leaf inclination (with steeper angles higher in the canopy) help to achieve tolerable intensities of incident light (Kuroiwa 1971; Falster & Westoby 2003).

Temperature and humidity

At high leaf temperatures, C₃ photosynthesis is strongly impaired by photoinhibition. Steeper leaf angles are thought to increase water use efficiency and to decrease the risk of overheating (King 1997; Falster & Westoby 2003). A close coupling leaf temperature commonly is commonly assumed in modelling, although it is well-known that leaf temperature may differ from ambient temperature due to transpiration, convective heat loss (Miller 1972; Smith 1978b). It has only recently been shown that canopy leaf temperature is indeed under close regulation, the leaves of many tree species maintaining an optimum temperature across 50° of latitude (Helliker & Richter 2008).

The degree of canopy closure also affects humidity within the canopy (Baldochi 1989). Higher humidity generally causes stomatal opening and has been shown to increase photosynthetic rates (Cowan 1977; Farquhar 1978; Lange *et al.*; Bunce 1982). As a downside, a high canopy humidity may promote infestation by fungal pests (e.g. Del Ponte *et al.* 2006).

Canopy-air CO₂ concentration

The canopy-air CO₂ concentration ($[CO_2]_c$) is characterized by strong diurnal, seasonal and multi-annual variation. Typically, $[CO_2]_c$ increases during the night due to respiration, and remains elevated for several hours after sunrise before declining (Ziska *et al.* 2001). The degree of coupling of above- and within-canopy $[CO_2]$ is governed by canopy structure Verma & Rosenberg (1976); Rasse *et al.* (2002). $[CO_2]_c$ may strongly affect net plant productivity (Rasse *et al.* 2002).

1.3.3 Direct vs. indirect methods of measuring structural parameters of canopies

Numerous methods have been developed to measure certain aspects of canopy structure, each having their assets and drawbacks (e.g. measurement speed, manual labor, cost, invasiveness). Oftentimes, an original basic approach was later refined using more advanced technology.

Direct methods

Methods like layer-by-layer stratified clipping (Monsi & Saeki 1953) to determine the LAI (leaf area index) or compass-protractors (Campbell & Norman 1989; Muraoka *et al.* 1998) to measure leaf inclination and azimuthal orientation gave useful insights into regulation of light capture efficiency, while being very labour-intensive. Such methods are referred to as ‘direct’ methods (Campbell & Norman 1989; Pearcy & Yang 1996) because information is derived from looking at individual leaves. Other examples of direct methods are allometry and litter collection (see e.g. Breda 2003). In many cases, technical advances reduced the amount of labor

involved in applying direct methods. For instance, Lang (1990) developed a non-image-based device to automatically record 3D positions, ultimately allowing to determine positions and orientations of leaves in a canopy. This approach was later advanced by Rakocevic *et al.* (2000); it has a strong benefit when investigating the topology of a canopy, but is too labor-intensive to be used even on moderate scale. Commercial instrumentation like the ‘Li-COR 3100C Area Meter’ (Li-COR Biosciences, Lincoln, Nebraska, USA) allow economic area measurements on cut leaves.

Indirect methods

In contrast to direct methods, ‘indirect’ methods provide statistical information, i.e. information on a particular stand. For example, the point quadrats method (Levy & Madden 1933; Wilson 1960) allows measuring leaf area per unit ground by passing needles through vegetation and recording the number of contacts between needle and vegetation. The same information can nowadays be obtained by optical methods. The *gap fraction*, i.e. the probability of not hitting a leaf when casting a ray through a canopy (Chen & Cihlar 1995) can be determined using a hemispherical lens. Gap fraction may either be determined photometrically, i.e. using light intensity as a function of incidence angle (implemented e.g. in the ‘Li-COR LAI-2000 Canopy Analyzer’, Li-COR Biosciences, Lincoln, Nebraska, USA), or image-based, by applying image segmentation to hemispherical images (implemented e.g. in *SCANOPY*; Regent Instruments, Ottawa, Ontario, Canada).

1.3.4 Existing 3D approaches to measuring structural parameters of canopies

Techniques making use of three-dimensional information have only developed in the past years, namely with the emergence of low-priced digital photography. Previous attempts (Herbert 1995; Ivanov *et al.* 1995) used conventional photography and photogrammetric methods to obtain 3D information. Since image correspondences had to be established by hand, only very sparse 3D information could be obtained. Nevertheless, the authors demonstrated the utility of 3D information for answering ecophysiological questions. More recently, Omasa *et al.* (2003; 2007) used airborne LIDAR (light detection and ranging) to reconstruct forest canopies. Using modified lasers to overcome problems with reflective properties of leaf tissue, and highly precise INS (inertia navigation systems), the authors were able to create good-quality reconstructions. However, the technique is very cost-intensive (e.g. it requires a helicopter) and acquisition takes fairly long because of the small sensor footprint. Omasa *et al.* (2007) used a LIDAR sensor to reconstruct an individual plant under laboratory conditions to map multi-sensor data to the 3D model (e.g. thermographic information). Quan *et al.* (2006) developed a semi-automatic technique to create a complete 3D surface model of a plant. However, the system requires a high degree of manual intervention and is primarily geared towards computer graphics rather than biological applications.

1.3.5 New approaches to measuring structural parameters

In this dissertation, two novel stereo-based approaches to measuring structural parameters are proposed. The first is an optical-flow based approach which was investigated in a feasibility study (Biskup *et al.* 2009). The second, correlation-based, approach (Biskup *et al.* 2007) is presented along with case studies demonstrating the quantification of leaf angle distribution. The same approach was used to elucidate whether maximum ETR (electron transport rate) or the structure of the upper canopy is responsible for differences in yield between soybean cultivars under elevated atmospheric [CO₂].

Leaf angles

In Biskup *et al.* (2007) and Rascher *et al.* ([AgrForestMeteorol]), 3D reconstructions of individual soybean plants or the outer parts of soybean canopies were performed. Using the 3D model, areas corresponding to leaves or parts of leaves were segmented by manual or automatic procedures. The inclination of these segments was determined with respect to a reference plane. Likewise, the azimuth orientation (compass direction) of the segments was determined based on known orientations of the cameras.

1.3.6 Possible applications of the newly developed 3D techniques

Canopy photosynthesis models

Modelling canopy photosynthesis is a long-standing idea. Based on pioneering work by Boyson Jensen (1932), Monsi & Saeki (1953) established the theory for modelling light penetration into canopies and the resulting canopy photosynthesis. In short, they applied Beer's law, $I = I_0 e^{-K \cdot LAI}$, to estimate light attenuation, with I denoting the PPFD with respect to a horizontal plane, and K denoting the extinction coefficient. However, actual canopies violate Beer's law because leaves have a finite size and are not distributed uniformly. Furthermore, leaves are usually not horizontal. These deviations are reflected in K , typically ranging from 0.7 to 1.0 for planophile leaf angle distributions and ranging from 0.3 to 0.5 for erectophile leaf angle distributions (Monsi & Saeki 1953). Taking into account leaf transmittance, the light response curve of photosynthesis and dark respiration, Monsi & Saeki (1953) calculated the canopy photosynthesis P . The Monsi-Saeki model was later confirmed for a broad range of real canopies. Despite its good predictive quality, several assumptions proved too general: photosynthetic characteristics actually vary between leaves, especially between dark and shaded leaves (e.g. Boardman 1977). However, Saeki (1959) pointed out that the contribution of shaded leaves to canopy photosynthesis is usually marginal (also see Long *et al.* 2006b; Humphries & Long 1995). Another generalization was the assumption of diffuse light (i.e. overcast sky). Under clear-sky conditions, the proportion of direct light is substantial, thus light intensities will be overestimated by

the Monsi-Saeki model. The authors developed the notion of an *optimal* LAI, i.e. the LAI that maximizes canopy photosynthesis. According to their predictions, P_{\max} is achieved at steeper leaf angles under high irradiance, and at horizontal leaf angles under low light intensities. The predicted trend has been observed in real canopies, but leaf inclinations are typically below their predicted values. This deviation is possibly due to inter-specific competition (Hirose 2005).

The Monsi-Saeki theory provided the basis for later models (e.g. De Wit 1965; Idso & De Wit 1970; Röhrig *et al.* 1999). Common to all approaches is the necessity to supply an estimate of the leaf angle distribution to the model. While the leaf angle distributions are well-established for a variety of species (e.g. Falster & Westoby 2003), especially such species that are capable of heliotropic leaf movements may differ profoundly in their leaf angle distribution even between cultivars (Wofford & Allen 1982; Rosa *et al.* 1991; Rosa & Forseth 1995; Bawhey *et al.* 2003). Moreover, leaf inclination may be affected by the water status of the plant (Rosa *et al.* 1991). Thus, being able to measure leaf angles with a method as proposed in this dissertation (Biskup *et al.* 2007) can be useful to parameterize canopy photosynthesis models.

Virtual plants

The increased availability of processing power enables new approaches to modelling canopy photosynthesis and other canopy processes. Rather than making simplified assumptions about light attenuation (e.g. according to Beer's law; Monsi & Saeki 1953), it has become possible to explicitly model plant organs in three-dimensional space. Depending on its scope and purpose, a model may incorporate reflective, optical or mechanical properties, temperature, growth processes or a combination of several. Such spatially explicit, structural-functional plant models have brought about the term *virtual plant* (for review, see De Visser *et al.* 2002; Godin 2000). A typical approach to generating plant models is by *Lindenmayer systems* (L-systems; Lindenmayer 1968), formal grammars that have proved useful to generate a vast array of biological shapes and topologies. L-systems generate self-similar fractals. The initial theory did not allow for modelling plant shapes and was later refined for this purpose (Frijters & Lindenmayer; Hogeweg & Hesper 1974). The first realistic images were presented by A. R. Smith (Smith 1978a; 1984). Originating from computer-graphics oriented generation of plant models (Prusinkiewicz *et al.* 1988), the research group of P. Prusinkiewicz refined the L-systems theory and applied it to many areas relevant to plant biology, such as architecture and physiology of growing trees (Allen *et al.* 2005), growth simulation on the basis of biomechanical models (Prusinkiewicz 2004; Smith *et al.* 2007), models for developmental biology (Giavitto *et al.* 2002) and interaction of growing plants with environmental factors (water availability, light; Měch & Prusinkiewicz 1996).

Using an alternative approach to L-systems, Barczi *et al.* (2007) developed a simulation architecture, AMAPsim, that is able to integrate multiple user-supplied external models, each capturing a certain structural or functional aspect. In the core of the system lies the plant model that

defines how a plant develops. The plant model consists of *virtual buds* with a potential growth determined by their physiological age. The buds grow according to stochastic processes, resulting in a plant architecture that accurately mimics real plants. External models, such as light interception models (Soler *et al.* 2003; Chenu *et al.* 2007), source-sink related models (GreenLab; Yan *et al.* 2004), xylem transport or biomechanical models (Sellier *et al.* 2006) may interact with the core model via well-defined interfaces. AMAPsim is a promising approach because it is designed for integration of multiple models, and because the underlying growth model allows modification of development processes at particular physiological ages, in particular tissues, without affecting the rest of the plant (Barczi *et al.* 2007; Rey *et al.* 2007).

Another, well-established virtual plant model is YPLANT (Percy & Yang 1996; Falster & Westoby 2003). YPLANT capitalizes on the static structure of a plant and is used for computing light interception and whole-plant carbon gain. Structural parameters (internode and leaf positions) may be collected on real plants using a digitizing device (Percy & Yang 1996; Sinoquet & Rivet 1997; Rakocevic *et al.* 2000). Since YPLANT does not simulate growth, the digitized positions and the topology derived thereof are only a snapshot of the developing plant.

Structural comparison of crop cultivars

Structural parameters such as leaf angle distribution and vertical foliage distribution can help to discriminate differences in growth and development between different cultivars. e.g. as basis for breeding decisions. In Rascher *et al.* ([AgrForestMeteorol]), the stereo system described in Biskup *et al.* (2007) was used to augment measurements of leaf area index (LAI) and specific leaf weight (SLW) to compare the canopy structure of the soybean cultivar Pioneer 93B15 under ambient and future (elevated) CO₂. Several authors suggested that light use efficiency of a canopy may be increased by targeted modification of leaf inclination, namely by achieving steeper inclined upper canopy leaves that permit deeper light penetration (Sakamoto & Shaw 1967; Kuroiwa 1971; Humphries & Long 1995; Reynolds *et al.* 2000).

Leaf movement

As illustrated in Biskup *et al.* (2007) by the example of nyctinastic leaf movement in soybean, measurements of leaf angles at an adequate frequency may elucidate short-term responses to stimuli such as light, temperature changes, mechanical irritation or application of substances. While conventional techniques have been applied successfully to study leaf movement (e.g. Herbert 1983; Rosa *et al.* 1991; Rosa & Forseth 1995; Herbert 1992; Jurik & Akey 1994), a stereo technique bears the advantage of being non-invasive, which may be especially important when investigating thigmo-sensitive plants. Moreover, imaging techniques allow higher acquisition rates, possibly with multiple plants at a time. Plant movements are generally thought to be brought about by *osmotic motors* (Moran 2007; Côté 1995). In many cases, opposing volume and turgor changes in specialized organs, *pulvini* cause leaf motion: powered by H⁺ ATPase in

the plasma membrane, fluxes of K^+ , Cl^- and sometimes malate change the osmotic potential, not unlike the mechanism regulating guard cell conductivity (Schroeder & Hedrich 1989). Leaf movements may be very fast; for instance, the shrinking violet (*Mimosa pudica*) displays a pronounced seismonastic response in the range of seconds (Fromm & Eschrich 1988). The almost instantaneous response of the Venus flytrap (*Dionea muscipula*) is achieved by the osmotic motor releasing the pre-tensed, unstable leaf (Forterre *et al.* 2005). A paraheliotropic response to stressful light intensities may be induced within minutes (Koller *et al.* 1995; Forseth & Ehleringer 1983). On the other hand, removing stress factors may cause an equally fast relaxation.

The high temporal resolutions possible with the 3D techniques introduced in Biskup *et al.* (2007) and Biskup *et al.* (2009) gives access to the kinetics of stimulus response reactions that manifest in changing leaf orientation.

Shade avoidance

Shade-intolerant plants, i.e. plants that are not capable of long-term survival under low light intensities (Gilbert *et al.* 2001) must avoid being overtopped and shaded by other plants. One way to detect the risk of shading early is the perception of a proximity signal (Ballaré *et al.* 1990; Gilbert *et al.* 2001; Franklin & Whitelam 2005). The signal consists of the ratio of red (R; 655 nm to 665 nm) and far-red (FR; 725 nm to 735 nm) photon irradiances. This ratio is close to 1 and fairly stable under different weather conditions. Due to scattering of the poorly absorbed FR, the R:FR ratio underneath a canopy is strongly decreased, ranging from 0.05 to 0.7 (Franklin & Whitelam 2005). The proximity signal is perceived via phytochrome photoreceptors, but there is evidence that a green-light receptor is involved at least in *Arabidopsis thaliana* (Mullen *et al.* 2006). Shade responses may manifest in shoot growth, causing a plant to overtop competitors (e.g. Gilbert *et al.* 2001), or differential petiole growth in rosette plants, causing leaves to bend up to avoid shade (Mullen *et al.* 2006). The intensity of the proximity signal depends on the size, vertical distribution and spatial orientation of leaves surrounding a plant. To estimate signal intensity, Gilbert *et al.* (2001) used LAI and leaf angle information to compute the leaf area projected on a cylinder representing the plant receiving the proximity signal.

3D growth of plant surfaces

On a microscopic scale, the sequential replica method (Williams & Green 1988; Williams 1991) can be used to track the three-dimensional position of individual cells over several division cycles. The method is non-destructive; in short, a deformable material (dental polymer moulds) is used to create replicas of plant tissue. Then, epoxy resin is used to prepare casts for observation in a scanning electron microscope (SEM). Kwiatkowska (2004) used two SEM views of the same object to perform 3D reconstructions of the positions of cell walls to measure

the surface growth of the shoot apical meristem of *A. thaliana*, a structure of approx. 200 µm in diameter. Three-dimensional information gives a valuable insight into the spatio-temporal development of the meristematic tissue.

Coen *et al.* (2004) devised a conceptual framework for modelling 3D growth, using the regional parameters growth rate, anisotropy, direction and rotation. The virtue of their approach is that it allows to study control by, as well as response to, genetic regulation. The authors suggest using their framework to test hypotheses about genetic regulation, comparing modelled morphogenesis with actual measurements on mutants.

Optical-flow-based 3D reconstruction lends itself to measuring growth (in terms of surface expansion in three dimensions) of fruit or leaves (Küsters 2004; Scharr & Küsters 2002). The surface of fruit is usually convex, and leaves often move while growing, thus causing projective artifacts when measuring growth rates based on 2D information. Measuring growth in 3D avoids such artifacts. Sufficient surface structure (contrast) is essential for accurate growth measurements with optical-flow-based techniques. In Biskup *et al.* (2009), the positive effects of spray marking and structured light on the quality of 3D reconstruction are demonstrated by a range of example plant organs.

Canopy growth

Rather than looking at single leaves, the increase in leaf material may be studied in terms of increasing envelope surface area. As demonstrated in (Biskup *et al.* 2009), the proposed small-baseline approach may deliver such an envelope. Differential measurements at consecutive time points allows quantification of canopy growth.

1.4 Application: elevated atmospheric CO₂ concentrations

1.4.1 Future atmospheric gas concentrations

Global change subsumes a variety of gradual, consistent atmospheric, ecological and other environmental changes, some of which are likely to be of anthropogenic origin. The most prominent phenomenon is an increase in atmospheric [CO₂] which is mostly due to combustion of fossile fuels by both industry and cars (IPCC 2007). CO₂ acts as a greenhouse gas, i.e. it increases absorption of infrared radiation emitted by earth, thereby increasing the temperature of the atmosphere. Atmospheric [CO₂] has risen by approx. 30% since the beginning of the industrial revolution to a current level of approx. 380 ppm (IPCC 2007; Tans 2008), a value unprecedented over more than 400000 years (Petit *et al.* 1999). The future development of atmospheric temperature is uncertain because of various feedback effects, e.g. evaporation of water, which is also a greenhouse gas, or melting polar ice which reduces albedo (IPCC 2001), but future [CO₂] will undoubtedly increase (IPCC 2007).

Increasing concentrations of atmospheric nitrogen oxides, which arise from increased combustion of fuels, produce rising levels of surface ozone (O_3). O_3 , apart from acting as a greenhouse gas, is toxic for animals (e.g. WHO 2003) and plants (e.g. Bermejo *et al.* 2003), there most notably by reducing content and activity of the enzyme ribulose-1,5-bisphosphate carboxylase/oxygenase (Rubisco), thus reducing carbon assimilation (Heath 1994; Reid *et al.* 1999). Like $[CO_2]$, $[O_3]$ is expected to rise by as much as 20% until the middle of this century (IPCC 2001).

When considering global food supply, any large scale effects on crop yields due to changes in the atmospheric concentrations of CO_2 and O_3 are of great importance. Elevated $[CO_2]$ could, as a substrate of photosynthesis, increase yields. On the other hand, elevated $[O_3]$, being a severe stress factor for plants, could counter such effects. Even by now, elevated $[O_3]$ causes crop damages on an economically important scale. E.g., 30 million hectares (worth 19 billion US\$; USDA 2006) of soybean are grown in the US; annual losses due to O_3 damages have been estimated to amount to 2 billion US\$ (Murphy *et al.* 1999).

1.4.2 Free air carbon enrichment (FACE)

To estimate the impact of changes in $[CO_2]$ and $[O_3]$, several *free air concentration enrichment* facilities (FACE) have been set up around the world. Enrichment of atmospheric gases is achieved by measuring the momentary concentration and instantaneously adding the appropriate amount of gas via nozzles arranged around the test plot (Miglietta *et al.* 2001). Fumigation with CO_2 is typically done only at daytime when carbon assimilation takes place to reduce costs, and when sufficient wind is present to ensure homogeneous fumigation. FACE sites were typically set up to study a small number of important crop plants (soybean, corn, rice) or forest ecosystems (e.g. loblolly pine (*Pinus taeda*) in the Duke Forest FACE experiment (Rogers & Ellsworth 2002) or *Populus* in EuroFACE, Italy (Miglietta *et al.* 2001) in detail, often over several years.

Enclosure versus FACE studies

Experimental set-ups seem to have strong influence on observed effects of elevated $[CO_2]$. Chamber (enclosure) studies tend to overestimate biomass increase as compared to FACE experiments. Long *et al.* (2004) (also see Long *et al.* 2006a) suggest a variety of reasons for systematic errors, the most important being (1) using pot-grown instead of field-grown plants, which has previously been observed to have influence on the response to elevated CO_2 , (2) reduced transmission of sunlight, (3) increased temperature, (4) increased water vapor pressure deficit, (5) altered air flow. The authors advocate the use of FACE experiments to measure $[CO_2]$ response under conditions as realistic as possible. Some authors stated contrasting opinions, arguing that carefully set up enclosure experiment may be well-suited, provided that confounding

factors such as growth conditions are ruled out (Ziska & Bunce 2007; Körner 2006). Given the multitude and diversity of direct and indirect responses to elevated [CO₂], the use of several approaches seems justified to elucidate the mechanisms.

1.4.3 Effects of elevated atmospheric [CO₂] concentrations on plants

CO₂ fertilization

A well-known effect of elevated [CO₂] is *CO₂ fertilization*, an increase in growth mainly due to stimulation of photosynthesis (Farquhar & von Caemmerer; Makino & Mae 1999). The effect is used commercially in greenhouse cultivation, where [CO₂] is typically raised to approx. 700 ppm (Nelson 2002). In terrestrial C₃ plants, the stimulation of photosynthesis is caused by two properties of Rubisco: firstly, its Michaelis constant (K_M) for the substrate CO₂ is close to contemporary ambient [CO₂] (J. & Salvucci 2002), thus elevation of [CO₂] will cause an increase the carboxylation rate. Secondly, photorespiration gets suppressed because CO₂ competitively inhibits the Rubisco oxygenation reaction (Long 1991; Long *et al.* 2004).

In C₄ plants, because their photosynthetic apparatus nearly always operates under CO₂-saturated conditions, little immediate fertilization occurs. However, because stomatal conductance will decrease, an indirect stimulation of photosynthesis and production due to improved water use efficiency may result (Ghannoum *et al.* 2000; Leakey *et al.* 2004). There are pronounced differences in the degree of fertilization between genera and between ecosystems (Makino & Mae 1999). In most ecosystems, positive effects on net primary production are limited by the availability of nitrogen (Vitousek *et al.* 1997) and also phosphorus and calcium in tropical soils.

Adverse effects of elevated [CO₂]

Aside from the positive effects on assimilation, elevated [CO₂] has a number of negative effects, manifesting as yield decrease. An increased assimilation rate due to an improved efficiency of Rubisco under elevated [CO₂] usually causes accumulation of carbohydrates in the leaf, slowing down the carboxylation reaction by end product inhibition (Arp 1991; Sawada *et al.* 2001). Notably, plants possessing a large and adaptable sink capacity (e.g. in the form of roots and tubers) are not affected by down-regulation of photosynthesis (Usuda & Shimogawara 1998). Along the same line, the leaf sheath in rice has been shown to provide temporary sink capacity, effectively avoiding down-regulation of photosynthesis (Watanabe *et al.* 1997). Extreme starch accumulation may reduce photosynthesis by physically damaging chloroplasts (e.g. Cave *et al.* 1981) or by slowing diffusing of CO₂ in the chloroplast (e.g. Nafziger & Koller 1976). The carbon:nitrogen (C:N) ratio typically increases under prolonged exposure to elevated [CO₂] (Roger *et al.* 2000) states an average increase of C:N by 12% when doubling [CO₂]. This increase may be irrelevant for pure energy crops, but critical for the nutritional value in terms of protein content (Hocking & Meyer 1991; Conroy *et al.* 1994; Rogers *et al.* 1996; Pal *et al.*

2004).

Recently, elevated [CO₂] was found to effectively disable the herbivore defense mechanism in soybean (Zavala *et al.* 2008). The authors found that higher levels of carbohydrates made soybean grown under elevated [CO₂] more attractive to two herbivore species (Japanese soybean beetle (*Popillia japonica*) and western corn rootworm (*Diabrotica virgifera virgifera*)). At the same time, the wound hormone Jasmonic acid was down-regulated. The authors propose that increased herbivory under the condition of suspended defense mechanisms may exceed the yield increase due to elevated [CO₂]. While the study was conducted in an intense monoculture, it is an example of the manifold effects of elevated [CO₂].

The soil fauna may be strongly affected by atmospheric CO₂ concentrations. Lesaulnier *et al.* (2008) observed an increase in heterotrophic decomposers and ectomycorrhizal fungi on one hand, and a decrease on nitrate-reducers on the other hand at the Rhineland FACE site, a population of *Populus tremuloides*. The total abundance of microbes did not change. The authors view the increased production of detritus under elevated [CO₂] as the main reason for the observed rearrangement in soil biota populations.

1.4.4 Measurements at SoyFACE

Several measurement campaigns in the context of this dissertation (Biskup *et al.* 2007; Rascher *et al.* [AgrForestMeteorol]) were conducted on soybean at the SoyFACE facility at Urbana, IL, USA (Rogers *et al.* 2004; Ainsworth & Long 2005; Morgan *et al.* 2006). At SoyFACE, soybean and corn, both the most important crops used in the Midwest of the USA are cultivated according to standard agricultural practice. There were four experimental blocks: one control plot with ambient (378 ppm) [CO₂], elevated (550 ppm) [CO₂], elevated (1.5 × ambient) [O₃], and a combination of elevated [CO₂] and [O₃], in four replicates. Each plot was 20 m in diameter. Measurements in the scope of this dissertation were carried out on plots under ambient and elevated [CO₂].

1.5 Plant growth

Growth is a fundamental property of plants. It is defined as the irreversible increase in volume and substance (Nultsch 2001; Raven *et al.* 2004). In contrast to most animals, plants are typically sessile and thus have to cope with fluctuations in environmental conditions. Due to their modular structure, plants grow during their entire lifetime (Scanlon 1998; Walter & Schurr 1999). Modifications of the building plan are a means to adapt to environmental conditions. Cell turgor is the driving force behind plant growth, whereas cell wall extensibility restricts growth (Vissenberg *et al.* 2000; Cosgrove *et al.* 2002). The dynamics of leaf and root growth reflects their adaptation to the exposure of these organs to the environment: roots live in a

slowly changing temperature regime, but experience high spatial heterogeneity of nutrients. Consequently, they exhibit little regulation and respond quickly to changes in environmental conditions (Nagel *et al.* 2006). Leaves of dicots are exposed to strong diurnal variations of light and temperature and thus have developed circadian growth patterns (Walter & Schurr 2005). In contrast, growth zones of monocot leaves are protected by older leaves and thus less exposed to environmental fluctuations (Ben-Haj-Salah & Tardieu 1995; Walter & Schurr 2005).

Assuming exponential growth $A(t_2) = A(t_1)e^{RGR(t_2-t_1)}$, the relative growth rate RGR is defined as follows:

$$RGR[d^{-1}] = \frac{100}{t_2 - t_1} \ln\left(\frac{A(t_2)}{A(t_1)}\right)$$

1.5.1 Spatial and temporal patterns of leaf growth in dicots

The process of plant growth is the result of an interplay between a huge number of genes and many environmental factors, each of which may vary over time (Koornneef *et al.* 2004). Growth occurs simultaneously in many parts of the plant; the distribution of growth rates is shaped by carbon allocation and structure formation (Walter & Schurr 1999).

Leaf growth exhibits a variety of patterns, both temporally and spatially. During the development of dicot leaves, a fixed amount of cells is produced (meristematic growth). Then, the cells undergo expansion until maturity is reached. On a temporal dimension, the mean diel growth rates gradually decrease until maturity. For instance, mean growth rates of tobacco leaves decrease exponentially, reaching maturity after approx. two weeks (e.g. Avery 1933; Walter & Schurr 1999). Leaf development proceeds from tip to base in a wave-like fashion (van Volkenburgh 1985). While the majority of cells of growing leaf tissue transition from division to elongation, the two processes are not entirely separated (Heckenberger 1998).

More pronounced than this leaf ageing is the diel variation of growth rates (circadian rhythm) (Dale 1988; van Volkenburgh 1999; Walter & Schurr 2005). Dicot leaves are adapted to coping with drastic changes and maintaining optimal performance. Leaves of monocots usually exhibit a maximum RGR during the middle of the day, whereas dicots do not show a general preference (Walter & Schurr 2005). The difference may arise from the absence of an endogenous control in monocots where growth rates have been found to be coupled to meristem temperature (Ben-Haj-Salah & Tardieu 1995).

On a spatial dimension, leaves of some dicot species, e.g. *N. tabacum* Walter & Schurr (1999; 2005), *Coccoloba uvifera* and *Sanchezia nobilis* (Walter *et al.* 2004), *Rhizinus communis* (Walter 2000) and *A. thaliana* (Wiese *et al.* 2007) have been shown to exhibit a base-tip gradient of growth rates. While such patterns may be obscured by small-scale temporal and spatial vari-

ations, such patterns clearly emerge when integrating over 24 h. The presence of a base-tip gradient is thought to originate from earlier reduction and cessation of cell division and elongation in the tip region (Poethig & Sussex 1985; Granier & Tardieu 1998; Schmundt & Schurr 1998). On the other hand, e.g. leaflets of *Glycine max* (Ainsworth *et al.* 2005) or *Populus deltoides* (Walter *et al.* 2005; Matsubara *et al.* 2006) lack a base-tip gradient.

1.5.2 Classical measurement methods

A straight-forward way of assessing leaf growth is to measure leaf length and elongation with a regular spacer. The approach allows measuring large sample sizes. Using allometric relationships (i.e. empirical form factors; Schurr 1997; Walter & Schurr 1999), the area of a leaf can be determined with sufficient precision, allowing to determine growth rates on a coarse scale based on calibration measurements for a particular species or cultivar. This approach, while inexpensive and simple, does not offer spatial resolution. Fresh and dry weight of a leaf are also good, albeit destructive, indicators of growth (e.g. Leister *et al.* 1999). The temporal resolution of elongation measurements was considerably enhanced by the application of linear variable differential transducers (LVDT; Watts 1974; Degli Agosti *et al.* 1997).

1.5.3 Measuring growth at sub-leaf resolution

The first attempt to measure spatially resolved leaf growth was reported by Avery (1933), who applied ink dots. A similar approach, albeit facilitated by image processing, was taken by Küsters (2004), who used spray marks applied with a toothbrush to enhance contrast for image processing, and by Hamamoto *et al.* (2006), who applied ink with an ink jet printer and subsequently tracked the trajectories of the dots with motion analysis software. Using modern image sequence processing techniques, Schmundt & Schurr (1998) were able to measure leaf growth at a high spatial and temporal resolution, without depending on spray markers. The authors employed the *structure tensor* technique (Bigün & Granlund 1987; Schmundt & Schurr 1998; Haußecker 1999). In short, motion (as when observing growth processes in time) gives rise to grey level displacements between consecutive images of the same plant organ. The orientation of such displacements in the space-time cube immediately yields the velocities. The structure tensor mathematically describes the local orientation of grey values. The approach, now termed DISP (digital image sequence processing) in the context of growth measurements, was successfully employed in several studies (e.g. Walter 2000; Ainsworth *et al.* 2005; Matsubara *et al.* 2006; Berns *et al.* 2007; Wiese *et al.* 2007) and was also extended to allow measuring three-dimensional growth of plant organs (Küsters 2004).

1.5.4 High-throughput leaf growth measurements

The DISP method, while giving a wealth of information, is less suitable under high-throughput requirements, which call for a simple and robust approach. Using imaging techniques, the projected area of a whole plant can be measured to obtain growth time series (Leister *et al.* 1999; Granier *et al.* 2006; Walter *et al.* 2007). Using *A. thaliana*, there is little overlap during the first weeks of growth. By correlating area with fresh and dry weight measurements, Walter *et al.* (2007) verified that increase in projected leaf area is a good estimate for growth rates. Temporal resolution is in the range of days. However, differences in projected leaf area that arise from differences in habitus between phenotypes, e.g. hormone-induced differential growth (Nielsen & Ulvskov 1997) or altered leaf inclination in phytochrome mutants (Mullen *et al.* 2006), cannot be detected with this method. To combine the spatial resolution of DISP methods with the high-throughput benefits of image-based area measurements, a two-step approach seems useful: in a first step, a high-throughput technique could be used to identify candidate phenotypes, which could be analyzed in more detail using DISP.

1.5.5 Leaf disc growth measurements

Excised leaf discs typically retain their ability to grow for several days or even weeks (Powell & Griffith 1960; Glinka & Meidner 1968; Nunes *et al.* 1983; Walter 2000; Stiles & Van Volkenburgh 2004; Walter & Schurr 2005). However, accurate image-based measurement of relative growth rates (RGR) is hampered by the fact that sinking water levels cause a decrease in projected area, which may be tolerable if actual RGR is high but will lead to grossly incorrect results at small growth rates. Especially when diel characteristics of growth are investigated, the dynamics will be skewed because of the varying contribution of the actual growth signal. In this dissertation, an image-based screening system is presented (Biskup *et al.* 2009) which overcomes these problems by measuring leaf disc area in 3D instead of its projection.

1.5.6 Growth as a phenotypic characteristic

Growth is a complex, quantitative phenotypic trait: the potential growth rate of a particular organ is determined by a multitude of genes. *A. thaliana* is a suitable model plant for conducting quantitative trait loci (QTL) analyses (El-Lithy *et al.* 2004). In the context of metabolic phenotypes, alterations of diel growth dynamics in conjunction with quantitative analysis of substances at different daytimes (e.g. Wiese *et al.* 2007), are more indicative than comparisons of day-to-day area increase; diel RGR patterns may be affected by a mutation, without a substantial impact of total diel RGR (Wiese *et al.* 2007). In this dissertation, phenotypic differences due to altered starch metabolism were shown (Biskup *et al.* 2009). Moreover, a novel combination of non-invasive imaging methods was used to study the dynamics of growth and photosynthesis under stress conditions (Jansen *et al.* [FunctPlantBiol]).

2 Synopsis

The objective of this dissertation was to develop and implement 3D imaging techniques to measure structural parameters of plant canopies, individual leaves and leaf discs. On a large (ecosystem) scale, an accurate model of an extended canopy was created (Biskup *et al.* 2009). On a medium scale, a novel stereo imaging system (Biskup *et al.* 2007) was used to reconstruct soybean canopies (few m²) to measure leaf orientation. The approach revealed that yield increases under elevated [CO₂] are caused by an increase in maximum electron transport rate ETR_{max} rather than by structural differences in the outer canopy (Rascher *et al.* [AgrForestMeteorol]). On an even smaller scale, leaf inclination angles of individual soybean plants were measured to diagnose drought stress and to track leaf movements (Biskup *et al.* 2007). The principle of 3D reconstruction was also applied in the development of a high-throughput image-based system for growth phenotyping of leaf discs, demonstrating the increased measurement accuracy crucial for revealing subtle differences in diel growth cycles due to difference in treatment or phenotype (Biskup *et al.* 2009).

3 Personal bibliography

3.1 Publications of dissertation

Biskup B., Küsters R., Scharr H., Walter A. & Rascher U. (2009a) Quantification of plant surface structures from small baseline stereo images to measure the three-dimensional surface from the leaf to the canopy scale. *Nova Acta Leopoldina (in press)* **96**.

Biskup B., Scharr H., Fischbach A., Wiese-Klinkenberg A., Schurr U. & Walter A. (2009b) Diel growth cycle of isolated leaf discs analyzed with a novel, high-throughput three-dimensional imaging method is identical to that of intact leaves. *Plant Physiology* **149**, 1452–1461.

Biskup B., Scharr H., Schurr U. & Rascher U. (2007) A stereo imaging system for measuring structural parameters of plant canopies. *Plant, Cell and Environment* **30**, 1299 – 1308.

Rascher U., Biskup B., Leaky A. D. B., McGrath J. M., Nelson R. & Ainsworth E. A. ([Agr-ForestMeteorol]) Maximum photosynthetic electron transport rate, not upper canopy structure, determines crop yield in soybean varieties under elevated CO₂. *Agricultural and Forest Meteorology (submitted)*.

3.2 Other publications

Biskup B., Gradmann D. & Thiel G. (1999) Calcium release from InsP₃-sensitive internal stores initiates action potential in *Chara*. *FEBS Letters* **453**, 72–76.

Jansen M., Gilmer F., Biskup B., Nagel K. A., Rascher U., Fischbach A., Briem S., Dreissen G., Tittmann S., Braun S., De Jaeger I., Metzloff M., Schurr U., Walter A. & Scharr H. ([FunctPlantBiol]) Simultaneous phenotyping of leaf growth and chlorophyll fluorescence via GROWSCREEN FLUORO allows detection of stress tolerance in *Arabidopsis thaliana* and other rosette plants. *Functional Plant Biology (in preparation)*.

White P. J., Biskup B., Elzenga T. M., Homann U., Maathuis F. J. M., Thiel G. & Wissing F. (1999) Advanced patch-clamp techniques and single channel analysis. *Journal of Experimental Botany* **50**, 1037–1054.

4 References

- Ainsworth E. A. & Long S. P. (2005) What have we learned from 15 years of free air CO₂ enrichment (FACE)? a meta-analytic review of the responses of photosynthesis, canopy properties and plant production to rising CO₂. *New Phytologist* **165**, 351–372.
- Ainsworth E. A., Schurr U. & Walter A. (2005) *Glycine max* leaflets lack a base-tip gradient in growth rate. *Journal of Plant Research* **118**, 343–346.
- Allen M., Prusinkiewicz P. & DeJong T. (2005) Using L-systems for modeling source-sink interactions, architecture and physiology of growing trees: the L-PEACH model. *New Phytologist* **166**, 869–880.
- Arp W. J. (1991) Effects of source-sink relations on photosynthetic acclimation to elevated CO₂. *Plant, Cell and Environment* **14**, 869–875.
- Avery G. S. (1933) Structure and development of tobacco leaves. *American Journal of Botany* **20**, 565–592.
- Baker J. G. (1980). Manual of photogrammetry. In (eds. J. C. Baker, K. M. O’Connell & R. A. Williamson) chapter, 103–185. Pub. American Society of Photogrammetry 4 edition.
- Baldocchi D. D. (1989). Canopy atmosphere water vapor exchange: can we scale from a leaf to a canopy? In Black T. A., Spittlehouse D. L., Novak M. D. & Price D. T., editors, *Estimation of Areal Evapotranspiration*. Pub. 177 21–41 Wallingford, UK. IAHS Press.
- Balegh S. E. & Biddulph O. (1970) The photosynthetic action spectrum of bean plants. *Plant Physiology* **46**, 1–5.
- Ballaré C. L., Scopel A. L. & Sanchez R. A. (1990) Far-Red Radiation Reflected from Adjacent Leaves: An Early Signal of Competition in Plant Canopies. *Science* **247**, 329–332.
- Barczy J. F., Rey H., Caraglio Y., De Reyffe P., Barthélémy D.D. Q. X. & Fourcaud T. (2007) Amapsim: A structural whole-plant simulator based on botanical knowledge and designed to host external functional models. *Annals of Botany* **0**, 1–14.
- Bawhey C. I., Grant R. H. & Gao W. (2003) Digital measurement of heliotropic leaf response in soybean cultivars and leaf exposure to solar uvb radiation. *Agricultural and Forest Meteorology* **120**, 161–175.
- Ben-Haj-Salah H. & Tardieu F. (1995) Temperature affects expansion rate of maize leaves without change in spatial distribution of cell length. *Plant Physiology* **109**, 861–870.

- Bermejo V., Gimeno B. S. Sanz J., de la Torre D. & Gil J. M. (2003) Assessment of the ozone sensitivity of 22 native plant species from mediterranean annual pastures based on visible injury. *Atmospheric Environment* **37**, 4667–4677.
- Berns M., Matsubara S., Wiese A., Gilmer F., Schurr U., Walter A. & Höcker U. (2007) Diel leaf growth pattern in cry1cry2 mutants of *Arabidopsis thaliana* under different light conditions. *Comparative Biochemistry and Physiology A-Molecular & Integrative Physiology* **146**, 233.
- Bigün J. & Granlund G. H. (1987). Optimal orientation detection of linear symmetry. In *IEEE First International Conference on Computer Vision* 433–438 London, Great Britain. Linköping University, Sweden.
- Biskup B., Scharr H., Fischbach A., Wiese-Klinkenberg A., Schurr U. & Walter A. (2009) Diel growth cycle of isolated leaf discs analyzed with a novel, high-throughput three-dimensional imaging method is identical to that of intact leaves. *Plant Physiology* **149**, 1452–1461.
- Boardman N. K. (1977) Comparative photosynthesis of sun and shade plants. *Annual Review of Plant Physiology* **28**, 355–377.
- Bouguet J.-Y. (2005). Calibration toolbox for matlab. URL http://www.vision.caltech.edu/~bouguetj/calib_doc/.
- Boysen Jensen P. (1932) *Die Stoffproduktion der Pflanzen*. Gustav Fischer Verlag Jena, Germany.
- Breda N. J. J. (2003) Ground-based measurements of leaf area index: a review of methods, instruments and current controversies. *J. Exp. Bot.* **54**, 2403–2417.
- Brox T., Bruhn A., Papenberg N. & Weickert J. (2004). High accuracy optical flow estimation based on a theory for warping. URL citeseer.ist.psu.edu/brox04high.html.
- Bunce J. A. (1982) Photosynthesis at ambient and elevated humidity over a growing season in soybean. *Photosynthesis Research* **3**, 307–311.
- Campbell G. S. & Norman J. M. (1989). The description and measurement of plant canopy structure. In *Plant Canopies: Their Growth, Form, and Function* (eds. G. Russell, B. Marshall & P. G. Jarvis) , pp. 1 – 19. Cambridge University Press, Cambridge, UK.
- Cave G., Tolley L. C. & Strain B. R. (1981) Effect of carbon dioxide enrichment on chlorophyll content, starch content and starch grain structure in trifolium subterraneum leaves. *Physiologia Plantarum* **51**, 171–174.
- Chen J. M. & Cihlar J. (1995) Plant canopy gap-size analysis theory for improving optical measurements of leaf-area index. *Applied Optics* **34**, 6211 – 6222.
- Chenu K., Franck N. & Lecoecur J. (2007) Simulations of virtual plants reveal a role for *SER-RATE* in the response of leaf development to light in *Arabidopsis thaliana*. *New Phytologist* **175**, 472 – 481.

- Clarke T. A. & Fryer J. G. (1998) The development of camera calibration methods and models. *Photogrammetric Record* **16**, 51 – 66.
- Coen E., Rolland-Lagan A. G., Matthews M., Bangham A. J. & Prusinkiewicz P. (2004) The genetics of geometry. *Proceedings of the National Academy of Sciences of the United States of America* **101**, 4728–4735.
- Conrady A. (1919) Decentering lens systems. *Monthly Notices of the Royal Astronomical Society* **79**, 384 – 390.
- Conroy J. P., Seneweera S., Basra A. S., Rogers G. & Nissenwooller B. (1994) Influence of rising atmospheric CO₂ concentrations and temperature on growth, yield and grain quality of cereal crops. *Australian Journal of Plant Physiology* **21**, 741–758.
- Cosgrove D. J., Li L. C., Cho H.-T., Hoffmann-Benning S., Moore R. C. & Blecker D. (2002) The growing world of expansin. *Plant and Cell Physiology* **43**, 1436–1444.
- Coté G. G. (1995) Signal transduction in leaf movement. *Plant Physiology* **109**, 729 – 734.
- Cowan I. R. (1977) Stomatal behaviour and environment. *Advances in Botanical Research* **4**, 117–228.
- Dale J. E. (1988) The control of leaf expansion. *Annual Review of Plant Physiology and Plant Molecular Biology* **68**, 267–295.
- De Visser P. H. B., Marcelis L. F. M., Van der Heijden G. W. A. M., Vos J., Struik P. C. & Evers J. B. (2002) Report 52: 3D modelling of plants: a review. Technical report Plant Research International B. V. Wageningen, The Netherlands.
- De Wit C. T. (1965) Photosynthesis of leaf canopies. Agricultural Research Report 663 Institute for Biological & Chemical Research on Field Crops and Herbage Wageningen, The Netherlands.
- Degli Agosti R., Jouve L. & Greppin H. (1997) Computer-assisted measurements of plant growth with linear variable differential transformer (LVDT) sensors. *Archives Scientifiques Genève* **50**, 233–244.
- Deisenhofer J., Epp O., Miki K., Huber R. & Michel H. (1985) Structure of the protein subunits in the photosynthetic reaction centre of *Rhodospseudomonas viridis* at 3 Å resolution. *Nature* **318**, 618–624.
- Del Ponte E. M., Godoy C. V., Li X. & Yang X. B. (2006) Predicting severity of Asian soybean rust epidemics with empirical rainfall models. *Phytopathology* **96**, 797–803.
- Dyer C. (2001). Volumetric scene reconstruction from multiple views. URL citeseer.comp.nus.edu.sg/467411.html.

- El-Lithy M. E., Clerkx E. J. M., Ruys G. J., Koornneef M. & Vreugdenhil D. (2004) Quantitative trait locus analysis of growth-related traits in a new *Arabidopsis* recombinant inbred population. *Plant Physiology* **135**, 1–15.
- Emerson R. (1958) The quantum yield of photosynthesis. *Annual Reviews of Plant Physiology* **9**, 1–24.
- Falster D. S. & Westoby M. (2003) Leaf size and angle vary widely across species: what consequences for light interception? *New Phytologist* **158**, 509 – 525.
- Farquhar G. D. (1978) Feedforward responses of stomata to humidity. *Australian Journal of Plant Physiology* **5**, 787–800.
- Farquhar G. D. & von Caemmerer S. (). Encyclopedia of Plant Physiology, Bd. 12B. Physiological Plant Ecology II: Water Relations and Carbon Assimilation. In (eds. O. Lange, P. Nobel & H. Ziegler) chapter. Springer Berlin.
- Faugeras O. D., Luong Q.-T. & Maybank S. J. (1992). Camera self-calibration: Theory and experiments. In *ECCV '92: Proceedings of the Second European Conference on Computer Vision* 321–334 London, UK. Springer-Verlag.
- Forseth E. N. & Ehleringer J. R. (1983) Ecophysiology of two solar tracking desert winter annuals. IV. effects of leaf orientation on calculated daily carbon gain and water use efficiency. *Oecologia* **58**, 10–18.
- Forseth I. N. & Teramura A. H. () Kudzu leaf energy budget and calculated transpiration: The influence of leaflet orientation. *Ecology* **67**, 564–571.
- Forterre Y., Skotheim J. M., Dumais J. & Mahadevan L. (2005) How the venus fly trap snaps. *Nature* **433**, 421–425.
- Franklin K. A. & Whitelam G. C. (2005) Phytochromes and shade-avoidance responses in plants. *Annals of Botany* **96**, 169–175.
- Frenkel A. W. (1995) Photosynthetic phosphorylation. *Photosynthesis Research* **46**, 73–77.
- Frijters D. & Lindenmayer A. (). *L Systems*, Lecture Notes in Computer Science. In (eds. G. Rozenberg & A. Salomaa) chapter, 24–52. Springer Berlin, Germany.
- Fromm J. & Eschrich W. (1988) Transport processes in stimulated and non-stimulated leaves of *Mimosa pudica*. II. energesis and transmission of seismic stimulation. *Trees — Structure and Function* **2**, 18–24.
- Fusiello A., Roberto V. & Trucco E. (1997). Efficient stereo with multiple windowing. In *Proceedings of the IEEE Conference on Computer Vision and Pattern Recognition (CVPR '97)* 858–863 Puerto Rico. IEEE Computer Society Press.

- Gamon J. A. & Pearcy R. W. (1989) Leaf movement, stress avoidance and photosynthesis in *Vitis californica*: Interactive effects of sunlight, temperature and water status. *Plant, Cell and Environment* **13**, 267–276.
- Ghannoum O., von Caemmerer S. & Conroy J. P. (2000) Plant water use efficiency of 17 Australian NAD-ME and NADPME C₄ grasses at ambient and elevated CO₂ partial pressure. *Australian Journal of Plant Physiology* **28**, 1207–1217.
- Giavitto J. L., Godin C., Michel O. & Prusinkiewicz P. (2002). Computational models for integrative and developmental biology. In *Actes du Colloque Modélisation et simulation de processus biologiques dans le contexte de la génomique* 43 Autrans, France.
- Gilbert I. R., Jarvis P. G. & Smith H. (2001) Proximity signal and shade avoidance differences between early and late successional trees. *Nature* **411**, 792 – 795.
- Glinka Z. & Meidner H. (1968) The measurement of stomatal responses to stimuli in leaves and leaf discs. *J. Exp. Bot.* **19**, 152–166.
- Godin C. (2000) Representing and encoding plant architecture: A review. *Annals of Forest Science* **57**, 413–438.
- Granier C., Aguirrezabal L., Chenu K., Cookson S. J., Dauzat M., Hamard P., Thioux J., Rolland G., Bouchier-Combaud S., Lebaudy A., Muller B., Simonneau T. & Tardieu F. (2006) PHENOPSIS, an automated platform for reproducible phenotyping of plant responses to soil water deficit in *Arabidopsis thaliana* permitted the identification of an accession with low sensitivity to soil water deficit. *New Phytol.* **169**, 623–635.
- Granier C. & Tardieu F. (1998) Spatial and temporal analyses of expansion and cell cycle in sunflower leaves. *Plant Physiology* **116**, 991–1001.
- Hamamoto H., Kimura M. & Yamaguchi I. (2006) High resolution analysis of plant organ growth using non-contact inkjet marking. *Environmental and Experimental Botany* **57**, 62–69.
- Hartley R. I. (1992). Estimation of relative camera positions for uncalibrated cameras. In *ECCV '92: Proceedings of the Second European Conference on Computer Vision* 579–587 London, UK. Springer-Verlag.
- Hartley R. I. & Zisserman A. (2004) *Multiple View Geometry in Computer Vision*. Cambridge University Press, Cambridge, UK.
- Haußecker H. (1999). Handbook of computer vision and applications. In (eds. B. Jähne, H. Haußecker & P. Geißler) chapter. Academic Press San Diego, CA, USA.
- Heath R. L. (1994) Possible mechanisms for the inhibition of photosynthesis by ozone. *Photosynthesis Research* **39**, 439–451.

- Heckenberger U.R. U. . S. U. (1998) Effect of drought stress on cytological status of *Ricinus communis*. *Journal of Experimental Botany* **49**, 181 – 189.
- Heikkilä J. (2000) Geometric camera calibration using circular control points. *IEEE Transactions on Pattern Analysis and Machine Intelligence* **22**, 1066–1077.
- Helliker B. R. & Richter S. L. (2008) Subtropical to boreal convergence of tree-leaf temperatures. *Nature* **454**, 511–515.
- Herbert T. J. (1983) The influence of axial rotation upon reception of solar radiation by plant leaves. *Journal of Theoretical Biology* **105**, 603 – 618.
- Herbert T. J. (1992) Geometry of heliotropic and nyctinastic leaf movements. *American Journal of Botany* **79**, 547 – 550.
- Herbert T. J. (1995) Stereo photogrammetry of plant leaf angles. *Photogrammetric Engineering and Remote Sensing* **61**, 89 – 92.
- Hill R. & Scarisbrick R. (1940) Production of oxygen by illuminated chloroplasts. *Nature* **146**, 61–62.
- Hirose T. (2005) Development of the monsi-saeki theory on canopy structure and function. *Annals of Botany* **95**, 483–494.
- Hocking P. J. & Meyer C. P. (1991) Carbon dioxide enrichment decreases critical nitrate and nitrogen concentrations in wheat. *Journal of Plant Nutrition* **14**, 571–584.
- Hogeweg P. & Hesper B. (1974) A model study on biomorphological description. *Pattern Recognition* **6**, 165–179.
- Hoover W. H. (1937) The dependence of carbon dioxide assimilation in a higher plant on wavelength of radiation. *Smithsonian Miscellaneous Collections* **95**, 1–13.
- Horn B. K. P. & Schunck B. G. (1981) Determining optical flow. *Artificial Intelligence* **17**, 185–203.
- Humphries S. W. & Long S. P. (1995) WIMOVAC: a software package for modelling the dynamics of plant leaf and canopy photosynthesis. *Computer Applications in the Biosciences* **11**, 361 – 371.
- Idso S. B. & De Wit C. T. (1970) Light relations in plant canopies. *Applied Optics* **9**, 177–184.
- IPCC (2001) *The scientific basis. Contribution of working group I to the third assessment report of the intergovernmental panel on climate change*. Climate change 2001. Cambridge University Press Cambridge.
- IPCC (2007) *Fourth Assessment Report: Climate Change 2007: Working Group I Report: The Physical Science Basis*. Geneva: IPCC.

- Ivanov N., Boissard P., Chapron M. & Andrieu B. (1995) Computer stereo plotting for 3-D reconstruction of a plant canopy. *Agricultural and Forest Meteorology* **75**, 85 – 102.
- J. S. R. & Salvucci M. E. (2002) Rubisco: structure, regulatory interactions, and possibilities for a better enzyme. *Annual Reviews of Plant Biology* **53**, 449 – 475.
- Jurik T. W. & Akey W. C. (1994) Solar-tracking leaf movements in velvetleaf (*Abutilon theophrasti*). *Plant Ecology* **112**, 93–99.
- Jurik T. W., Zhang H. & Pleasants J. M. (1990) Ecophysiological consequences of non-random leaf orientation in the prairie compass plant, *SSilphium laciniatum*. *Oecologia* **82**, 180–186.
- Kao W. Y. & Forseth I. N. (1991) The effects of nitrogen, light and water availability on tropic leaf movements in soybean (*Glycine max*). *Plant, Cell and Environment* **14**, 287–294.
- Kao W. Y. & Forseth I. N. (1992) Diurnal leaf movement, chlorophyll fluorescence and carbon assimilation in soybean grown under different nitrogen and water availabilities. *Plant, Cell and Environment* **15**, 703–710.
- King D. A. (1997) The functional significance of leaf angle in eucalyptus. *Australian Journal of Botany* **45**, 619–639.
- Koller D., Björkman O. & Ritter S. (1995) Role of pulvinar chloroplasts in light-driven leaf movements of the trifoliolate leaf of bean (*Phaseolus vulgaris* L. *Journal of Experimental Botany* **46**, 1215–1222.
- Koornneef M., Alonso-Blanco C. & Vreugdenhil D. (2004) Naturally occurring genetic variation in *Arabidopsis thaliana*. *Annual reviews of plant biology* **55**, 141–172.
- Körner C. (2006) Plant CO₂ responses: an issue of definition, time and resource supply. *New Phytologist* **172**, 393–411.
- Kühlbrandt W., Wang D. N. & Fujiyoshi Y. (1994) Atomic model of plant harvesting complex by electron crystallography. *Nature* **367**, 614–621.
- Kuroiwa S. (1971). Prediction and measurement of photosynthetic productivity. In (ed. I. Setlick) chapter, 79–89. Pudoc Wageningen, The Netherlands.
- Küstern R. (2004) *Simultane Tiefen- und Flussbestimmung pflanzlicher Oberflächen*. PhD thesis Universität Heidelberg, Germany.
- Kwiatkowska D. (2004) Surface growth at the reproductive shoot apex of *Arabidopsis thaliana pin-formed 1* and wild type. *Journal of Experimental Botany* **55**, 1021 – 1032.
- Lang A. R. G. (1990) An instrument for measuring canopy structure. *Remote Sensing Reviews* **5**, 61 – 76.

- Lange O. L.L. R., Schulze E.-D. & Kappen L. () Responses of stomata to changes in humidity. *Planta* **100**, 76–86.
- Leakey A. D. B., Bernacchi C. J., Dohleman F. G., Ort D. R. & Long S. P. (2004) Will photosynthesis of maize (*Zea mays*) in the U. S. corn belt increase in future [CO₂] rich atmospheres? an analysis of diurnal courses of CO₂ uptake under free-air concentration enrichment (FACE). *Global Change Biology* **10**, 951–962.
- Leister D., Varotto C., Pesaresi P., Niwergall A. & Salamini F. (1999) Large-scale evaluation of plant growth in *Arabidopsis thaliana* by non-invasive image analysis. *Plant Physiology and Biochemistry* **37**, 671–678.
- Leopold J., H. G. & R. L. (2003) New developments in fast 3d-surface quality control. *Measurement* **33**, 179–187.
- Lesaulnier C., Papamichail D., McCorkie S., Ollivier B., Skiena S., Taghavi S., Zak D. & van der Lelie D. (2008) Elevated atmospheric CO₂ affects soil microbial diversity associated with trembling aspen. *Environmental Microbiology* **10**, 926–941.
- Levy E. B. & Madden E. A. (1933) The point method of pasture analysis. *New Zealand Journal of Agriculture* **46**, 267–279.
- Lindenmayer A. (1968) Mathematical models for cellular interaction in development. parts i and ii. *Journal of Theoretical Biology* **18**, 280–315.
- Long S. P. (1991) Modification of the response of photosynthetic productivity to rising temperature by atmospheric CO₂ concentrations. has its importance been underestimated? *Plant, Cell and Environment* **14**, 729–739.
- Long S. P., Ainsworth E. A., Leaky A. D. B., Nösberger J. & Ort D. R. (2006a) Food for thought: Lower-than-expected crop yield stimulation with rising CO₂ concentrations. *Science* **312**, 1918–1921.
- Long S. P., Ainsworth E. A., Rogers A. & Ort D. R. (2004) rising atmospheric carbon dioxide: Plants FACE the future. *Annual Reviews of Plant Biology* **55**, 591–628.
- Long S. S., Zhu X.-G., Naidu S. L. & Ort D. R. (2006b) Can improvement in photosynthesis increase crop yield? *Plant, Cell and Environment* **29**, 315 – 330.
- Lucas B. D. & Kanade T. (1981). An iterative image registration technique with an application to stereo vision. In *IJCAI81* 674–679.
- Ludlow M. M. & Björkman O. (1984) Paraheliotropic leaf movement in sirato as a protective mechanism against drought-induced damage to primary photosynthetic reactions: damage by excessive light and heat. *Planta* **161**, 505–518.

- Makino A. & Mae T. (1999) Photosynthesis and plant growth at elevated levels of CO₂. *Plant Cell Physiology* **40**, 999–1006.
- Matsubara S., Hurry V., Druart N., Benedict C., Janzik I., Chavarria-Krauser A., Walter A. & Schurr U. (2006) Nocturnal changes in leaf growth of *Populus deltoides* are controlled by cytoplasmic growth. *Planta* **223**, 1315–1328.
- Mémin E. & Pérez P. (1998). A multigrid approach to hierarchical motion estimation. In *Proceedings of the International Conference on Computer Vision, ICCV'98* 933–938 Bombay, India.
- Miglietta F., Peressotti A., Vaccari F. P., A. Z., P. D. & Scarascia-Mugnozza G. (2001) Free air CO₂ enrichment (FACE) of a poplar plantation: the POPFACE fumigation system. *New Phytologist* **150**, 465–476.
- Miller P. C. (1972) Subtropical to boreal convergence of tree-leaf temperatures. *Ecology* **53**, 22–45.
- Mitchell P. (1961) Coupling of phosphorylation to electron and proton transfer by a chemiosmotic type of mechanism. *Nature* **191**, 144–148.
- Monsi M. & Saeki T. (1953) Über den Lichtfaktor in den Pflanzengesellschaften und seine Bedeutung für die Stoffproduktion. *Japanese Journal of Botany* **14**, 22–52.
- Moran N. (2007) Osmoregulation of leaf motor cells. *FEBS Letters* **581**, 2337–2347.
- Morat J., Devernay F., Cornou S. & Ibanez Guzman J. (2007). Evaluation method for automotive stereo-vision systems. In *Proceedings of IEEE Intelligent Vehicles Symposium*.
- Morgan P. B., Mies T. A., Bollero G. A., Nelson R. L. & Long S. P. (2006) Season-long elevation of ozone concentration to projected 2050 levels under fully open-air conditions substantially decreases the growth and production of soybean. *New phytologist* **170**, 333–343.
- Mulder J. D., Jansen J. & van Rhijn A. (2003). An affordable optical head tracking system for desktop vr/ar systems. In *EGVE '03: Proceedings of the workshop on Virtual environments 2003* 215–223 New York, NY, USA. ACM.
- Mullen J. L., Weinig C. & Hangarter R. P. (2006) Shade avoidance and the regulation of leaf inclination in *Arabidopsis*. *Plant, Cell and Environment* **29**, 1099–1106.
- Muraoka H., Takenaka A., Tang Y., Koizumi H. & Washitani I. (1998) Flexible leaf orientations of *Arisaema heterophyllum* maximize light capture in a forest understorey and avoid excess irradiance at a deforested site. *Annals of Botany* **82**, 297–307.
- Murphy J. J., Delucchi M. A., McCubbin D. R. & Kim H. J. (1999) The cost of crop damage caused by ozone air pollution from motor vehicles. *Journal of Environmental management* **55**, 273–289.

- Měch R. & Prusinkiewicz P. (1996). Visual models of plants interacting with their environment. In *SIGGRAPH '96: Proceedings of the 23rd annual conference on Computer graphics and interactive techniques* 397–410 New York, NY, USA. ACM.
- Nafziger E. D. & Koller R. M. (1976) Influence of leaf starch concentration on CO₂ assimilation in soybean. *Plant Physiology* **57**, 560–563.
- Nagel K. A., Schurr U. & Walter A. (2006) Dynamics of root growth stimulation in nicotiana tabacum in increasing light intensity. *Plant, Cell and Environment* **29**, 1936–1945.
- Nelson P. V. (2002) *Greenhouse Operation and Management*. Prentice Hall PTR Upper Saddle River, USA.
- Nielsen T. H. & Ulvskov P. (1997) Cytokinins and leaf development in sweet pepper (*Capsicum annuum* L.). II. sink metabolism in relation to cytokinin-promoted leaf expansion. *Planta* **188**, 78–84.
- Nultsch W. (2001) *Allgemeine Botanik*. Thieme.
- Nunes M. A., Correira M. M. & Lucas M. D. (1983) NaCl-stimulated proton efflux and cell expansion in sugar-beet leaf discs. *Planta* **158**, 103–107.
- Olson C. F., Matthies L. H., Wright J. R., Li R. & Di K. (2007) Visual terrain mapping for mars exploration. *Computer Vision and Image Understanding* **105**, 73–85.
- Omasa K., Hosoi F. & Konishi A. (2007) 3d lidar imaging for detecting and understanding plant responses and canopy structure. *Journal of Experimental Botany* **58**, 881–898.
- Omasa K., Qiu G. Y., Watanuki K., Yoshimi K. & Akiyama Y. (2003) Accurate estimation of forest carbon stocks by 3–D remote sensing of individual trees. *Environmental Science & Technology* **37**, 1198 – 1201.
- Ort D. R. & P. L. S. (2003). Converting Solar Energy into Crop Production. In (eds. M. J. Chrispeels & D. E. Sadava) chapter, 240–269. American Society of Plant Biologists/Jones and Bartlett Boston, MA, USA.
- Pal M., Karthikeyapandian V., Jain V., Srivastava A. C., Raj A. & Sengupta U. K. (2004) Biomass production and nutritional levels of berseem (*Trifolium alexandrinum*) grown under elevated CO₂. *Agriculture, Ecosystems & Environment* **101**, 31–38.
- Pearcy R. W. & Yang W. (1996) A three-dimensional crown architecture model for assessment of light capture and carbon gain by understory plants. *Oecologia* **108**, 1–12.
- Petit J. R., Jouzel J., Raynaud D., Barkov N. I., Barnola J. M., Basile I., Bender M., Chappellaz J., Davis M., Delaygue G., Delmotte M., Kotlyakov V. M., Legrand M., Lipenkov V. Y., Lorius C., Pepin L., Ritz C., Saltzman E. & Stievenard M. (1999) Climate and atmospheric history of the past 420,000 years from the vostok ice core, antarctica. *Nature* **399**, 429–436.

- Poethig R. S. & Sussex I. M. (1985) The cellular parameters of leaf development in tobacco: a clonal analysis. *Planta* **165**, 170–184.
- Pollefeys M., Gool L. J. V., Vergauwen M., Cornelis K., Verbiest F. & Tops J. (2001). Image-based 3d acquisition of archaeological heritage and applications. In Arnold D. B., Chalmers A. & Fellner D. W., editors, *Virtual Reality, Archeology, and Cultural Heritage* 255–262. ACM.
- Pollefeys M., Koch R., Vergauwen M. & Van Gool L. J. (2000) Automated reconstruction of 3d scenes from sequences of images. **55**, 251–267.
- Powell R. D. & Griffith M. M. (1960) Some anatomical effects of kinetin and red light on disks of bean leaves. *Plant Physiol.* **35**, 273–275.
- Preim B. & Bartz D. (2007) *Visualization in Medicine: Theory, Algorithms, and Applications (The Morgan Kaufmann Series in Computer Graphics)*. Morgan Kaufmann Publishers Inc. San Francisco, CA, USA.
- Prusinkiewicz P. (2004) Modeling plant growth and development. *Current Opinion in Plant Biology* **7**, 79–83.
- Prusinkiewicz P., Lindenmayer A. & Hanan J. (1988). Developmental models of herbaceous plants for computer imagery purposes. In *ACM SIGGRAPH* volume 22 Atlanta, Georgia. ACM SIGGRAPH.
- Quan L., Tan P., Zeng G., Yuan L., Wang J. & Kang S. B. (2006). Image-based plant modeling. In *SIGGRAPH '06: ACM SIGGRAPH 2006 Papers* 599–604 New York, NY, USA. ACM.
- Rakocevic M., Sinoquet H., Christophe A. & Varlet-Grancher C. (2000) Assessing the geometric structure of a white clover (*Trifolium repens* L.) canopy using 3–D digitising. *Annals of Botany* **86**, 519–526.
- Rascher U., Biskup B., Leaky A. D. B., McGrath J. M., Nelson R. & Ainsworth E. A. ([Agr-ForestMeteorol]) Maximum photosynthetic electron transport rate, not upper canopy structure, determines crop yield in soybean varieties under elevated CO₂. *Agricultural and Forest Meteorology* (submitted).
- Rasse D. P., Stolaki S., Peresta G. & Drake B. G. (2002) Patterns of canopy-air CO₂ concentration in a brackish wetland: analysis of a decade of measurements and the simulated effects on the vegetation. *Agricultural and Forest Meteorology* **114**, 59–73.
- Raven P. H., Evert R. F. & Eichhorn S. E. (2004) *Biology of plants*. Freeman.
- Reid C. D., Fiscus E. L. & Burkey K. O. (1999) Combined effects of chronic ozone and elevated CO₂ on rubisco activity and leaf components in soybean (*Glycine max*). *Journal of Experimental Botany* **49**, 1999–2011.

- Rey H., Dauzat J., Chenu K., Barczy J.-F., Dosio G. A. A. & Lecoœur J. (2007) Using a 3-d virtual sunflower to simulate light capture at organ, plant and plot levels: Contribution of organ interception, impact of heliotropism and analysis of genotypic differences. *Annals of Botany* **0**, 1–13.
- Reynolds P. M., van Ginkel M. & Ribaut J.-M. (2000) Avenues for genetic modification of radiation use efficiency in wheat. *Journal of Experimental Botany* **51**, 459–473.
- Roden J. (2003) Modeling the light interception and carbon gain of individual fluttering aspen (*Populus tremuloides* michx) leaves. *Trees – Structure and Function* **17**, 117–126.
- Roger G., Barrett D. & Lutze J. (2000) The effects of elevated [CO₂] on the C:N and C:P mass ratios of plant tissues. *Plant and Soil* **224**, 1–14.
- Rogers A., Allen J., Davey P. A., Morgan P. B., Ainsworth E. A., Bernacchi C. J., Cornic G., Dermody O., Dohleman F. G., Heaton E. A., Mahoney J., Zhu Z.-G., DeLucia E. H., Ort D. R. & Long S. P. (2004) Leaf photosynthesis and carbohydrate dynamics of soybeans grown throughout their life-cycle under free-air carbon dioxide enrichment. *Plant, Cell and Environment* **27**, 449 – 458.
- Rogers A. & Ellsworth D. S. (2002) Photosynthetic acclimation of *Pinus taeda* (loblolly pine) to long-term growth in elevated pCO₂ (face). *Plant, Cell and Environment* **7**, 851–858.
- Rogers G., Milham P. J., Gillings M. & Conroy J. P. (1996) Sink strength may be the key to growth and nitrogen responses in N-deficient wheat at elevated CO₂. *Australian Journal of Plant Physiology* **23**, 253–264.
- Röhrig M., Stützel H. & Alt C. (1999) A three-dimensional approach to modeling light interception in heterogeneous canopies. *Agronomy Journal* **91**, 1024–1032.
- Rosa L. M., Dillenburg L. R. & Forseth I. N. (1991) Responses of soybean leaf angle, photosynthesis and stomatal conductance to leaf and soil water potential. *Annals of Botany* **67**, 51–58.
- Rosa L. M. & Forseth I. N. (1995) Diurnal patterns of soybean leaf inclination angles and azimuthal orientation under different levels of UVB radiation. *Agricultural and Forest Meteorology* **78**, 107–119.
- Ross J. (1981) *The Radiation Regime and Architecture of Plant Stands*. Dr. W. Junk Publishers, The Hague, The Netherlands.
- Saeki T. (1959) Variation of photosynthetic activity with aging of leaves and total photosynthesis in a plant community. *Botanical Magazine, Tokyo* **72**, 404–408.
- Sakamoto C. M. & Shaw R. H. (1967) Light distribution in field soybean canopies. *Agronomy Journal* **59**, 7–9.

- Sawada S., Kuninaka M., Watanabe K., Sato A., Kawamura H., Komine K., Sakamoto T. & Kasai M. (2001) The mechanism to suppress photosynthesis through end-product inhibition in single-rooted soybean leaves during acclimation to CO₂ enrichment. *Plant Cell Physiology* **42**, 1093–1102.
- Saxena A., Chung S. H. & Ng A. Y. (2008) 3-d depth reconstruction from a single still image. *Int. J. Comput. Vision* **76**, 53–69.
- Scanlon M. J. (1998) Force fields and phyllotaxy: an old model comes to age. *Trends in Plant Science* **3**, 413–414.
- Scharr H. (2004). Optimal filters for extended optical flow. In *International Workshop on Complex Motion (IWCM)* 14–29.
- Scharr H. & Küsters R. (2002). A linear model for simultaneous estimation of 3d motion and depth. In *IEEE Workshop on Motion and Video Computing*.
- Scharstein D., Szeliski R. & Zabih R. (2001). A taxonomy and evaluation of dense two-frame stereo correspondence algorithms. URL www.middlebury.edu.
- Schmundt D.S. M. J. & Schurr U. (1998) Quantitative analysis of the local growth rates of growth of dicot leaves at a high temporal and spatial resolution, using image sequence analysis. *The Plant Journal* **16**, 505–514.
- Schroeder J. I. & Hedrich R. (1989) Involvement of ion channels and active transport in osmoregulation and signaling of higher plant cells. *Trends in Biochemical Sciences* **14**, 187–192.
- Schurr U. (1997). Progress in Botany. In (eds. H.-D. Behnke, Lüttge, K. Esser, J. W. Kadereit & M. Runge) chapter, 355–373. Springer Berlin.
- Sellier D., Fourcaud T. & Lac P. (2006) A finite-element model for investigating effect of aerial architecture on tree oscillations. *Tree Physiology* **26**, 807–817.
- Sinoquet H. & Rivet P. (1997) Measurement and visualisation of the architecture of an adult tree based on a three-dimensional digitising device. *Trees: Structure and Function* **11**, 265 – 270.
- Smith A. R. (1978a) About the cover: reconfigurable machines. *Computer* **11**, 3–4.
- Smith A. R. (1984). Plants, fractals and formal languages. In *Proceedings of SIGGRAPH '84 (Minneapolis, Minnesota, July 22–24, 1984)* volume 18 1–10 ACM SIGGRAPH, New York, USA.
- Smith C., Godin C., Gudon Y., Prusinkiewicz P. & Costes E. (2007). Simulation of apple tree development using mixed statistical and biomechanical models. In *5th International Workshop on Functional-Structural Plant Models* 31, 1–4 Napier, New Zealand.

- Smith W. K. (1978b) Subtropical to boreal convergence of tree-leaf temperatures. *Science* **201**, 614–616.
- Soler C., Sillion F. & de Reffye P. (2003) An efficient instantiation algorithm for simulating radiant energy in transfer in plant models. *ACM Transactions on Graphics* **22**, 204–233.
- Stevens K. A. & Brookes A. (1988) Integrating stereopsis with monocular interpretations of planar surfaces. *Vision Research* **28**, 371–386.
- Stiles K. A. & Van Volkenburgh E. (2004) Role of K⁺ in leaf growth: K⁺ uptake is required for light-stimulated H⁺ efflux but not solute accumulation. *Plant, Cell Environ.* **27**, 315–325.
- Tans P. (2008). Trends in atmospheric carbon dioxide. National Oceanic and Atmospheric Administration.
- Trucco E. & Verri A. (1998) *Introductory Techniques for 3-D Computer Vision*. Prentice Hall PTR Upper Saddle River, USA.
- USDA (2006). <http://www.ers.usda.gov/news/soybeancoverage.htm>.
- Usuda H. & Shimogawara K. (1998) The effects of increased atmospheric carbon dioxide on growth, carbohydrates, and photosynthesis in radish, *Raphanus sativus*. *Plant Cell Physiology* **39**, 1–7.
- van der Mark W. & Gavrilu D. M. (2006) Real-time dense stereo for intelligent vehicles. *IEEE Transactions on Intelligent Transportation Systems* **7**, 38–50.
- van Volkenburgh E. (1999) Leaf expansion – an integrating plant behaviour. *Plant, Cell and Environment* **22**, 1463–1473.
- van Volkenburgh E.S. M. G. . C. R. E. (1985) Loss of capacity for acid-induced wall loosening as a principle cause of the cessation of cell enlargement in light-grown bean leaves. *Planta* **163**, 500 – 505.
- Verma S. B. & Rosenberg N. J. (1976) Vertical profiles of carbon dioxide concentration in stable stratification. *Agricultural Meteorology* **16**, 359 – 369.
- Vissenberg K., Martinez-Vilchez I. M.V. J.-P., Miller J. G. & Fry S. C. (2000) In vivo colocalization of xyloglucan endotransglycosylase activity and its donor substrate in the elongation zone of *Arabidopsis* roots. *Plant Cell* **12**, 1229–1237.
- Vitousek P. M., Aber J. D., Howarth R. W., Likens G. E., Matson P. A., Schindler D. W., Schlesinger W. H. & Tilman D. G. (1997) Human alteration of the global nitrogen cycle: Sources and consequences. *Ecological Applications* **7**, 737–750.
- Walter A. (2000) *Räumliche und zeitliche Wachstumsmuster in Wurzeln und Blättern dikotyler Pflanzen*. PhD thesis University of Heidelberg.

- Walter A., Christ M. M., Barron-Gafford G. A., Grieve K. A., Murthy R. & Rascher U. (2005) The effect of elevated CO₂ on diel leaf growth cycle, leaf carbohydrate content and canopy growth performance of *Populus deltoides*. *Global Change Biology* **11**, 1207–1219.
- Walter A., Rascher U. & Osmond B. (2004) Transitions in photosynthetic parameters of midvein and interveinal regions of leaves and their importance during leaf growth and development. *Plant Biology* **6**, 184–191.
- Walter A., Scharr H., Gilmer F., Zierer R., Nagel K. A., Ernst M., Wiese A., Virnich O., Christ M. M., Uhlig B., Jünger S. & Schurr U. (2007) Dynamics of seedling growth acclimation towards altered light conditions can be quantified via GROWSCREEN: a setup and procedure designed for rapid optical phenotyping of different plant species. *New Phytol.* **174**, 447–455.
- Walter A. & Schurr U. (1999) The modular character of growth in nicotiana tabacum plants under steady-state nutrition. *J. Exp. Bot.* **50**, 1169–1177.
- Walter A. & Schurr U. (2005) Dynamics of leaf and root growth: Endogenous control versus environmental impact. *Annals of Botany* **95**, 891–900(10).
- Watanabe Y., Nakamura Y., & R. I. (1997) Relationship between starch accumulation and activities of the related enzymes in the leaf sheath as a temporary sink organ in rice plant (*Oryza sativa* L.) . *Australian Journal of Plant Physiology* **24**, 563–569.
- Watts W. R. (1974) Leaf extension in *Zea mays*. *Journal of Experimental Botany* **25**, 1085–1096.
- Wheatstone C. (1838) Contributions to the physiology of vision—part the first. on some remarkable, and hitherto unobserved, phenomena of binocular vision. *Philosophical Transactions of the Royal Society of London* 371–394.
- WHO (2003) *Health Aspects of Air Pollution with Particulate Matter, Ozone and Nitrogen Dioxide. Report of WHO Working Group*. WHO Bonn, Germany.
- Wiese A., Christ M. M., Virnich O., Schurr U. & Walter A. (2007) Spatio-temporal leaf growth patterns of *Arabidopsis thaliana* and evidence for sugar control of the diel leaf growth cycle. *New Phytologist* **174**, 752–761.
- Williams M. H. (1991) A sequential study of cell divisions and expansion patterns on a single developing shoot apex of *Vinca major*. *Annals of Botany* **68**, 541–546.
- Williams M. H. & Green P. B. (1988) Sequential scanning electron microscopy of a growing plant meristem. *Protoplasma* **147**, 77–79.
- Wilson J. W. (1960) Inclined point quadrats. *New Phytologist* **59**, 1–8.
- Wofford T. J. & Allen F. L. (1982) Variation in leaflet orientation among soybean cultivars. *Crop Science* **22**, 999–1004.

- Würmlin S., Lamboray E., Stadt O. G. & Gross M. H. (2002). 3d video recorder. In *PG '02: Proceedings of the 10th Pacific Conference on Computer Graphics and Applications* 325 Washington, DC, USA. IEEE Computer Society.
- Yan H. P., Kang M. Z., de Reffye P. & Dingkuhn M. (2004) A dynamic, architectural plant model simulating resource-dependent growth. *Annals of Botany* **93**, 591–602.
- Yoon K. J. & Kweon I. S. (2006). Stereo matching with symmetric cost functions. In *Proceedings of the 2006 Conference on Computer Vision and Pattern Recognition (CVPR '06) II*: 2371 – 2377.
- Zavala J. A., Casteel C. L., DeLucia E. H. & Berenbaum M. R. (2008) Anthropogenic increase in carbon dioxide compromises plant defense against invasive insects. *Proceedings of the National Academy of Sciences of the United States of America* **105**, 5129–5133.
- Zelnik-Manor L. & Irani M. (2002) Multiview constraints on homographies. *IEEE Transactions on Pattern Analysis and Machine Intelligence* **24**, 214–223.
- Zhang R., Tsai P.-S., Cryer J. E. & Shah M. (1999) Shape from shading: A survey. *IEEE Transactions on Pattern Analysis and Machine Intelligence* **21**, 690–706.
- Zhang Z. (1999). Flexible camera calibration by viewing a plane from unknown orientations. In *International Journal of Computer Vision* 666 – 673.
- Zhang Z. (2000) A flexible new technique for camera calibration. *IEEE Transactions on Pattern Analysis and Machine Intelligence* **22**, 1330 – 1334.
- Zhang Z. (2002). Camera calibration with one-dimensional objects. In Heyden A., Sparr G., Nielsen M. & Johansen P., editors, *ECCV (4)* volume 2353 of *Lecture Notes in Computer Science* 161 – 174. Springer.
- Ziska L. H. & Bunce J. A. (2007) Predicting the impact of changing CO₂ on crop yields: some thoughts on food. *New Phytologist* **175**, 607–618.
- Ziska L. H., Ghannoum O., Baker J. T., Conroy J., Bunce J. A., Kobayashi K. & Okada M. (2001) A global perspective of ground level, ‘ambient’ carbon dioxide for assessing the response of plants to atmospheric CO₂. *Global Change Biology* **7**, 789–796.

5 Publications of the dissertation

5.1 First publication: A stereo imaging system for measuring structural parameters of plant canopies

Status: **Published** (September 10, 2007)

Biskup B., Scharr H., Schurr U. & Rascher U. (2007) A stereo imaging system for measuring structural parameters of plant canopies. *Plant, Cell and Environment* **30**, 1299 – 1308.

Own contribution

- Preliminary experiments
- Comparison of stereo algorithms
- Selection of system components and algorithms
- Software design and implementation
- Validation
- Experimental design
- Experiments
- Data analysis
- Preparation of manuscript

A stereo imaging system for measuring structural parameters of plant canopies

BERNHARD BISKUP, HANNO SCHARR, ULRICH SCHURR & UWE RASCHER

Institute of Chemistry and Dynamics of the Geosphere ICG-III (Phytosphere), Research Centre, Jülich GmbH, 52425 Jülich, Germany

ABSTRACT

Plants constantly adapt their leaf orientation in response to fluctuations in the environment, to maintain radiation use efficiency in the face of varying intensity and incidence direction of sunlight. Various methods exist for measuring structural canopy parameters such as leaf angle distribution. However, direct methods tend to be labour-intensive, while indirect methods usually give statistical information on stand level rather than on individual leaves. We present an area-based, binocular stereo system composed of commercially available components that allows three-dimensional reconstruction of small- to medium-sized canopies on the level of single leaves under field conditions. Spatial orientation of single leaves is computed with automated processes using modern, well-established stereo matching and segmentation techniques, which were adapted for the properties of plant canopies, providing high spatial and temporal resolution (angle measurements with an accuracy of approx. $\pm 5^\circ$ and a maximum sampling rate of three frames per second). The applicability of our approach is demonstrated in three case studies: (1) the dihedral leaflet angle of an individual soybean was tracked to monitor nocturnal and daytime leaf movement showing different frequencies and amplitudes; (2) drought stress was diagnosed in soybean by quantifying changes in the zenith leaflet angle distribution; and (3) the diurnal course of the zenith leaf angle distribution of a closed soybean canopy was measured.

Key-words: canopy; leaf movement; screening; stereo imaging; systems biology; 3D reconstruction.

Abbreviations: CDT, central daylight time; FWHM, full width at half maximum; HSV, hue, saturation, (brightness) value; LAI, leaf area index; LIDAR, light detection and ranging system; MTA, mean tilt angle; RANSAC, random sampling consensus; ROI, regions of interest; SoyFACE, soybean free-air concentration enrichment.

INTRODUCTION

Plants, being sessile organisms, must constantly adapt to a spatially and temporally fluctuating environment. This

Correspondence: B. Biskup. Fax: +49-2461/61-2492; e-mail: b.biskup@fz-juelich.de

adaptation is manifested in long-term growth patterns as well as in short-term changes in foliage orientation. Therefore, the structure of plant canopies is highly dynamic, changing on various timescales, from minutes to seasons (Schurr, Walter & Rascher 2006). A predominant factor governing adaptations is the intensity and incidence direction of sunlight. Structural changes in plants have been studied for decades and different approaches for measuring structural parameters of plant canopies have been taken in the past, addressing different scales, from small herbaceous plants to entire forest stands (Campbell & Norman 1989). A classical direct approach for determining leaf angle distributions is to use compass-protractors or inclinometers to measure individual leaf angles (Ross 1981; Herbert 1983; Campbell & Norman 1989; Daughtry 1990). The method is semi-invasive, as leaves are touched while angles are measured and it is labour-intensive; thus the possible temporal resolution is limited. In his seminal work, Lang (1973) proposed a system to digitize three-dimensional (3D) coordinates (also see Lang 1990). Selecting appropriate geometrical structures (e.g. triangles) on the leaf surface, the author was able to measure orientation of single leaves in space quite efficiently. Sinoquet and co-workers have advanced this technique, using an electromagnetic digitizer to compose 3D models of entire plant stands. They carried out extensive work on the modelling of plant canopies (Sinoquet & Rivet 1997; Sinoquet *et al.* 1998; Rakocevic *et al.* 2000). One drawback of the digitization approach is the long acquisition time. Rakocevic *et al.* (2000) reported 3–7 h for a 10 × 10 cm canopy of white clover. While this approach arguably yields very comprehensive information about position and orientation of leaves and stem, short-term dynamic changes in leaf orientation are inaccessible.

LIDAR systems have been greatly advanced in recent years and have been used successfully to reconstruct tree canopies on different scales. LIDAR systems have been applied to forest canopies to estimate parameters like tree height, diameter at breast height or biomass (Lefsky *et al.* 1999; Omasa *et al.* 2003; Parker, Harding & Berger 2004; Tanaka, Park & Hattoria 2004; Omasa, Hosoi & Konishi 2007). However, LIDAR systems are still expensive, and if single leaf resolution is desired, scanning time increases considerably. Because 3D reconstruction requires a rigid scene, leaf-level measurements with LIDAR seem feasible

only in laboratory studies where wind can be avoided, and for plants that do not exhibit short-term leaf movement.

Gap fraction analysis (Chen & Cihlar 1995) is a well-established indirect measurement method, commercially available, for example, in the Li-Cor LAI-2000 plant canopy analyser (Li-Cor Biosciences, Lincoln, NE, USA). The gap fraction is the fraction of view not obscured by foliage in a particular zenith view angle class. The method makes assumptions about foliage distribution and azimuthal symmetry and is therefore not suitable for measuring leaf angles in smaller stands for which these assumptions do not hold. Other indirect methods exist that usually make some assumptions about the canopy structure and tend to be specialized (see, e.g. Campbell & Norman 1989; Deckmyn, Nijs & Ceulemans 2000). Indirect approaches share the property of providing statistical rather than per-leaf information. Several authors have used film-based stereo photography (Herbert 1995; Ivanov *et al.* 1995) or stereo imaging to obtain 3D reconstructions of plants. Andersen, Reng & Kirk (2005) have developed a trinocular stereo system for automatic inspection of crops. They tested their system on ray-traced images of cereal plants. Nielsen, Andersen & Granum (2005a) conducted a comparative study using multi-camera configurations to reconstruct ray-traced images of broad-leaved as well as narrow-leaved plants. The focus of their work was to compare different algorithms to ground truth (also see Nielsen *et al.* 2005b), which would have been hard to obtain for a real plant scene. They found that the combination of descriptive parameters such as presence or absence of texture, surface orientation, depth range or proportion of occlusion influences the quality of reconstruction, resulting in a complicated trade-off.

Here, we present a binocular field stereo system that can be used to create partial 3D models of the outer canopy of small stands (currently a few square meters), allowing access to structural information on the level of single leaves, if necessary at a comparatively high temporal resolution of three frames per second. The system is assembled of moderately priced, consumer-grade digital single-lens reflex cameras. In this paper, we describe a processing pipeline which is based on established algorithms and which allows the separation of single leaves and the semi-automated quantification of leaf orientation in space, independent of the viewing angle. We demonstrate the accuracy of the system by three applications: (1) studying temporal dynamics of leaflet inclination in a soybean plant; (2) quantifying changes in leaflet inclination angle distribution in a small drought-stressed soybean canopy; and (3) measuring the diurnal course of the zenith leaf angle distribution of a closed soybean canopy.

STEREO CAMERA SYSTEM

Image acquisition hardware

Image pairs were acquired using two identical, unmodified EOS 350D Digital Rebel XT single-lens reflex cameras with Canon EF 50 mm f/1.8 I fixed focal length lenses (Canon Co.

Ltd., Tokyo, Japan). The camera model was chosen because of its resolution of 8 megapixels, the comparably low sensor noise, the moderate price and the possibility of remote control. The lenses were selected because of their reasonably low distortion and their general-purpose field of view. The cameras were triggered simultaneously either by using a custom-made remote control release cable (directly coupled focusing and trigger channels), or by a custom-made control cable switched via the parallel port of a personal computer. Identical settings (focal length, aperture, shutter time, etc.) were used for both cameras. The cameras were set to manual mode to ensure synchronous triggering (within 20 ms), thus avoiding non-deterministic focusing and exposure time calculations. Synchronous triggering is important for outdoor measurements because plants may be very susceptible to wind, and stereo matching requires a rigid scene. Field measurements with soybean under different wind conditions showed that reconstruction was reliable in moderate wind and moving canopy; however, it failed in stormy conditions. The cameras were set to produce JPEG images with a resolution of 3456×2304 pixels at 24-bit colour depth and best available image quality. Images in our case studies were downsampled by a factor of 5. The resulting resolution (691×460 pixels) was sufficient for reconstruction. Cameras were mounted in a fixed position relative to each other on a 500 mm X-95 bar (Linus Photonics GmbH & Ko. KG, Göttingen, Germany). To maximize the overlapping field of view, the cameras were adjusted such that their optical axes converged somewhere within the observed scene. The distance between camera centres, the stereo baseline, is a trade-off between precision and loss of information due to occlusion: the larger the baseline, the more precise the depth estimate will be, but the higher the proportion of occluded leaf area. Depending on the application, a tripod was used to mount the stereo rig, or the rig was moved by hand to capture images from arbitrary directions. Rather than attempting an accurate positioning of the cameras (hardware calibration) which would be difficult with our consumer-grade cameras and stereo rig, cameras and rig were calibrated and images were subjected to epipolar rectification (see next section). We used the following stereo rig settings (baseline b , working distance w): (1) for accuracy measurements: $b = 13.0$ cm, $w \approx 57$ cm; (2) leaf movement case study: $b = 16.9$ cm, working distance of approx. $w \approx 2$ m; (3) drought stress case study: $b = 18.2$ cm, w between 2 and 4 m; (4) $b = 46.1$ cm, $w \approx 2.80$ m (mean canopy height).

Calibration of cameras and stereo rig

Stereo calibration is a prerequisite for metric 3D reconstruction. It amounts to finding the intrinsic parameters (focal length, principal point, radial and tangential distortion) of the cameras and the extrinsic parameters (rotation matrix and translation vector) of the stereo rig (Conrady 1919; Brown 1966, 1971; Hartley & Zisserman 2004). The knowledge of these parameters allows to relate pairs of image points (left, right) to 3D world points. The stereo rig was calibrated before each series of measurements. Lenses

were focused to the appropriate distance and the focus setting was fixed with adhesive tape to avoid changes in the intrinsic camera parameters (especially focal length and principal point) after calibration.

Stereo calibration was carried out using the OpenCV computer vision library (Intel Inc., Santa Clara, CA, USA). This approach uses a chessboard of known dimensions observed from a number of unknown positions (Zhang 1999, 2000; Fig. 1a). It is a flexible and robust and thus pragmatic approach to calibration, originally targeted at desktop vision systems rather than highly controlled laboratory or industry set-ups; the calibration target can simply be printed out with a laser printer and put on a flat surface which, however, is not required to be crafted with high accuracy. We typically used calibration targets of 7×10 chessboard fields, each field 40 or 80 mm in size (depending on the distance of the stereo rig to the scene), taking image pairs of at least 20 different positions all over the working volume. The target should not appear too small in the image to be useful for calibration (Zhang 2000). As a rule of thumb, we ensured it covered at least one-fourth of the entire image. Thus, working distance is limited by the size of the calibration target.

Epipolar rectification

The calibration parameters were used to rectify image pairs for epipolar geometry (Fig. 1c,d). During this step, new projections of both images are generated such that epipolar lines coincide with scan lines (i.e. pixel lines). This reduces the following stereo correspondence search to a 1D problem (as opposed to 2D in the unrestricted case, drastically reducing computing time (see, e.g. Trucco & Verri 1998; Hartley & Zisserman 2004). At the same time, lens distortions are removed. Simple bilinear interpolation was used for resampling the rectified images, producing satisfactory results. Stereo rectification produces a distortion-free image pair of the same dimensions as the original images, with corresponding features having the same y image coordinate, and a new set of calibration parameters ($2 \times$ intrinsic, $1 \times$ extrinsic). These parameters are valid for the virtual cameras used to obtain the new projections. The virtual cameras have parallel optical axes ('standard camera configuration').

Colour segmentation of foliage

Oftentimes, the green colour of plants can be used to discard the background. Because segmentation for green leaves is difficult to perform in the RGB (R : red, G : green, B : blue) colour space, the stereo image pair was transformed into the HSV (H : hue, S : saturation, V : colour brightness value) colour space. Next, a three-channel thresholding was applied to remove all but the green plant pixels. For each channel, only those pixels were accepted whose H , S and V values were all within configurable bounds. Bounds (thresholds) were set to $\min = 49^\circ$, $\max = 169^\circ$ for H ; $\min = 19.6\%$, $\max = 100\%$ for S ; and $\min = 13.7\%$,

$\max = 100\%$ for V , indoors and outdoors. Once selected by manual inspection, the bounds resulted in good segmentation of green plant material from the background and usually did not have to be adjusted except for V in very low illumination. We tested the segmentation approach using the same thresholds on broad-leaved plants other than soybean, with similar success. Lee (1998) proposed a more elaborate HSV Bayesian classification approach which enables separation into different species; however, for the experiments presented here, our simple scheme suffices. To remove jagged object borders, the segmentation mask obtained in the previous step was subjected to binary morphological opening/closing. This was done to improve the quality of visualization.

Stereo matching

Stereo matching is a fundamental problem of computer vision (see, e.g. Brown, Burschka & Hager 2003), for a review). For binocular stereo vision, it amounts to finding corresponding pixels between two images taken from different viewpoints. The difference in image coordinates between corresponding points (typically in the x direction) is called disparity. Knowing the calibration parameters of the stereo rig and pixel disparities, a 3D reconstruction of the scene can be achieved.

We used an area-based (correlation-based) stereo algorithm. Firstly, the so-called disparity space was calculated, that is, the correlation criterion $C(x, y, d)$ for a range of potential disparities. This was achieved by comparing a fixed window in one image to a shifting window in the second. The extremum of the cost function was assumed to denote the actual disparity (see, e.g. Trucco & Verri 1998). We tested several combinations of stereo algorithms and came to the conclusion that the procedure described here is well suited for plant canopies. The correlation criterion C_2 (Faugeras *et al.* 1993) was used. Given the greyscale images as functions of the x and y image coordinates, $I_1(x, y)$ and $I_2(x, y)$, C_2 is calculated as

$$C_2(x, y, d) = \frac{\sum_{i,j} I_1(x+i, y+j) \times I_2(x+d+i, y+j)}{\sqrt{\sum_{i,j} I_1(x+i, y+j)^2} \times \sqrt{\sum_{i,j} I_2(x+d+i, y+j)^2}} \quad (1)$$

where the correlation window is given by $(2n+1) \times (2m+1)$, i and j are window pixel indices (i runs from $-n$ to n and j runs from $-m$ to m), and d denotes horizontal disparity. Note that vertical disparity is assumed to be zero, as is appropriate, because the algorithm operates on rectified images. The true disparity is assumed where C_2 is maximal. We used a rectangular correlation window of 17×7 pixels for all experiments.

Matching is robust against changes in illumination due to the fact that C_2 is invariant to changes in image intensity of the form $I' = aI_1$ and $I_2 = bI_2$. To increase the resolution of depth estimation, that is, to achieve sub-pixel accuracy, a three-point parabola fit was applied to the extremum of the correlation function in disparity space (Fusiello, Roberto

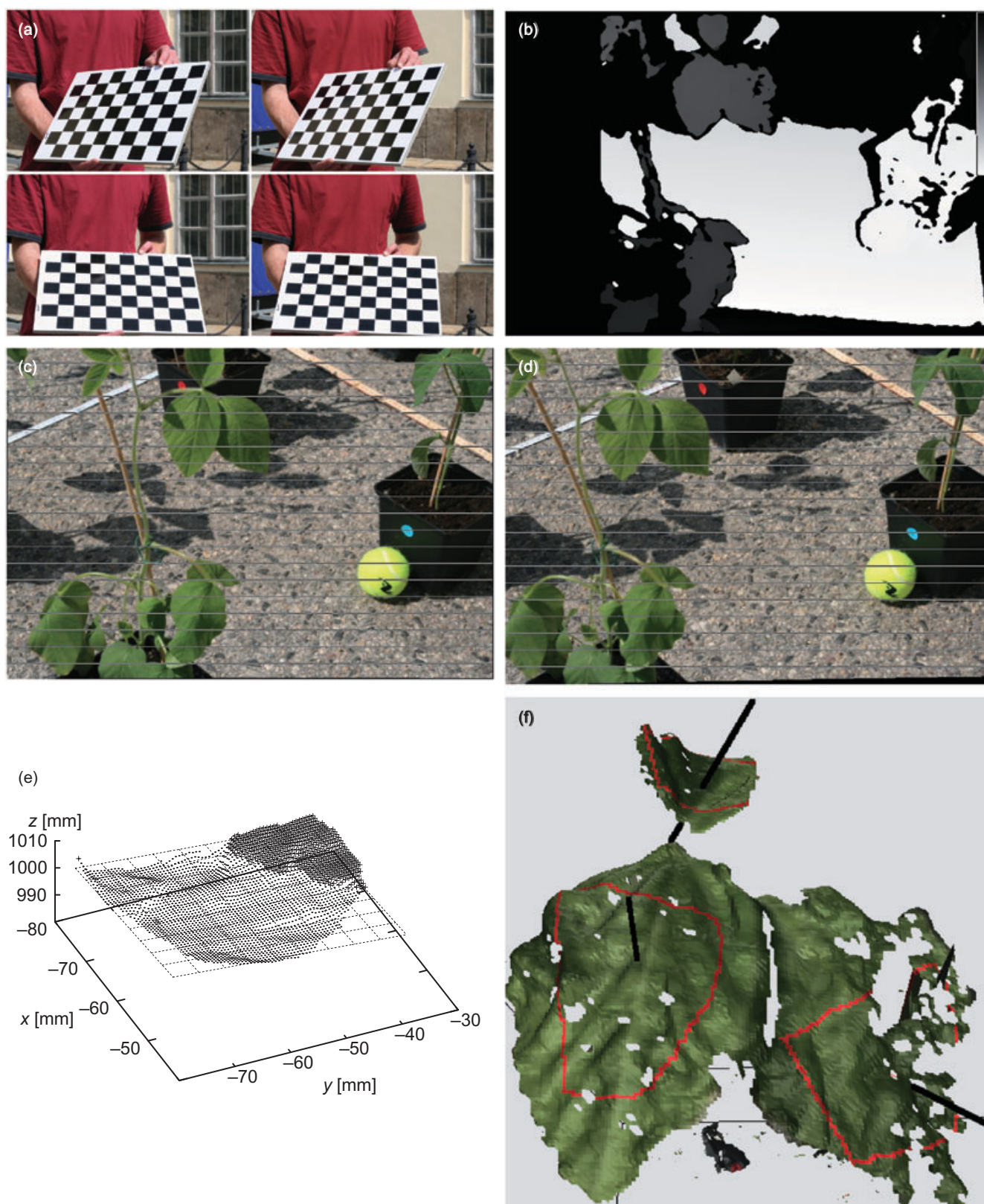


Figure 1. Stereo set-up and procedure to derive three-dimensional (3D) surface of leaves in natural canopies. (a) Chessboard calibration pattern. (b) Disparity map. Scale bar indicates disparity range from -35 (black) to $+99$ pixels (white). Pixels for which the left-right consistency check failed are black. (c,d) Stereo image pair after epipolar rectification. Corresponding features have approx. the same y image coordinate in both images. (e) Plane fitted to ROI using RANSAC algorithm. Thin points denote inliers (distance to plane < 1 SD); thick points denote outliers. Triangle denotes RANSAC sample with highest proportion of inliers. (f) 3D reconstruction of a soybean leaf consisting of three leaflets. Black lines: normal vectors to fitted plane; red contour: projected ROI used for plane fitting.

& Trucco 1997). Incorrect disparity estimates (e.g. due to matching ambiguities or occlusions) were largely eliminated by applying a left-right consistency check (Fua 1991; Faugeras *et al.* 1993): only correspondences that were consistently found matching left-to-right and right-to-left were accepted. For efficiency, both disparity searches were performed in the same disparity space (Mühlmann *et al.* 2002). The result of stereo matching is a disparity image (Fig. 1b).

3D reconstruction

To calculate Euclidean coordinates from known disparities, stereo triangulation was performed. In the general case of arbitrarily oriented cameras, 3D reconstruction amounts to solving a linear system of equations. However, because we used rectified images, the reconstruction problem reduces to the special case $Z = fbd^{-1}$ where Z denotes depth, f denotes focal length, b is the stereo baseline and d is the disparity (Trucco & Verri 1998). The remaining components of the Euclidean coordinates are calculated as $X = xZf^{-1}$ and $Y = yZf^{-1}$ where x and y are the image coordinates of the left point of a corresponding pair of rays.

Leaf inclination angles

Guided by the input images, ROIs corresponding to single leaflets were selected interactively such that edges of roughly 10 pixels (at 20% resolution) were excluded, preventing border effects due to occlusions and fixed correlation window shape. Each ROI consisted of a set of 3D points belonging to a single leaf or a part of it.

A planar surface model was used to extract leaflet inclination angles. This model was fitted to the 3D point set encompassed by each individual ROI (Fig. 1f). To cope with noise, false matches and filter artefacts, a robust algorithm was needed. Plane fitting was done in a two-step approach. (1) A RANSAC robust fit (Fischler & Bolles 1981) was performed to remove outliers. The basic assumption of RANSAC is that data are composed of *inliers*, that is, data points that can be explained by the given model, and *outliers*, that is, data points not fitting the model. RANSAC operates by repeatedly drawing a minimal set of data points (three 3D points in the case of a plane) and determining the number of inliers according to some distance criterion (± 1 SD in our case). The data set corresponding to the largest number of inliers is then chosen for further refinement of the fit. (2) The refined plane fit was done by analysing the covariance matrix \mathbf{J} of the outlier-free point cloud. The eigenvector with respect to the smallest eigenvalue of \mathbf{J} corresponds to the normal vector of the plane, while the remaining eigenvectors span the plane. The variance of point distances to the fitted plane (i.e. the model error) was used to accept or reject ROI.

We were interested in leaflet inclination angles (zenith angles), φ . To determine φ , we used a horizontal reference plane. This could be an artificial target as in the leaf movement and the closed canopy experiments, or simply the ground, as in the drought stress experiment. The leaflet

inclination, φ , corresponding to the dihedral angle between two planes $a_1X + b_1Y + c_1Z + d_1 = 0$ and $a_2X + b_2Y + c_2Z + d_2 = 0$, that is, between the leaflet and the reference plane is given by

$$\varphi = \arccos \hat{\mathbf{n}}_1 \cdot \hat{\mathbf{n}}_2 \quad (2)$$

$$= \arccos \frac{a_1b_1 + a_2b_2 + a_3b_3}{\sqrt{a_1^2 + b_1^2 + c_1^2} \sqrt{a_2^2 + b_2^2 + c_2^2}} \quad (3)$$

where $\hat{\mathbf{n}}_1$ and $\hat{\mathbf{n}}_2$ are the normal vectors to the planes.

Automatic segmentation of leaf regions

In order to cope with a larger amount of leaves and images, an automatic segmentation technique was developed. This technique yields planar regions suitable for measuring leaf angles; it consists of the following steps. (1) Input images were subjected to a graph-based segmentation algorithm (Felzenszwalb & Huttenlocher 2004). Using appropriate parameters, this algorithm yields segments corresponding to entire leaves or leaf fragments, typically cut along the midvein (Fig. 2). The algorithm, while being computationally efficient, is aimed to capture conceptually important global regions of the image and is thus well suited for the task at hand. (2) Planes were fitted to the 3D point set of each segment, using only those regions classified as leaf material by *HSV* thresholding. The zenith angle φ and the azimuth angle ψ were computed for each segment with respect to a reference plane and compass north. (3) The area A_{3D} was computed on the 3D surface patch of each segment. (4) The only segments that were kept were those for which several statistical properties were within empirically determined thresholds (see legend of Fig. 2). (5) Using A_{3D} as weights, weighted histograms were computed for φ and ψ at each sampled point in time.

Accuracy

To determine the accuracy of measured angles viewed from various directions and in a realistic set-up, we glued two soybean leaflets to planar surfaces. One plane acted as the reference. The other plane was inclined forward or backward, its inclination angle adjusted by means of a water-level inclinometer (precision approx. 1°). We set the inclination angle to various values and measured the dihedral angle between the two planes (Fig. 3). We used real leaflets because the quality of reconstruction depends on the texture of the scene. Except for very steep viewing angles, our system was able to produce a dense disparity map for the entire leaflet surface. The slope of the linear regression, $m = 1.02$ compared with 1 for the theoretical relationship $y = x$ shows that the stereo method is able to measure dihedral angles from a wide range of viewing angles. The average deviation between angles measured by stereo and reference angles was $1.9 \pm 0.3^\circ$.

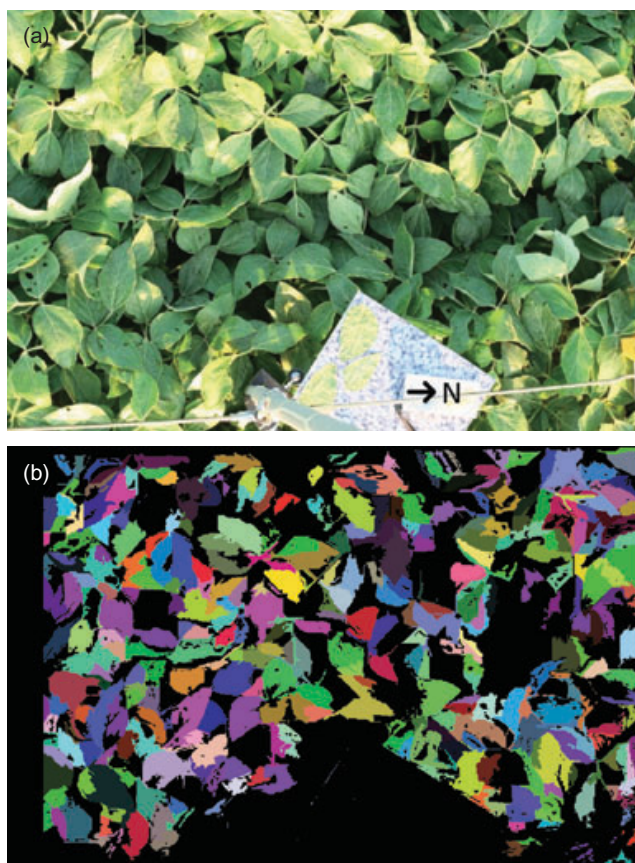


Figure 2. Automatic segmentation of leaf regions. (a) Left input image (0646 h) with reference plane and compass at bottom. A constant mask was used to discard segments on the reference plane. (b) Label image resulting from segmentation. Segmentation parameters: $\sigma = 0.5$, $k = 100$, $\text{min} = 100$ (Felzenszwalb & Huttenlocher 2004). Binary masks previously obtained from *HSV* colour segmentation and from applying the left-right consistency check were both applied to the label image to exclude invalid regions (black). Only such segments were considered for determining the zenith leaf angle distribution for which all of the following criteria held true: (1) variance $\sigma^2 < 1 \text{ mm}^2$; (2) the 3D surface area A_{3D} was between 200 and 5000 mm^2 ; (3) $\varphi \leq 80^\circ$; (4) the segment size was between 100 and 1000 pixels (image resolution: 691×461 pixels); (5) at least 20% of the segment pixels were inliers according to the RANSAC fit. Only segments with $20^\circ \leq \varphi \leq 70^\circ$ were used to estimate azimuth angles.

CASE STUDIES

Experiments with potted plants

Soybean plants (*Glycine max* L. Merr. Erin) were cultivated in a greenhouse of the Research Centre Jülich, Germany, at 26°C at daytime and 18°C at night, with 16:8 light : dark regime. Relative humidity was 45% at daytime and higher (unregulated) at night. The plants were 18 d old when the experiments were performed. Drought stress-treatment plants were cultivated like the control plants for 11 d, then received no more water for the remaining 7 d. To increase drought stress, these plants were kept at 30% relative humidity for the last 2 d before the experiments began.

Both control and drought-stressed plants were exposed to direct sunlight and moderate wind for about 5 h immediately prior to the measurements.

Closed-canopy experiment

Images were taken on 30 July 2006 in a 16 ha soybean (*G. max*) field at the SoyFACE facility in Champaign, IL, USA ($40^\circ 02' \text{N}$, $88^\circ 14' \text{W}$, 228 m a.s.l.); see, for example Rogers *et al.* (2004) for a detailed description. The same $1.20 \times 0.80 \text{ m}$ canopy patch within a field grown at ambient gas concentrations was imaged every 2 min to record a full diurnal course. The diurnal course was repeated, but only one time series is shown.

Nocturnal leaf movement

Three soybean plants were arranged in a laboratory at a distance of approx. 2 m from the stereo rig. Using a control program developed by the authors, the acquisition system was set up to take a stereo image pair every 10 min to generate a times series. The time series was acquired between 0020 and 0920 h. The built-in camera flashes were used to illuminate the scene. For each point in time, the dihedral angle between leaflet and a horizontal reference plane was determined. Leaves were droopy, being oriented down from the horizontal plane.

During night-time, the dihedral angle of a single soybean leaflet oscillated between -45° and -75° , with a period of approx. 4 h. With sunrise, oscillations became faster (period length: approx. 70 min) while exhibiting a smaller amplitude. Leaves became more horizontal, that is, remained less inclined, with the dihedral angle oscillating between -37° and -55° (Fig. 4). The phase length of the dominant oscillation decreased abruptly after sunrise, demonstrating the signalling effect of light on leaf movements. Oscillations

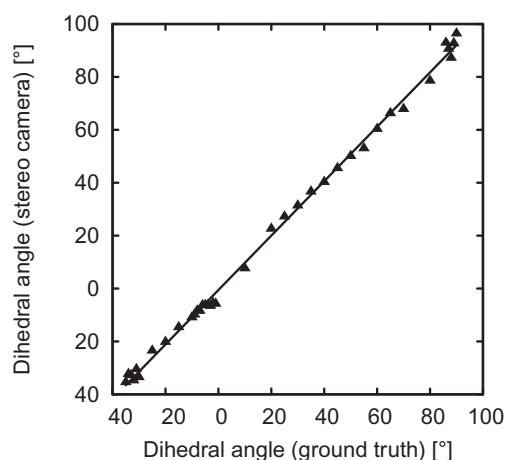


Figure 3. Accuracy of dihedral angle measurements. X-axis: reference angles obtained with water-level inclinometer. Y-axis: angles measured with stereo system. Line: linear regression ($y = 1.02x - 2.26$, $R^2 = 0.9937$). The stereo rig was directed 57° downward from the horizontal plane.

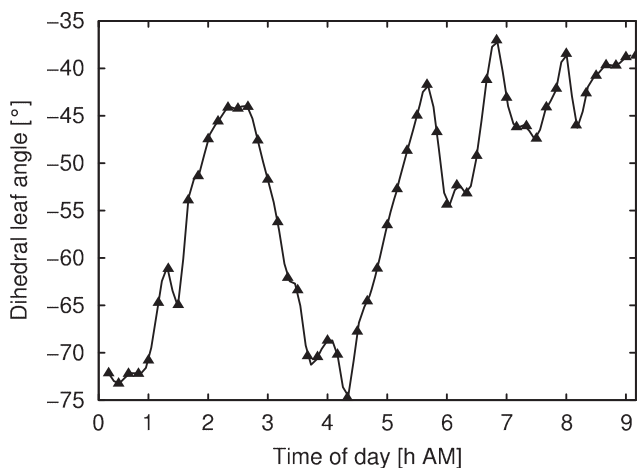


Figure 4. Leaf movement as quantified by stereo approach. Dihedral leaflet angle for one selected leaflet versus time. The measured leaflet angle results from a superimposition of longitudinal and lateral movement of the leaf under observation. Starting time: 0020 h; end time: 0920 h. Sunrise: 0554 h.

were obviously caused by several motion components, as was also observable in the image sequences. In addition, the stem, although fixed to a pole, showed slight circumnutations also affecting the angle of the single leaflet.

Leaf inclination during drought

Two batches of soybean plants, well watered and drought stressed, with nine replicates each, were set up in an alternating pattern in direct sunlight. Within 15 min, 18 stereo images were taken from arbitrary directions, from a distance between 2 and 4 m and an inclination of about 20° to 70°. No special care was taken to adjust the camera pose. Viewing directions were roughly chosen to cover the entire stand and to avoid excessive overlap. Image pairs were taken from the drought-stressed and well-watered soybean plants to diagnose differences in leaf inclination. 211 ROIs were marked in the images and classified by treatment (drought-stressed or control). Zenith angle distributions of drought-stressed and well-watered plants are shown in Fig. 5. Leaves of both treatments pointed down and were moved by slight wind, rendering a visual separation of the two treatments difficult. The stereo system, however, was capable of detecting the slight differences in the canopy. The median zenith leaflet angle for well-watered plants was 65.5° as opposed to 75.0° for drought-stressed plants. A two-sided Kolmogorov–Smirnov (KS) test revealed that the two distributions differ with high significance ($D = 0.27$, $P = 0.007$). The drought-stressed plants clearly had steeper inclined leaflets as opposed to the well-watered plants.

Diurnal course of leaf angle distribution in a closed, natural canopy

To obtain a time series of canopy structure changes, stereo images of the same plot of a soybean canopy were taken between 0615 and 1915 h CDT in 2 min intervals. The stereo

rig was mounted 4 m above the ground, pointing vertically downwards. Zenith and azimuth leaf angle distributions were determined for each sampled point in time by using the automatic segmentation technique described earlier (see also Fig. 2).

Figure 6a,b illustrates the temporal dynamics of leaf inclination. Starting out from 37°, the MTA rises by about 3° h⁻¹ until it reaches its peak of 58° at solar noon (1300 h). After solar noon, the MTA decreases again, but only at about 1° h⁻¹ to a final value of 50° at 1900 h. Superimposed on the dominant frequency, there are faster oscillations which are mostly due to leaf movement caused by wind. These oscillations are effectively suppressed by applying a 1 h running-average filter. Figure 6a shows that the zenith angle distribution is broader before noon, but transiently gets very narrow around solar noon. First results quantifying the circular mean azimuth angle of leaves (Batschelet 1982) indicated that the compass orientation of leaves was dominated by the local shape of the canopy due to planting rows (data not shown).

In our case study, individual measurements are affected to a certain degree by noise due to wind gusts or drastic illumination changes. However, by employing a simple smoothing filter, fluctuations on a diurnal scale may still be recovered. Moreover, if wind shields are used, the major source of noise can be alleviated. Other fluctuations on a scale of several minutes probably result from the limited size of the observed canopy patch. Such effects could be minimized by pooling observations from different patches.

DISCUSSION

We introduced a stereo system for measuring structural parameters of plant canopies and highlighted three possible

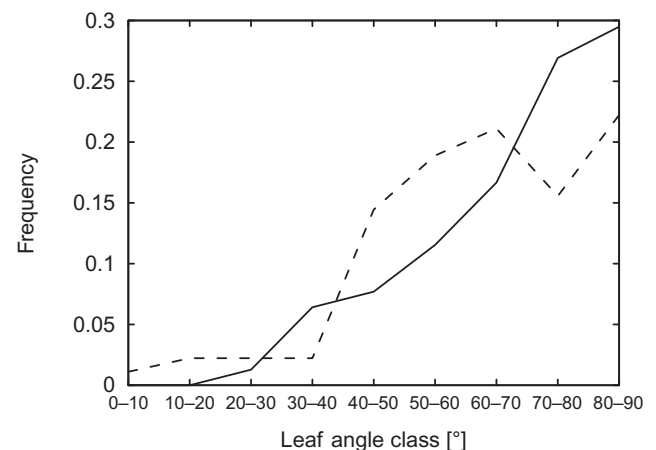


Figure 5. Soybean drought stress leaflet zenith angle distribution. Dotted line: control; solid line: drought-stressed. A zenith angle of 0° corresponds to a horizontal leaf. All observed leaflets were between 0° and 90°. In 18 images, zenith angles of 100 control plant leaflets and 111 leaflets on drought-stressed plants were measured. After thresholding by variance ($\sigma^2 < 50 \text{ mm}^2$), 90 control ROIs and 78 drought-stressed ROIs remained. Inclination angles are given for downward-pointing leaflets.

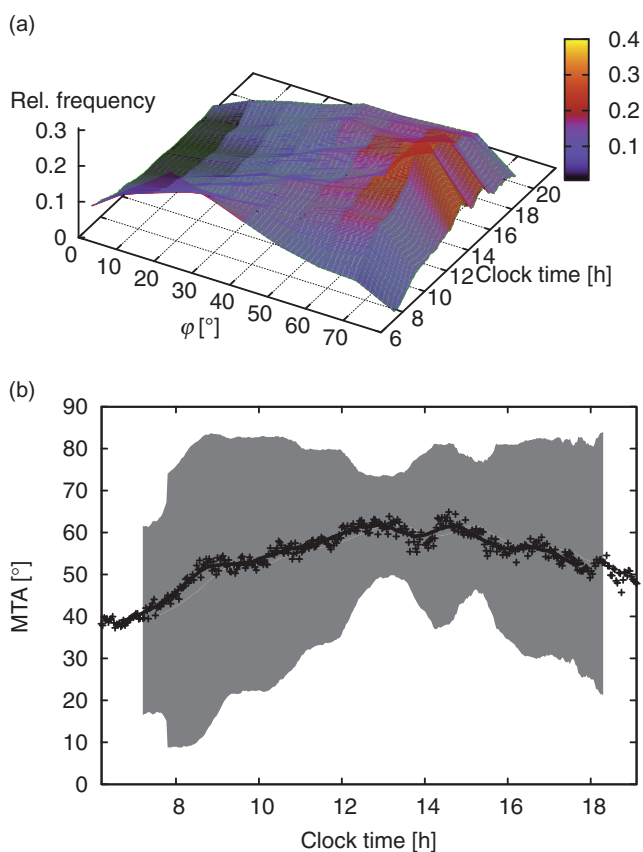


Figure 6. Temporal dynamics of the leaf angle distribution of a 1.20 m × 0.80 m canopy patch. Images were taken in 2 min intervals on 30 July 2006 from 0615 to 1915 h (local time, CDT; solar noon at 1300 h). (a) Time series of normalized zenith angle (φ) distribution (bin width: 10°; smoothed with a 1 h running average filter). (b) Time series of MTA. Line: 1 h running average; grey area: \pm FWHM of leaf angle distribution.

applications of our approach. Our simple stereo system built from commercially available components can provide a useful tool for obtaining quantitative data on canopy structure, including dynamic and short-term changes. The accuracy measurements (Fig. 3) suggest that our stereo approach is capable of repeatable leaf angle measurements from various directions. However, very steeply inclined leaves are inaccessible because their projected leaf area is too small for stereo matching. The inclination angle time series (Fig. 4) obtained from the leaf movement experiment indicates that angle measurements with our stereo system are able to resolve short-term changes in leaf inclination. The expressiveness of such experiments could be increased by determining the principal orientations of a leaf or leaflet (leaf normal, midvein and its transverse) separately rather than the ‘all-inclusive’ dihedral angle, allowing the monitoring of the dynamics of different motion components simultaneously (Herbert 1983). Our method can readily be applied under field conditions and is robust against wind movements and variations in illumination. It can thus readily deliver structural parameters (e.g. dihedral angle of single leaves, leaf angle distribution, time constants of leaf

movements) to scale leaf level processes to the canopy. We demonstrated the measurement of temporal dynamics of zenith angle distribution in a closed canopy (Fig. 6). Employing an automatic segmentation technique, leaf angle information can be extracted from a large amount of stereo images in a consistent fashion.

Leaves within natural canopies are constantly changing orientation because of endogenous mechanisms (Fig. 4) and external factors such as water availability, (Fig. 5) and direct methods to quantify these structural changes are necessary. Structural changes in canopies were recently highlighted to have the potential to increase photosynthetic efficiency of crops (Long *et al.* 2006). An optimized canopy architecture could increase crop yield considerably, provided that excessive light would be transmitted more efficiently into lower layers of the canopy (Humphries & Long 1995). Within limits, canopy structure can be ‘designed’ using classic breeding techniques or genetic modification (Reynolds, van Ginkel & Ribaut 2000); better knowledge of canopy structure could further enhance such efforts. Our approach could also be applied on the level of single plants and for automated mutant screening, revealing, for example, mutations that affect endogenous plant movement, or static leaf orientation. Structural parameters obtained by optical remote sensing are also important to parameterize vegetation-atmosphere transfer models. Three-dimensional canopy structure greatly influences radiation and turbulent energy transfer and directly measured input parameters are identified as important factors to increase reliability of current models (Yang & Friedl 2003).

ACKNOWLEDGMENTS

We thank J. Stroka for helping with data analysis and B. Uhlig for providing soybean plants. The authors are also grateful to L. Nedbal (University of South Bohemia, Nové Hradý, Czech Republic) and his group for their hospitality and for providing their laboratory and help with experiments, and to A. Walter for fruitful discussions and helpful comments. We acknowledge financial support by Forschungszentrum Jülich in the Helmholtz Society. This paper has been partially funded by DFG SPP1114 (SCHA 927/1–3) and by Deutscher Akademischer Austauschdienst DAAD (grant PPP D/05/50496). B. Biskup also acknowledges support of his PhD thesis by the Heinrich-Heine University of Düsseldorf, Germany. We thank T.A. Mies, E.A. Ainsworth and S.P. Long for assistance at SoyFACE. SoyFACE received funding by the Illinois Council for Food and Agricultural Research, Archer Daniels Midland Company and USDA/ARS.

REFERENCES

- Andersen H.J., Reng L. & Kirk K. (2005) Geometric plant properties by relaxed stereo vision using simulated annealing. *Computers and Electronics in Agriculture* **49**, 219–232.
- Batschelet E. (1982) *Circular Statistics in Biology*. Academic Press, London, England.

- Brown D.C. (1966) Decentering distortion of lenses. *Photometric Engineering* **32**, 444–462.
- Brown D.C. (1971) Lens distortion for close-range photogrammetry. *Photometric Engineering* **37**, 855–866.
- Brown M.Z., Burschka D. & Hager G.D. (2003) Advances in computational stereo. *IEEE Transactions on Pattern Analysis and Machine Intelligence* **25**, 993–1008.
- Campbell G.S. & Norman J.M. (1989) The description and measurement of plant canopy structure. In *Plant Canopies: Their Growth, Form, and Function* (eds G. Russell, B. Marshall & P.G. Jarvis), pp. 1–19. Cambridge University Press, Cambridge, UK.
- Chen J.M. & Cihlar J. (1995) Plant canopy gap-size analysis theory for improving optical measurements of leaf-area index. *Applied Optics* **34**, 6211–6222.
- Conrady A. (1919) Decentering lens systems. *Monthly Notices of the Royal Astronomical Society* **79**, 384–390.
- Daughtry C.S. (1990) Direct measurements of canopy structure. *Remote Sensing Reviews* **5**, 45–60.
- Deckmyn G., Nijs I. & Ceulemans R. (2000) A simple method to determine leaf angles of grass species. *Journal of Experimental Botany* **51**, 1467–1470.
- Faugeras O., Hotz B., Mathieu H., et al. (1993) Real time correlation based stereo: algorithm, implementations and applications. Technical Report RR-2013 INRIA.
- Felzenszwalb P.F. & Huttenlocher D.P. (2004) Efficient graph-based image segmentation. *International Journal of Computer Vision* **59**, 167–181.
- Fischler M.A. & Bolles R.C. (1981) Random sample consensus: a paradigm for model fitting with applications to image analysis and automated cartography. *Communications of the ACM* **24**, 381–395.
- Fua P. (1991) Combining stereo and monocular information to compute dense depth maps that preserve depth discontinuities. *12th International Joint Conferences on Artificial Intelligence*, Sydney, August, pp. 1292–1298.
- Fusiello A., Roberto V. & Trucco E. (1997) Efficient stereo with multiple windowing. In *Proceedings of the IEEE Conference on Computer Vision and Pattern Recognition (CVPR '97)*, pp. 858–863. IEEE Computer Society Press, Washington, DC, USA.
- Hartley R.I. & Zisserman A. (2004) *Multiple View Geometry in Computer Vision*. Cambridge University Press, Cambridge, UK.
- Herbert T.J. (1983) The influence of axial rotation upon reception of solar radiation by plant leaves. *Journal of Theoretical Biology* **105**, 603–618.
- Herbert T.J. (1995) Stereo photogrammetry of plant leaf angles. *Photogrammetric Engineering and Remote Sensing* **61**, 89–92.
- Humphries S.W. & Long S.P. (1995) Wimovac: a software package for modelling the dynamics of plant leaf and canopy photosynthesis. *Computer Applications in the Biosciences* **11**, 361–371.
- Ivanov N., Boissard P., Chapron M. & Andrieu B. (1995) Computer stereo plotting for 3-D reconstruction of a plant canopy. *Agricultural and Forest Meteorology* **75**, 85–102.
- Lang A.R.G. (1973) Leaf orientation of a cotton plant. *Agricultural Meteorology* **11**, 37–51.
- Lang A.R.G. (1990) An instrument for measuring canopy structure. *Remote Sensing Reviews* **5**, 61–76.
- Lee W.S. (1998) *Robotic Weed Control System for Tomatos*. PhD thesis, University of California/Davis, Davis, CA, USA.
- Lefsky M.A., Cohen W.B., Acker S.A., Parker G.G., Spies T.A. & Harding D. (1999) Lidar remote sensing of the canopy structure and biophysical properties of Douglas-fir western hemlock forests. *Remote Sensing of Environment* **70**, 339–361.
- Long S.P., Zhu X.-G., Naidu S.L. & Ort D.R. (2006) Can improvement in photosynthesis increase crop yield? *Plant, Cell & Environment* **29**, 315–330.
- Mühlmann K., Maier D., Hesser J. & Männer R. (2002) Calculating dense disparity maps from colour stereo images, an efficient implementation. *International Journal of Computer Vision* **47**, 79–88.
- Nielsen M., Andersen H.J. & Granum E.I. (2005a). Comparative study of disparity estimations with multi-camera configurations in relation to descriptive parameters of complex biological objects. In *Proceedings of the ISPRS Workshop BenCOS 2005: Towards Benchmarking Automated Calibration, Orientation and Surface Reconstruction from Images, held in conjunction with ICCV 2005* (ed. O. Hellwich, I. Niini, C. Ressel, V. Rodehorst, D. Scharstein & P. Sturm) Vol. XXXVI, pp. 63–68. Beijing, China. International Society for Photogrammetry and Remote Sensing ISPRS Working Groups – WG III/1 Automatic Calibration and Orientation of Optical Cameras – WG III/2 Surface Reconstruction, Silver Spring, MD, USA.
- Nielsen M., Andersen H.J., Slaughter D.C. & Granum E.I. (2005b). Ground truth evaluation of 3D computer vision on non-rigid biological structures. In *Precision Agriculture '05* (ed. J. Stafford), pp. 549–556. Wageningen Academic Publishers, Wageningen, the Netherlands.
- Omasa K., Qiu G.Y., Watanuki K., Yoshimi K. & Akiyama Y. (2003) Accurate estimation of forest carbon stocks by 3-D remote sensing of individual trees. *Environmental Science & Technology* **37**, 1198–1201.
- Omasa K., Hosoi F. & Konishi A. (2007) 3D LIDAR imaging for detecting and understanding plant responses and canopy structure. *Journal of Experimental Botany* **58**, 881–898.
- Parker G.G., Harding D.J. & Berger M.L. (2004) A portable LIDAR system for rapid determination of forest canopy structure. *Journal of Applied Ecology* **41**, 755–767.
- Rakocevic M., Sinoquet H., Christophe A. & Varlet-Grancher C. (2000) Assessing the geometric structure of a white clover (*Trifolium repens* L.) canopy using 3-D digitising. *Annals of Botany* **86**, 519–526.
- Reynolds P.M., van Ginkel M. & Ribaut J.-M. (2000) Avenues for genetic modification of radiation use efficiency in wheat. *Journal of Experimental Botany* **51**, 459–473.
- Rogers A., Allen J., Davey P.A., et al. (2004) Leaf photosynthesis and carbohydrate dynamics of soybeans grown throughout their life-cycle under free-air carbon dioxide enrichment. *Plant, Cell & Environment* **27**, 449–458.
- Ross J. (1981) *The Radiation Regime and Architecture of Plant Stands*. Dr. W. Junk Publishers, The Hague, the Netherlands.
- Schurr U., Walter A. & Rascher U. (2006) Functional dynamics of plant growth and photosynthesis – from steady-state to dynamics – from homogeneity to heterogeneity. *Plant, Cell & Environment* **29**, 340–352.
- Sinoquet H. & Rivet P. (1997) Measurement and visualisation of the architecture of an adult tree based on a three-dimensional digitising device. *Trees: Structure and Function* **11**, 265–270.
- Sinoquet H., Thanisawanyangkura S., Mabrouk H. & Kasemsap P. (1998) Characterization of the light environment in canopies using 3D digitising and image processing. *Annals of Botany* **82**, 203–212.
- Tanaka T., Park H. & Hattoria S. (2004) Measurement of forest canopy structure by a laser plane range-finding method: improvement of radiative resolution and examples of its application. *Agricultural and Forest Meteorology* **125**, 129–142.
- Trucco E. & Verri A. (1998) *Introductory Techniques for 3-D Computer Vision*. Prentice Hall PTR, Upper Saddle River, NJ, USA.
- Yang R.Q. & Friedl M.A. (2003) Modeling the effects of three-dimensional vegetation structure on surface radiation and

5.2 Second publication: Quantification of plant surface structures from small baseline stereo images to measure the three-dimensional surface from the leaf to the canopy scale

Status: **in press** (accepted August 29, 2008)

Biskup B., Küsters R., Scharr H., Walter A. & Rascher U. (2009) Quantification of plant surface structures from small baseline stereo images to measure the three-dimensional surface from the leaf to the canopy scale. *Nova Acta Leopoldina (in press)* **96**.

Own contribution

- Stereo measurements (with Ralf Küsters)
- Measurement of soybean canopies on different scales
- Implementation of small baseline algorithm and adaptation to different plants
- Preparation of manuscript (with co-authors)

Quantification of plant surface structures from small baseline stereo images to measure the three-dimensional surface from the leaf to the canopy scale

Bernhard Biskup*, Ralf Küsters*, Hanno Scharr*, Achim Walter* and Uwe Rascher*†

* Institute of Chemistry and Dynamics of the Geosphere ICG-III: Phytosphere,
Forschungszentrum Jülich, Stettener Forst, 52425 Jülich, Germany

† Corresponding author. E-mail: u.rascher@fz-juelich.de

Keywords: remote sensing, three-dimensional surfaces, leaf surface, canopy structure, growth.

Abbreviations: LIDAR = light detection and ranging; TLS = total least squares; PRI = Photochemical Reflectance Index

Abstract

Structural changes are one key feature of plant life and determine performance of plants in their natural environment. Shape and structure of single organs (e.g. leaves) and whole canopies constantly adjust to environmental factors. Currently only a limited number of methods are available to directly measure these structural changes under natural conditions. Here, we present and review the potential of small baseline stereo for mapping the surface of plant organs and canopies in 3 dimensions. To avoid occlusion, we suggest using a small baseline stereo approach, where images from different camera positions differ only slightly. Scaling this approach to the canopy is possible, and we mapped extended canopies of several meters diameter. On the ecosystem scale, a robotic arm was used to take mosaics of stereo images of the 40×40 m² canopy of the tropical rainforest mesocosm of Columbia University's Biosphere 2 Laboratory, an enclosed artificial ecological model system. This revealed a map of the outer canopy demonstrating the potential to give better insight into light penetration within the canopy and to provide quantitative data about the structure of the outer canopy of plant ecosystems.

Zusammenfassung

Strukturänderungen sind ein charakteristisches Merkmal pflanzlichen Lebens und haben einen maßgeblichen Einfluss auf die Leistungsfähigkeit von Pflanzen. Form und Struktur einzelner Organe (z. B. Blätter) und ganzer Kronendächer passen sich permanent ihren Umweltbedingungen an. Zur Zeit existiert nur eine begrenzte Zahl von Verfahren zur Messung der Oberflächenstruktur von Pflanzen unter natürlichen Bedingungen. In dieser Arbeit wird das Potential von Small-Baseline-Stereoverfahren zur Vermessung pflanzlicher Oberflächen und Kronendächern dar, d.h. Einzelbilder wurden von nah beieinander liegenden Positionen aufgenommen und daraus eine Tiefenkarte errechnet. Das Verfahren ist auch für größere Kronendächer geeignet; es wurden 3D-Modelle von Kronendächern mit mehreren Metern Durchmesser erzeugt. Auf Ökosystemskala wurden mittels eines Roboterarmes zahlreiche Stereobilder eines 40×40 m² Kronendachs des tropischen Mesokosmos im Biosphere 2 Labor (einem abgeschlossenen, künstlichen ökologischen Modellsystem der Columbia University) aufgenommen und fusioniert. Das resultierende 3D-Modell ist von großem Nutzen für die Untersuchung der Lichtdurchdringung und die Gewinnung quantitativer Daten über die Struktur des äußeren Kronendachs pflanzlicher Ökosysteme.

1. Introduction

Plants constantly adjust to changing environmental conditions. Being sessile organisms, a wealth of acclimation mechanisms affect plant structure by altering the distribution of growth of single organs such as leaves or the interplay and arrangement of their modules, which e.g. changes foliage orientation. Thus, the structure of plant canopies is highly dynamic, changing on various time scales, from minutes to seasons (for recent review see SCHURR et al. 2006). Structural changes in plants have been studied for decades and different approaches to quantify the structural parameters of plant canopies have been developed in the past (e.g. CAMPBELL and NORMAN 1989, SINOQUET and RIVET 1997, SINOQUET et al. 1998, RAKOCEVIC et al. 2000). However, most of these methods require the plant being fixed in the lab or are too time consuming (such as laser scanning methods) to account for fast changes in natural conditions (RAKOCEVIC et al. 2000 reported a time of 3-7 h needed for a 10 cm x 10 cm canopy of white clover).

On the microscopic scale, usually stereo microscopes are used together with correlation based reconstruction approaches (see e.g. LIAO et al. 1997, OMASA 2000). On the large scale, photogrammetry has established a variety of approaches to map the surface of earth in three dimensions: digital elevation models have been elaborated with enormous precision by methods such as relief displacement, shadow length analysis and aerial stereoscopic photography (see e.g. HIRSCHMÜLLER et al. 2005).

Considering this background there is surprisingly little information available on the three-dimensional structure of plant canopies and ecosystems, which pose the specific challenge of changing their shape and structure frequently. To our knowledge, there is currently no reliable field method available for reconstructing plant structure on a medium scale, i.e. from the level of single leaves (cm resolution) to canopies (a few meters). Stereo imaging methods are often hampered by the limited contrast of plant leaves and the cleft structure of plant canopies, which consist of almost 2-dimensional leaves parted by great discontinuities. These structural properties make it difficult to use standard stereo algorithms on plant canopies. Thus alternative methods were used to get information about plant ecosystems, with active radar and light detection and ranging (LIDAR) methods currently being the most frequently used.

LIDAR is used to quantify biomass and to retrieve structural information about whole forest stands for forest management (MALTAMO et al. 2005). LIDAR devices emit light onto a target and the travel time from the device to the target and back to the device is used to determine the height of an object. Because return signals are received from structures at different heights (such as canopy stories), LIDAR is capable of determining the vertical distribution of foliage. However, the top of the canopy may be hard to detect if insufficient leaf material is present (LEFSKY et al. 2002). By turning the LIDAR device or by moving it across an area, height distributions of complex surfaces, such as forest canopies being reconstructed from airplane measurements, can be obtained. In general, LIDAR provides a sparser sampling than optical approaches (BALTSAVIAS 1999). Results from LIDAR allow understanding dynamic vegetation changes which helps to improve forest management. Moreover, LIDAR vegetation data is discussed as a measure of carbon stocks in the frame of the Kyoto protocol (TURNER et al. 2003, PATENAUDE et al. 2005). Recently on the smaller spatial scale, scanning LIDAR techniques have successfully been employed to create three-dimensional (3-D) reconstructions of single broad-leaved plants (OMASA et al. 2006). Despite great technical advantages high spatial resolution results in long scanning times, which to date limits the applicability of high resolution LIDAR to laboratory experiments

During the past years it became obvious that processes well understood on the single leaf level cannot linearly be scaled up to the canopy level to understand ecosystem processes. Hence, the need was emphasized to

- (i) Monitor growth and phenotype of crops to facilitate improved management practices there. Analysis of plant reaction towards environmental stresses would allow rapid screening for optimized crop lines.
- (ii) Better understand and model foliage changes and light interception in canopies. These input parameters are necessary to increase precision of carbon models. Micrometeorological parameters have to be validated and parameterized for turbulences within plant canopies and to correctly parameterize plant mediated exchange processes in soil-vegetation-atmosphere-transfer and mechanistic ecosystem models.
- (iii) Get first insight into structural changes of the outer canopy as a response to environmental factors. Structural changes are an inherent feature of plants to adjust to different environments and the importance of structural changes as a trait of physiological acclimation and hence survival probability are just about to be realized (NIINEMETS et al. 2005).
- (iv) Remote sensing will help to better understand the radiative transfer processes within a canopy with the help of 3-D structural information, which will allow retrieving and correcting for effects related to bidirectional reflectance distribution functions (BRDF): due to their complex structure, leaf reflectance commonly depends both on the incidence angle of the sun and the viewing angle. (BARTON and NORTH 2001).

With this communication we address this gap in knowledge and present a proof-of-concept evaluation on 3-D imaging of plant surfaces from the single leaf to the canopy. We use a small baseline stereo approach, meaning a stereo reconstruction approach where the camera positions differ only little in comparison with the distance to the object. The method can be established with comparably small financial investment. Texture of plant surfaces is often sufficient for this approach and images of leaves and small canopies can often directly be used for 3-D reconstruction. However, it has to be pointed out that some plant organs, such as leaves of certain species may have to be pretreated for texture enhancement (e.g. by applying spray markers or illuminating with structured light). On the canopy scale, however, single leaves provide enough texture to calculate distance as long as the camera system provides sufficient spatial resolution.

2. Small baseline approach to quantify three-dimensional surfaces

2.1 Background

Stereo imaging is a way to measure 3-D surface structure non-destructively. There is a wide variety of 2-camera stereo image reconstruction schemes (see SCHARSTEIN and SZELISKI 2002 for a recent overview and performance comparison; also see BROWN et al., 2003). The basic idea of stereo reconstruction is to find positions in the acquired images corresponding to the same surface point (the so-called correspondence problem) and triangulate its depth using the known camera geometry. Camera geometry can be determined using freely available calibration tools (see e.g. http://www.vision.caltech.edu/bouguetj/calib_doc/index.html). Due to this work it is rather straightforward to calibrate single cameras for their intrinsic parameters as well as 2 cameras with respect to their relative positions and orientations (extrinsic parameters). The major remaining problem is to solve the correspondence problem

for as many points as possible. Point or feature based approaches look for distinct image structures like corners or junctions that can be detected reliably in both images. Discriminative features (see e.g. SHI and TOMASI 1994) can be matched even if their positions are far apart from each other in the two images. While these features deliver highly accurate depth estimates there are only few of them in an image and the reconstruction is usually too sparse for a full surface reconstruction. Area or correlation based approaches search for similar patches in both images. As for features their positions are also allowed to be separated considerably. Thus, large position changes due to large distances between the two cameras, i.e. wide baseline stereo, can be handled. Unfortunately, using correlation, patch positions can only be determined with pixel accuracy (i.e. discrete depth steps) leading to staircase-like depth reconstructions unless additional subpixel estimations are performed. Among the most promising approaches, even though not yet listed on the Middlebury web page (experimental comparison of stereo algorithms, <http://cat.middlebury.edu/stereo/>; see SCHARSTEIN and SZELISKI 2002), are optical flow based methods (SLESAREVA et al. 2005). They benefit from the tremendous accuracy increases in optical flow estimation achieved in the last decade (PAPENBERG et al. 2006). Originally designed to measure motion in temporal image sequences, they also solve the correspondence problem. Using optimized numerical differentiation schemes, even higher accuracy can be achieved when more than 2 images are used (SCHARR 2005) due to lower systematic errors. As explained in more detail below, the approach proposed in the current paper uses the optical flow assumption on usually 3-5 images acquired by a single camera shifted via a moving stage, together with a local total least squares estimation scheme. This approach thus benefits from the high accuracy of multiple-image optical flow without the need for elaborate camera calibration: internal parameters are fixed, and external parameters are known from the motion of the moving stage ('hardware calibration').

2.2 *Experimental set-up*

Generally the experimental set-up is an advancement of the 2-D growth set-up (see WALTER and SCHURR 2005), adding the additional dimension with the moving stage. Multi-camera images were acquired using a standard 640x480, black/white CCD video camera (XC-75, Sony, Tokyo, Japan). The relative spectral response of the camera ranged from 400 nm (0.5) to 1000 nm, reaching its maximum (1) at 500 nm (Sony). Images were acquired according to the near-baseline approach (see e.g. HARTLEY and ZISSERMAN, 2004) with a small parallel shift (the so-called stereo baseline) of the camera position to the distance of the object (parallel shift : distance to object = 1 : 100). For small objects such as leaves, this resulted in a parallel shift of a few millimeters only, prohibiting the use of separate cameras. We thus used a computer controlled moving stage (VTM80, OWIS, Stauffen, Germany) allowing high accuracy camera movements (repetition error < 1 μ m) via a step motor. Images could be acquired within a few seconds, which is necessary to ensure that the object does not move during the measurement. If fast motions e.g. due to wind are an issue, multiple synchronized cameras should be used instead of a single one on a moving stage (BISKUP et al. 2007). However, with two cameras, a near-baseline setup can only be achieved when the working distance is sufficiently high, depending on the size of the camera bodies. To compensate for noise of the CCD chip, 5-20 images were averaged with a frame rate of 25Hz.

Physiological performance and structure of plants adapt to environmental conditions and e.g. leaves move according to direction and intensity of light. Thus, measurements of plant surfaces and structure often involve natural conditions with day/night changes of light or fluctuating light conditions that are common in the field (RASCHER & NEDBAL 2006). This may pose special challenge for time series of optical flow estimates for which measuring light

conditions have to be kept constant. For laboratory measurements (Fig 1 and 2) we illuminated the plants with two light sources, (i) photosynthetic active light ($\lambda < 800$ nm) and (ii) infrared (IR) LED panel ($\lambda = 940$ nm; Conrad Elektronik, Hirschau, Germany). An IR long-pass filter ($\lambda > 940$ nm; Schott, Mainz, Germany) was used with the camera lens. This set-up allows separation of surface measurements under constant illumination in the near infrared, which is physiologically not effective for plants, and changes in photosynthetically active illumination, which is necessary to apply e.g. day/night cycles.

By restricting the imaged spectrum to a narrow band and by applying artificial illumination, the influence of variations in brightness of natural illumination was reduced. This is especially important when acquiring image sequences for growth measurements (WALTER and SCHURR 2005). However, natural intensity variations during acquisition of one image set was consistently low and thus did not cause problems with optical flow estimation. Long-term intensity variations can be allowed for by explicit modeling (HAUSSECKER and FLEET 2001, SCHUCHERT and SCHARR, 2007).

2.3 Algorithm

Optical flow is a concept for measuring motion in image sequences. The assumption used to do this is that intensity values of surface elements projected onto the camera sensor do not change (much) from one image to the next – the so-called brightness constancy assumption. Temporal brightness changes at a given pixel position are assumed to arise from motion of imaged objects, or from camera motion. Interpreting the acquired image sequence as a continuous spatio-temporal volume, allows for the calculation of derivatives in this data set. For each point, the spatio-temporal direction in which intensities change least is the direction where the intensity point is assumed to have moved. Such moving intensity point produces a linear structure of constant brightness in the spatio-temporal volume if moving at constant velocity, or a bent structure if it accelerates or decelerates. Fulfilling the brightness constancy assumption means formally that the total derivative of the acquired intensity I has to be zero or $dI(x,y,t)/dt = 0$, where x , y , and t denote the spatial and temporal image (pixel) coordinates. Applying chain rule we get

$$\frac{\partial I}{\partial x} \frac{dx}{dt} + \frac{\partial I}{\partial y} \frac{dy}{dt} + \frac{\partial I}{\partial t} = 0 \quad (1)$$

The partial derivatives of intensity I are calculated directly from the image data using suitable convolution kernels (derivative filters; cmp. SCHARR 2005). The remaining total derivatives of the spatial coordinates are the sought-for components of the displacement vector $\mathbf{u} = (u_x, u_y) = (dx/dt, dy/dt)$. They are calculated via the so-called structure tensor technique (BIGÜN and GRANLUND 1987, HAUSSECKER and FLEET 2001), a local total least squares (TLS) estimator. The TLS data modeling technique (also termed orthogonal regression) bears the advantage over ordinary least squares in that it assumes observational errors in both the dependent and the independent variables, which is more appropriate.

In order to relate multi-image optical flow with surface reconstruction, we need to know how a surface point is projected into an image and how this projected position changes with time, i.e. camera position, in the acquired sequence. Using a high-quality, low-distortion lens, or

assuming an internally calibrated camera, we can correct for optical distortions, and are allowed to use a simple pinhole camera model. The only parameter varied from image to image is the horizontal camera position $X_c=V_x t$ where t is the time in the image sequence or, better, the image index and V_x is the image to image camera position distance. A 3-D surface point $(X,Y,Z)^T$ is projected to an image point $(x,y)^T$ using a pinhole at $(X_c,0,0)^T$ and focal length f (i.e. distance between image sensor and pinhole) by

$$\begin{pmatrix} x \\ y \end{pmatrix} = \frac{f}{Z} \begin{pmatrix} X - V_x t \\ Y \end{pmatrix} \quad (2)$$

Consequently the image to image position change of an image point $(x,y)^T$ due to the camera shift is the derivative with respect to t or

$$\frac{dx}{dt} = -\frac{f}{Z} V_x \quad \text{and} \quad \frac{dy}{dt} = 0 \quad (3)$$

We see that the y component u_y of the optical flow vanishes and we can calculate depth Z from its x -component u_x via $Z = -f V_x / u_x$.

2.4 Accuracy

The accuracy of the proposed method has been investigated in SCHARR (2006). Tests using data with available ground truth showed that *systematic* errors of optical flow estimation, i.e. in u_x and therefore also for depth Z , using 5 camera positions are well below 0.03 % (0.85 % for 3 positions) when no noise is present. This error can be further decreased when more images are used. This shows that the method gives very accurate results under optimal conditions. However, for less optimal conditions (e.g. noise, reflections, poorly structured surfaces), the error increases. For a signal-to-noise ratio of 0.025, which one usually gets with consumer grade cameras under challenging but still realistic light conditions, the error rises to 0.2 % (1 % for 3 cameras). This accuracy is achieved as long as the working depth interval and camera shifts are chosen such that the x -component u_x of the optical flow is in the range of 0.2 to 1 pixel and sufficient structure is present in the data. If structure information is not sufficient (so-called 'aperture problem'), or the optical flow assumption is not well fulfilled, the estimation breaks down. Fortunately, using TLS estimation, this break-down can be detected. When the aperture problem occurs, the error in the estimated disparity becomes very large. It can be calculated e.g. via local estimation of the Cramer-Rao lower bound (KAY 1993) on the error covariance matrix (NESTARES et al. 2000). When the optical flow assumption does not hold, the so-called model error becomes large. It is calculated via the residual of the numerical estimation process (HARTLEY and ZISSERMAN, 2004). The model error, as well as the lower bound on the variance of the estimated parameters, is directly linked to the variance of the noise in the data. Rejecting high error areas by thresholding model error and covariance estimate suppresses outliers reliably.

2.5 Performance

Optical-flow-based techniques tend to be more demanding in terms of computing power compared to correlation-based stereo algorithms. However, optical-flow-based techniques lend themselves to parallelization on computer clusters (e.g. KOHLBERGER et al. 2003) or massive parallelization on graphics cards, allowing real-time computation (e.g. STRZODKA and GARBE 2004). In practice, computing time is not limiting for most applications and all the case studies in this communication were processed on standard desktop computers without parallelization.

3. Surface reconstruction of single leaves and small plants

[Fig. 1 about here]

Fig. 1 shows 3-D reconstructions of *Arabidopsis thaliana* (L.) Heynh. obtained with different pre-treatments of the plant. The 3-D reconstruction of the untreated plant (Fig. 1(a,b)) shows notable depth variations and holes due to insufficient scene contrast (see also cross-section). Enhancing contrast by either spray marking the plant (Fig. 1(c,d)) or illuminating it with structured light (Fig. 1(e,f)) profoundly enhances the quality of reconstruction (compare height profiles in Fig. 1). Depending on the illumination angle used for the structured light projector, shadowed regions may occur in which no reconstruction is possible. To avoid interference with light signaling, an IR light source should be used. Another way to improve reconstruction quality is to operate at higher resolutions, at which, e.g., hairs and wrinkles in the cuticle may provide additional contrast.

[Fig. 2 about here]

For practical reasons, spray marking may be the easiest method to enhance contrast and thus we tested this straight forward method on a variety of different plant organs (Fig. 2). With all leaves and the cactus cladode tested, spray marking provided sufficient contrast for reliable 3-D surface reconstruction. Even small surface structures such as the spines on the *Opuntia* cladode were reconstructed with high accuracy (Fig. 2(a,b)). 3-D reconstruction was best when size of the marks (color dots) were comparably small, providing fine contrast on the leaf surface (see better 3-D reconstruction in Fig. 2(e,f); small dots vs. Fig. 2(c,d); large dots).

4. Surface reconstruction of a rainforest canopy

4.1 Test case: Biosphere 2 Laboratory

Encouraged by the success on the leaf and small plant level, the small baseline approach was applied to reconstruct the 3-dimensional surface of the tropical rainforest of Biosphere 2 Laboratory. The enclosed and controllable tropical rainforest mesocosm of Columbia University's Biosphere 2 Laboratory is an experimental model system which is encased in a glass and metal shell controlled for temperature, humidity, atmospheric gas composition, and precipitation (for details see LIN et al. 1999, RASCHER et al. 2004, WALTER and LAMBRECHT 2004). It was used to test the potential of the small baseline approach to reconstruct the outer surface of an extended canopy. The tropical rainforest mesocosm within Biosphere 2 Laboratory was not intended to represent any particular natural rainforest. However, its plant

species composition, leaf area index (LAI: 4-5), canopy height (15 m), and other factors (LEIGH 1999, LEIGH et al. 1999) are similar to natural rainforests. The mesocosm has a total projected area of 1940 m² and an atmospheric volume of 26,700 m³. The rainforest was planted with a mixture of some 410 species from humid rainforests from the old world and neotropics (LEIGH 1999, LEIGH et al. 1999). At the time of the measurements 110 species were remaining, composing an enclosed canopy of 15 meters height, with the highest tree (*Ceiba pentandra* L.) reaching 25 meters.

Stereo images of canopy elements of 0.4 and 2 meters diameter were acquired from the space frame of Biosphere 2 Laboratory under natural illumination (Fig. 3; Fig. 4(a,b)). Single leaves and illumination differences resulted in small scale contrast, which was further increased by a high pass Gaussian filter. The small baseline algorithm yielded good depth information for canopy patches, which were well illuminated (Fig. 3 for two representative examples). Insufficient stability was detected in dark areas, which corresponded to canopy leaves of lower canopy layers. Those dark areas were readily masked out in the depth images of the canopy (Fig. 3(b,d)).

[Fig. 3 about here]

Different distances between canopy and camera resulted in different spatial resolution for each image. Moreover, various shading effects occurred induced by the encasing steel structure or shading branches above the scene resulting in a realistic forest-plot situation in which light conditions are likely to be non homogeneous and patchy. Error classification of canopy element depth reconstruction is shown in the lower row of Fig. 4, where the black and white areas indicate patches for which depth could not be calculated, while the grey areas indicate that satisfying information was available for surface reconstruction. Overall, good results were obtained in most image regions for the 3-dimensional surface reconstruction - regardless of the size and shape of leaves within the image (see e.g. the star like leaves in Fig. 4(c)). Insufficient information for depth reconstruction was primarily obtained in image regions that were characterized by great brightness heterogeneity, induced by e.g. shading (see e.g. diagonal shades in Fig. 4a and d).

[Fig. 4 about here]

4.2 *Assembly of single canopy elements to full canopy reconstruction*

For surface reconstruction of the full rainforest canopy of Biosphere 2 Laboratory, the moving stage was mounted on a two-axis, computer controllable robot arm (model HS-310P, Vinten TSM Inc., New York, USA). This rigid computer arm allowed for precise pointing of the camera along the horizontal and vertical axis, i.e. for panning and tilting of the camera (Fig. 5(b)). The whole set-up, including a control computer, was mounted at the east wall within the space frame of the tropical rainforest mesocosm of Biosphere 2 Laboratory, 15 meters above ground, providing a good view on the major part of the rainforest canopy (Fig. 5(a)). The stereo camera set-up itself was mounted on a 1 meter pole reaching into the free air space enabling a 180° view in horizontal and vertical direction. The camera position was about at mean height of the canopy with the big *Ceiba pentandra* tree and some vegetation at a nearby hill reaching higher. The center of the rainforest canopy is bowl-shaped and thus was clearly lower than the camera stand. Because of the highly varying distance between canopy surface

and camera (3 - 40 meters), single images varied from showing a few leaves only to showing canopy elements of several meters dimension.

[Fig. 5 about here]

We used 3 parallel camera positions, each with a 5 cm parallel shift for stereo reconstruction. At all scales stereo reconstruction yielded good results. The whole canopy was imaged using 140 stereo images, taken at viewing directions with equidistant pan- and tilt-angles. Images were captured without overlap in the horizontal plane (Fig. 5(c)). With moving the camera off the horizontal plane single, images increasingly overlapped and had to be cut to their non-overlapping regions (Fig. 5(c)). 122 stereo images were finally used to reconstruct the full canopy of the tropical mesocosm.

3-D points calculated by the proposed approach were first obtained in the coordinate frame of the respective camera, i.e. a coordinate frame with origin at the camera projection center and depth direction being the viewing direction. The 3-D point coordinates were transformed into a common world coordinate frame (with the central camera at the origin, its x and y axis aligned with the world X and Y axes) using external camera parameters (rotation and translation) known from the robot position, forming the reconstructed canopy. World coordinates were calculated for pixels with high confidence values only (grey regions in Fig. 4, lower row) and used for further processing. In our case study 3.5 Million pixels yielded reliable information to calculate world coordinates. From there on two alternative procedures were pursued. (i) All available pixels were combined to a single map, representing the 3-dimensional surface of the tropical mesocosm of Biosphere 2 Laboratory with a resolution of few cm, where points closer to the camera were reconstructed more accurately (Fig. 6(d)). This resulted in a very dense surface mesh, which however still did not yield single leaf orientation and which had the disadvantage of different spacing between the single points. (ii) Every reconstructed depth image was divided in 4 quadrants (any other division may be used for different spatial resolution) and the average world coordinate for each quadrant was calculated. This resulted in a lower number of surface points (in our case 488) which was easier to handle and display. Since points were spaced by constant angles from each other, single points could be used to easily calculate a surface mesh (Fig. 6(e)).

[Fig. 6 about here]

5. Discussion

The results presented here show that it is possible to reconstruct 3-dimensional surfaces of a wide range of plant structures from single leaves to extended plant canopies with a small baseline, stereoscopic approach. This approach may prove less costly, faster and more flexible than LIDAR approaches. Compared to other methods, such as manual, semi-automatic three-dimensional digitizing (SONOHAT et al. 2002, SINOQUET et al. 2005), it provides a high degree of automation, thereby allowing higher experimental throughput. Hence, it is ideally suited to monitor temporal changes of structural canopy characteristics and to improve e.g. models of canopy light interception. Light interception models are an important requirement to understand the vegetation response in the context of agriculture or global climate change. The accuracy of light interception models is determined by the accuracy of 3-dimensional

measurements of vegetation canopies that have to be investigated at scales relevant for the model. The 3-dimensional structure of a plant canopy, which greatly affects light intensity within the canopy as well as other microclimatic conditions is currently recognized as a crucial and long neglected variable, which greatly affects the performance of plants in their natural environment and in ecosystem exchange processes and which produces substantial uncertainties in scaling leaf-level knowledge to the canopy and ecosystem (RASCHER et al. 2004).

This paves the way to apply this approach to airborne platforms where the movement of the aircraft can provide the different baselines of adjacent images. Thus far, structure of plant ecosystems cannot sufficiently be quantified and information such as leaf angle distribution, fraction cover or canopy roughness are products that greatly would contribute to link remote sensing data to vegetation models. Additionally information about canopy structure can greatly benefit optical remote sensing. The Photochemical Reflectance Index (PRI) for example is greatly influenced by BRDF effects of varying leaf orientation (BARTON and NORTH 2001). Leaves of natural canopies greatly depend on species, are influenced by diurnal changes and environmental factors (BISKUP et al. 2007) and currently hamper estimates of photosynthetic efficiency using the PRI and other optical approaches.

Rapid and flexible analysis of the 3-dimensional shape of a vegetation canopy might also provide a novel tool for growth analyses of crops or natural vegetation. The increase in height and compactness of a canopy can be extracted from two successive maps, to allow monitoring the effect of altered ecofactors determining growth (temperature, salt stress, etc.) and allowing to rapidly selecting plants for agricultural breeding purposes.

We thus argue that this stereo approach has the potential to serve as a serious alternative or complement (BALTSAVIAS 1999) to LIDAR methods, especially when sub-leaf resolution is needed, e.g. to determine leaf angle distribution. Our approach, being an optical technique, can provide instantaneous snapshots of moving objects such as canopies, facilitates object recognition and allows segmentation of individual leaves or plant organs (BISKUP et al. 2007) and thus also has potential to be beneficially combined with LIDAR approaches. The specific strength of our approach may be in long term ecological monitoring set-ups, where continuous measurements can provide data about structural changes in plant ecosystems. Yet, on the longer perspective also airborne approaches may be feasible to provide additional and crucial information for optical sensors. The algorithms used in this communication are freely available and parameters can easily be adjusted to fit the special needs.

Acknowledgements

B. Biskup acknowledges support of his PhD work by the Heinrich-Heine University of Düsseldorf, Germany. H. Scharr and R. Küsters were supported by the Deutsche Forschungsgesellschaft (SPP1114, LOCOMOTOR). We greatly thank Barry Osmond, whose support as director of Biosphere 2 Laboratory made this work possible. We also thank the maintenance crew of Biosphere 2 Laboratory, especially Allen Wright and Robert Arrington for climbing support.

References

BALTSAVIAS, E. P.: A comparison between photogrammetry and laser scanning. *ISPRS J. Photogramm.* 54, 83-94 (1999)

- BARTON, C. V. M. and NORTH, P. R. J.: Remote sensing of canopy light use efficiency using the photochemical reflectance index - Model and sensitivity analysis. *Remote Sens. Environ.* 78, 264-273 (2001)
- BIGÜN, J. and GRANLUND, G.: Optimal orientation detection of linear symmetry. In: *Proceedings of the First International Conference on Computer Vision ICCV'87*, 433-438. London: IEEE 1987
- BISKUP, B., SCHARR, H. SCHURR U. and RASCHER, U.: A stereo imaging system for measuring structural parameters of plant canopies. *Plant, Cell Environ.* 30, 1299-1308 (2007)
- BROWN, M.Z., BURSCHKA, D. and HAGER, G. D.: Advances in computational stereo. *IEEE Trans. Pattern Anal. Mach. Intell.* 25, 993-1008 (2003)
- CAMPBELL G. S. & NORMAN J. M.: The description and measurement of plant canopy structure. In: RUSSELL, G., MARSHALL, B. and JARVIS, P. (Eds.): *Plant Canopies: Their Growth, Form, and Function*. 1-19. Cambridge: Cambridge University Press 1989
- HARTLEY, R. and ZISSERMAN, A.: *Multiple View Geometry in computer vision*. Cambridge: Cambridge University Press 2004
- HAUSSECKER, H. and FLEET, D. J.: Computing optical flow with physical models of brightness variation. *IEEE Trans. Pattern Anal. Mach. Intell.* 23, 661-673 (2001)
- HIRSCHMÜLLER, H., SCHOLTEN, F. and HIRZINGER, G.: Stereo vision based reconstruction of huge urban areas from an airborne pushbroom camera (HRSC). In: *Lecture Notes in Computer Science: Pattern Recognition, Proceedings of the 27th DAGM Symposium, 30 August - 2 September 2005, Vienna, Austria, 3663*, 58-66. Heidelberg: Springer 2005
- KAY, S. M.: *Fundamentals of Statistical Signal Processing Vol 1: Estimation Theory*. New Jersey : Prentice-Hall 1993
- KOHLBERGER, T., SCHNÖRR, C., BRUHN, A. and WEICKERT, J.: Domain decomposition for parallel variational optic flow computation. In: MICHAELIS, B. and KRELL, G. (Eds.): *Proceedings of DAGM Symposium 2003, Lecture Notes in Computer Science*. 196-202. Berlin: Springer 2003
- LEIGH, L. S.: *The Basis for Rainforest Diversity and Biosphere 2*. PhD dissertation. University of Florida, Gainesville, FL, USA (1999)
- LEIGH, L. S., BURGESS, T., MARINO, B. D. V. and WEI, Y. D.: Tropical rainforest biome of Biosphere 2: structure, composition and results of first two years of operation. *Ecol. Eng.* 13, 65-94 (1999)
- LEFSKY, M. A., COHEN, W. A., PARKER, G. G. and HARDING, D. J.: Lidar remote sensing for ecosystem studies. *Biosci.* 52, 19-30 (2002)
- LIAO, W. H., AGGARWAL, S. J. and AGGARWAL, J. K.: The reconstruction of dynamic 3-D structure of biological objects using stereo microscope images. *Mach. Vision Appl.* 9, 166-178 (1997)
- LIN G. H., ADAMS, J., FARNSWORTH, B., WEI, Y. D., MARINO, B. D. V. and BERRY, J. A.: Ecosystem carbon exchange in two terrestrial ecosystem mesocosms under different atmospheric CO₂ concentrations. *Oecologia* 119, 97-108 (1999)
- MALTAMO, M., PACKALEN, P., YU, X., EERIKAINEN, K., HYYPPA, J. and PITKANEN, J.: Identifying and quantifying structural characteristics of heterogeneous boreal forests using laser scanner data. *Forest Ecol. and Manag.* 216, 41-50 (2005)

- NESTARES, O., FLEET, D. and HEEGER, D.: Likelihood functions and confidence bounds or total-least-squares problems. *IEEE Conference on Computer Vision and Pattern Recognition* 3, 523–530 (2000)
- NIINEMETS, Ü., LUKJANOVA, A., SPARROW, A. D. and TURNBULL, M. H.: Light-acclimation of cladode photosynthetic potentials in *Casuarina glauca*: trade-offs between physiological and structural investments. *Funct. Plant Biol.* 32, 571-582 (2005)
- OMASA, K.: 3-D color video microscopy. In: HÄDER, D. P. (Ed.): *Image analysis: methods and applications* 2nd edn. 257–273. Boca Raton, FL: CRC Press 2000
- OMASA, K., HOSOI, F. and KONISHI, A.: 3d lidar imaging for detecting and understanding plant responses and canopy structure. *J. Exp. Bot.* 58, 881–898 (2007)
- PAPENBERG, N., BRUHN, A., BROX, A., DIDAS, S. and WEICKERT, S.: Highly accurate optic flow computation with theoretically justified warping. *Int. J. Comput. Vision* 67, 141-158 (2006)
- PATENAUDE, G., MILNE, R. and DAWSON, T. P.: Synthesis of remote sensing approaches for forest carbon estimation: reporting to the Kyoto Protocol. *Environ. Sci. and Policy* 8, 161-178 (2005)
- RAKOCEVIC, M., SINOQUET, H., CHRISTOPHE, A. and VARLET-GRANCHER, C.: Assessing the geometric structure of a white clover (*Trifolium repens* L.) canopy using 3-D digitising. *Ann. Bot.* 86, 519–526 (2000)
- RASCHER, U., BOBICH, E. G., LIN, G. H., WALTER, A., MORRIS, T., NAUMANN, M., NICHOL, C. J., PIERCE, D., BIL, K., KUDEYAROV, V. and BERRY, J. A.: Functional diversity of photosynthesis during drought in a model tropical rainforest - the contributions of leaf area, photosynthetic electron transport and stomatal conductance to reduction in net ecosystem carbon exchange. *Plant, Cell Environ.* 27, 1239-1256 (2004)
- RASCHER, U. AND NEDBAL, L.: Dynamics of photosynthesis in fluctuating light. *Curr. Opin. Plant Biol.* 9, 671-678 (2006)
- SCHARR, H.: Optimal filters for extended optical flow. In 'Complex Motion, 1. Int. Workshop, Günzburg, Oct. 2004', *Lecture Notes in Computer Science* 3417. Berlin: Springer 2005
- SCHARR, H.: Towards a multi-camera generalization of brightness constancy. In 'Complex Motion, 1. Int. Workshop, Günzburg, Oct. 2004', *Lect. Notes Comput. Sc.*, 3417, Berlin: Springer 2006
- SCHARSTEIN, D. and SZELISKI, R.: A taxonomy and evaluation of dense two-frame stereo correspondence algorithms. *Int. J. Comput. Vision*, 47, 7–42 (2002)
- SCHUCHERT, T. AND SCHARR, H.: Simultaneous estimation of surface motion, depth and slopes under changing illumination. In 'Pattern Recognition: Proceedings of the 29th DAGM Symposium, Heidelberg, Germany', *Lecture Notes in Computer Science* 4713. Berlin : Springer 2007
- SCHURR, U., WALTER, A. and RASCHER, U.: Functional dynamics of plant growth and photosynthesis – from steady-state to dynamics – from homogeneity to heterogeneity. *Plant, Cell Environ.* 29, 340 – 352 (2006)
- SHI, J. and TOMASI, C.: Good features to track. In 'IEEE Computer Society Conference on Computer Vision and Pattern Recognition (CVPR'94)', 593–600. Seattle: IEEE Computer Society 1994

- SINOQUET, H. and RIVET, P.: Measurement and visualisation of the architecture of an adult tree based on a three-dimensional digitising device. *Trees-Struct. Funct.* 11, 265– 270 (1997)
- SINOQUET, H., SONOHAT, G., PHATTARALERPHONG, J. and GODIN, C.: Foliage randomness and light interception in 3-D digitized trees: an analysis from multiscale discretization of the canopy. *Plant Cell Environ.* 28, 1158-1170 (2005)
- SINOQUET, H., THANISAWANYANGKURA, S., MABROUK, H. and KASEMSAP, P.: Characterization of the light environment in canopies using 3D digitising and image processing. *Ann. Bot.* 82, 203 – 212 (1998)
- SLESAREVA, N., BRUHN, A. and WEICKERT, J.: Optic flow goes stereo: a variational method for estimating discontinuity-preserving dense disparity maps. In: KROPATSCH, W., SABLATNIG, R. and HANBURY, A. (Eds.): *Pattern Recognition. 27th DAGM Symposium, Proceedings.* 33-40. Berlin: Springer 2005
- SONOHAT, G., SINOQUET, H. C., VARLET-GRANCHER, C., RAKOCEVIC, M., JACQUET, A., SIMON, J. C. and ADAM, B.: Leaf dispersion and light partitioning in three-dimensionally digitized tall fescue-white clover mixtures. *Plant, Cell Environ.* 25, 529-538 (2002)
- STRZODKA, R. AND GARBE, C.: Real-time motion estimation and visualization on graphics cards. In 'Proceedings IEEE Visualization 2004', Washington: IEEE Computer Society 2004
- TURNER, W., SPECTOR, S., GARDINER, N., FLADELAND, M., STERLING, E. and STEININGER, M.: Remote sensing for biodiversity science and conservation. *Trends Ecol. Evol.*, 18, 306-314 (2003)
- WALTER, A. and LAMBRECHT, S. C.: Biosphere 2 Center as a unique tool for environmental studies. *J. Environ. Monitor.* 6, 267-277 (2004)
- WALTER, A. and SCHURR, U.: Dynamics of leaf and root growth – endogenous control versus environmental impact. *Ann. Bot.* 95, 891-900 (2005)

Fig. 1 3-D reconstructions of *Arabidopsis thaliana* (L.) Heynh. achieved with different pre-treatments of the plant. (a,b) No pre-treatment. (c,d) Spray-marked. (e,f) Illuminated with structured light. Left Column: input image; Right column: disparity map, grey values code for depth and areas of insufficient reconstruction were masked out (black patches). Insets: height profiles along the line shown in right column.

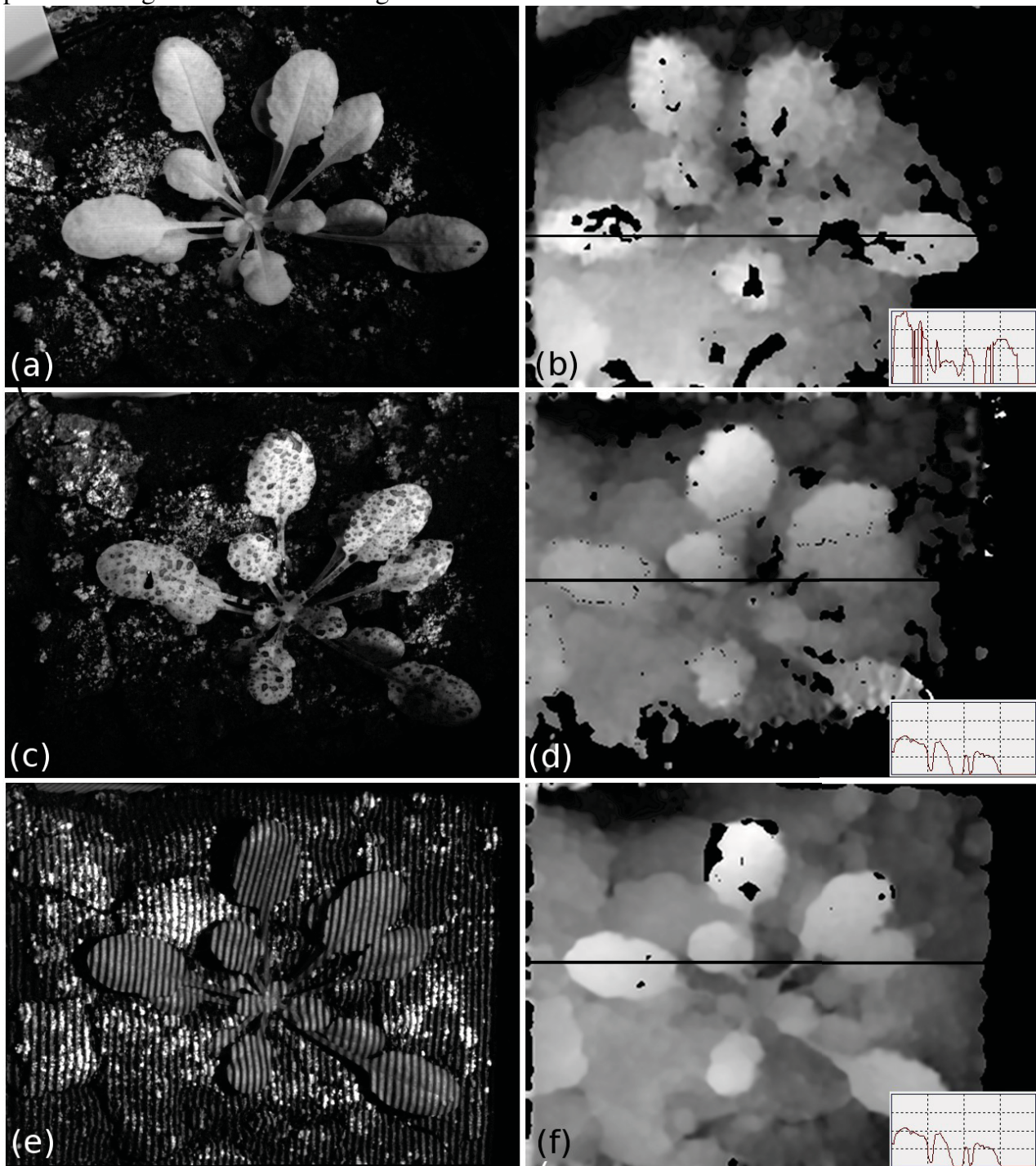


Fig. 2 Examples of 3-D reconstructions of plant organs pre-treated by spray marking. (a,b) *Opuntia phaeacantha* Engelm. cladodes; (c,d) *Fragaria x ananassa* Duch. leaf with comparably large spray dots (e,f) *Cucurbita pepo* L. leaf with comparably fine dots. From left to right: column 1: input image; column 2: disparity map. Insets: height profile along the line shown in (b).

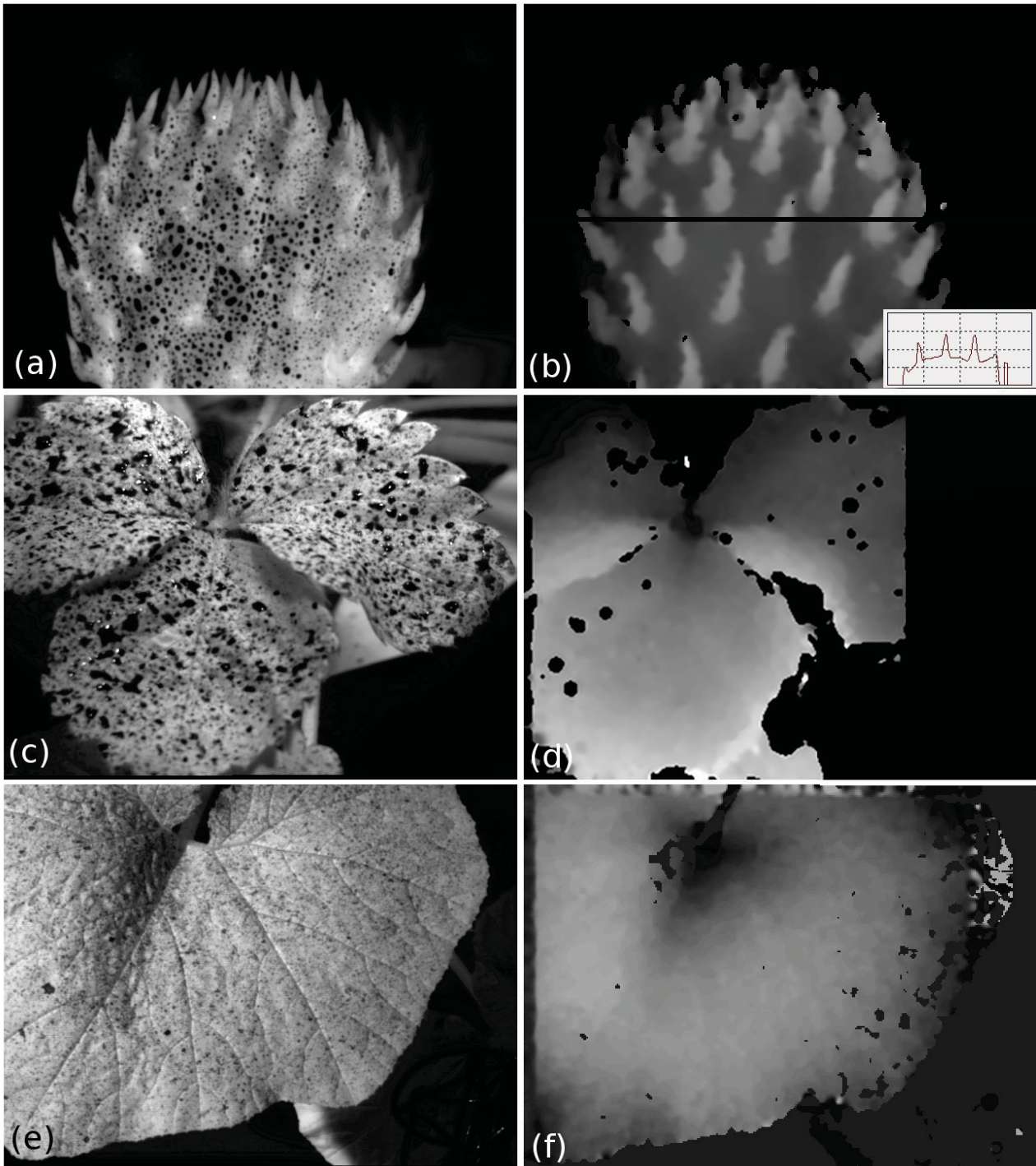


Fig. 3 Surface reconstruction of two medium sized canopy elements. Upper panels: *Ficus benjamini* L., lower panels: *Inga* cf. *sapindoides* Willd. (*left column*): original 2-D image of the canopies imaged from a distance of 2-8 meters. White bar indicates 0.1m. (*b,d*): distances to the camera as encoded in gray values. Pixels which did not yield a satisfying reconstruction were masked out (black patches).

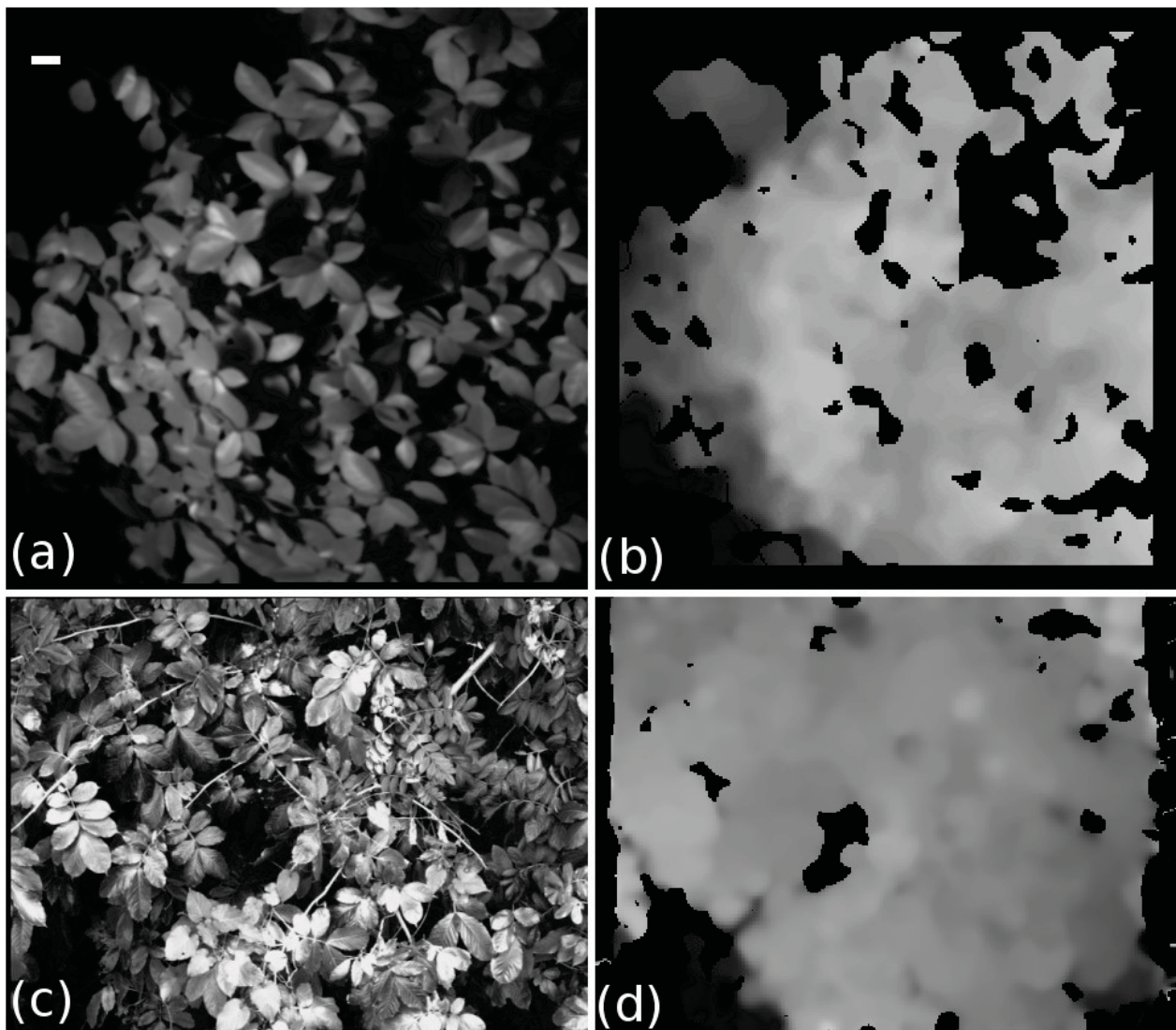


Fig. 4 Quality of 3-D information on canopy elements of the tropical mesocosm in Biosphere 2. Upper row: images of different canopy types, which were found in different distance to the camera set-up, resulting in different spatial resolution. Lower row: Images encoding outlier classification of the depth reconstruction. In black areas, the lower bound on the variance is too high and white areas indicate patches where the model error is too high. In the grey areas, sufficient information was available for surface reconstruction.

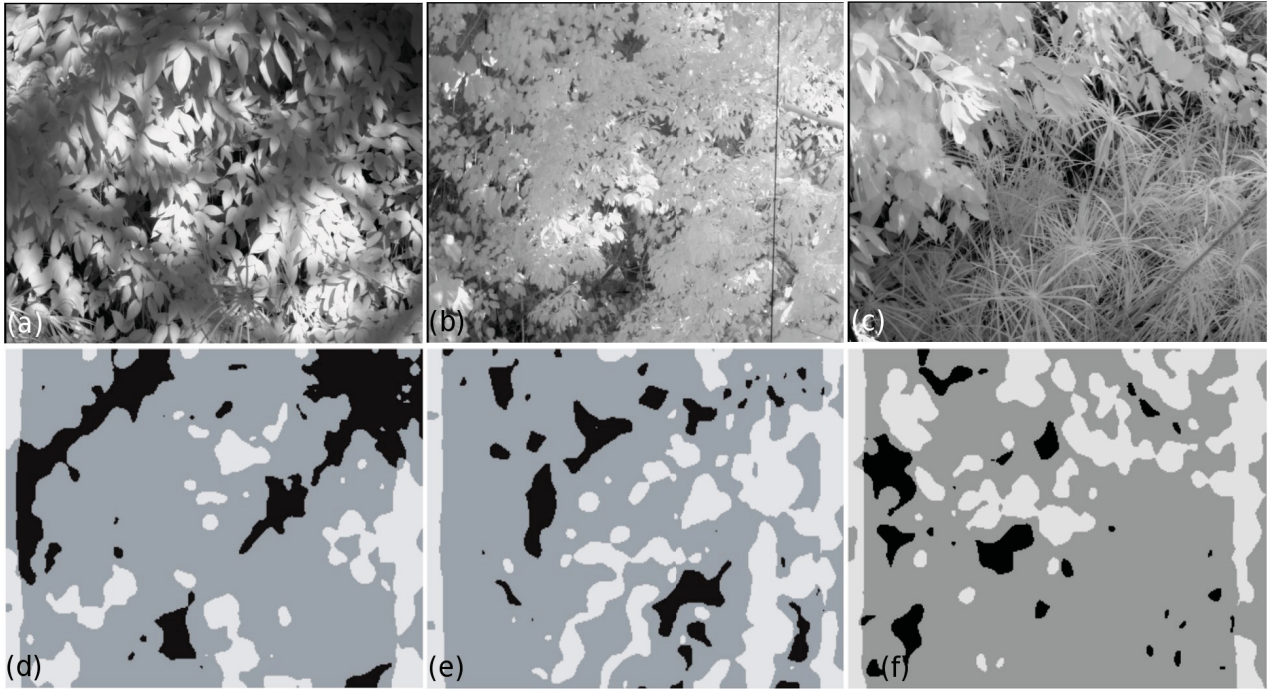


Fig. 5 Set-up and procedure for the assembly of single 3-D canopy elements the rainforest canopy of Biosphere 2 Center. (a): Picture of the stereo camera setup, mounted in the space frame of Biosphere 2 rainforest. (b): Schematic drawing of the controllable robot head, allowing horizontal and vertical scanning. (c, d): Schematic representation of horizontal and vertical camera movements that allow scanning the whole rainforest canopy using several adjacent images. Overlaps (see (d)) were eliminated in post-processing.

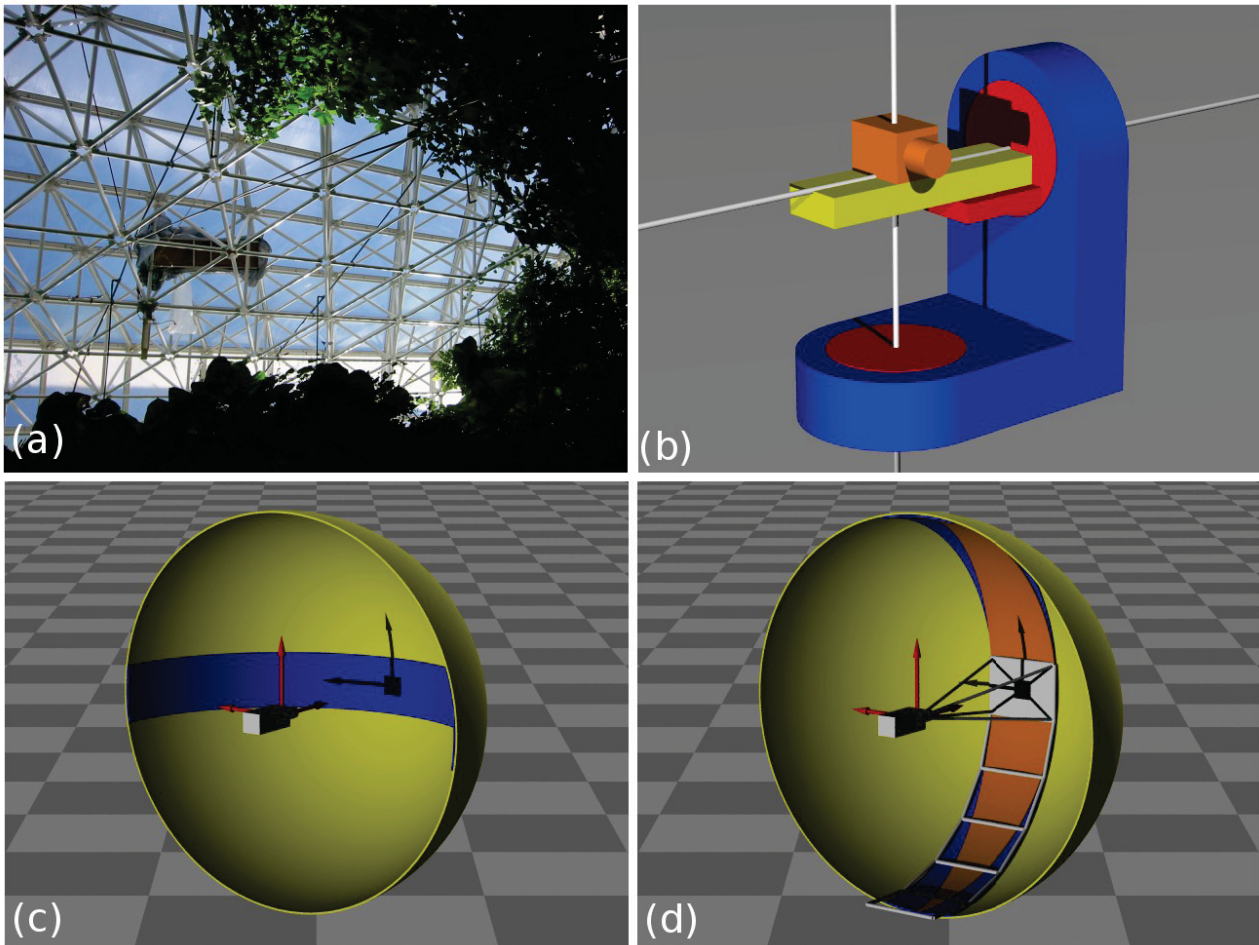
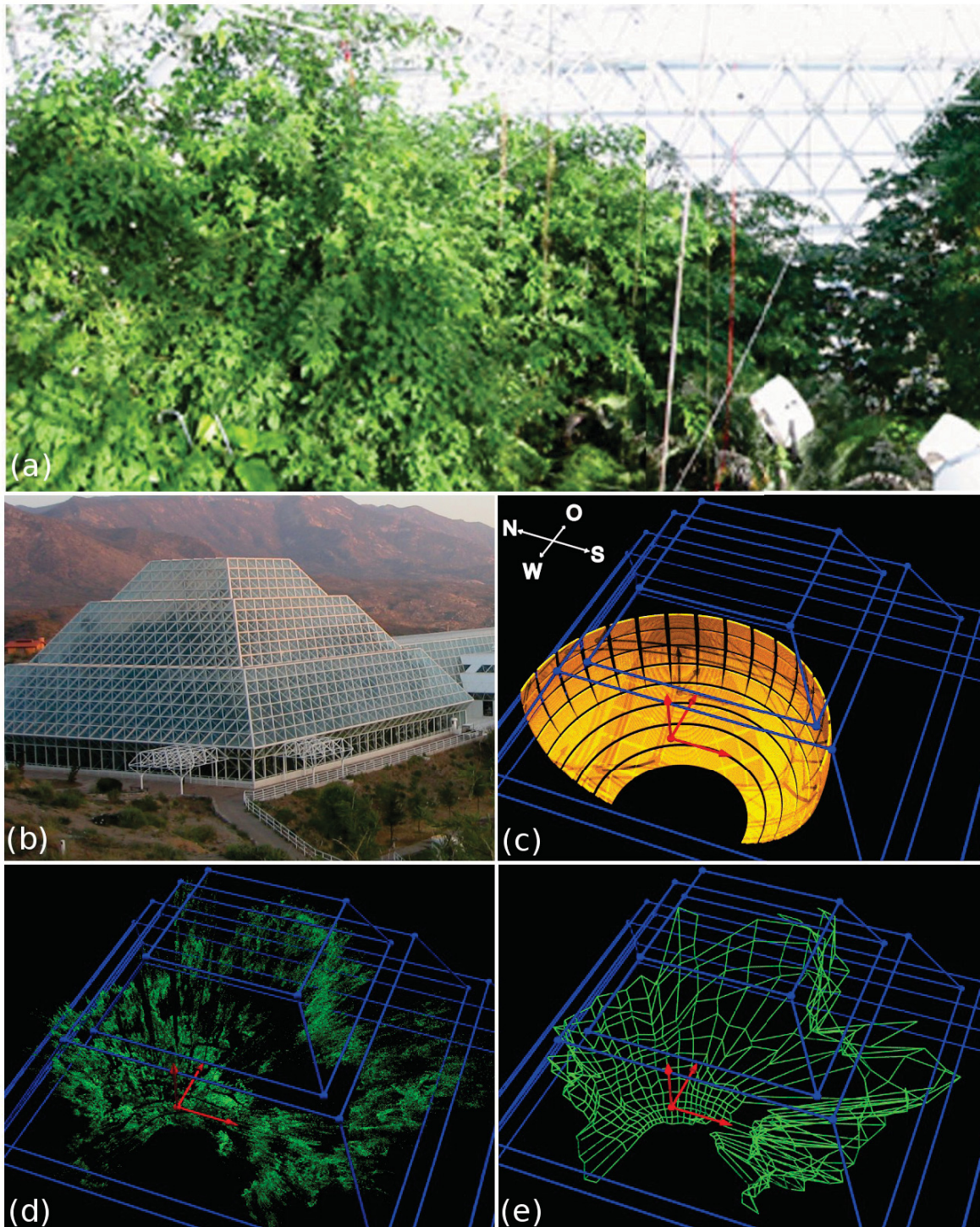


Fig. 6 Reconstruction of the surface structure of tropical rainforest mesocosm from the single images of the canopy element. (a): View of the tropical canopy of Biosphere 2 mesocosm, showing the complex 3-dimensional structure and heterogeneity of different species having different morphology. (b) Outside view of Biosphere 2 mesocosm. (c): Scheme how 122 single canopy elements were arranged to represent the whole canopy. (d): 3-D surface information of the canopy using all successfully reconstructed points (3.5 Million Pixels resulting from 122 single images were successfully reconstructed; for this presentation only 350 000 are plotted). (e): Reduction of the raw-data to a manageable resolution. In this example each canopy element was used to reconstruct 4 points. Averaging yielded a conceivable mesh representing the outer surface of the canopy.



5.3 Imaging and chlorophyll fluorescence analysis of the structure and function of the sunlit, upper canopy of soybean grown under free-air CO₂ enrichment

Status: **Submitted** (March 21, 2009)

Rascher U., Biskup B., Leaky A. D. B., McGrath J. M., Nelson R. & Ainsworth E. A. ([Agr-ForestMeteorol]) Maximum photosynthetic electron transport rate, not upper canopy structure, determines crop yield in soybean varieties under elevated CO₂. *Agricultural and Forest Meteorology (submitted)*.

Own contribution

- Design and implementation of measurement software
- Preliminary experiments (sensitivity measurements) on different soybean cultivars
- Stereo measurements (leaf orientation, vegetation profiles)
- Analysis and interpretation of experimental results
- Preparation of manuscript parts concerning stereo technique

1 Imaging and chlorophyll fluorescence analysis of the structure and
2 function of the sunlit, upper canopy of soybean grown under free-air
3 CO₂ enrichment.

4

5 Uwe Rascher^{1*}, Bernhard Biskup¹, Andrew D.B. Leakey^{2,3}, Justin M. McGrath³, Elizabeth A.
6 Ainsworth^{4,2,3*}

7

8 ¹Institute of Chemistry and Dynamics of the Geosphere ICG-3: Phytosphere, Forschungszentrum
9 Jülich, 52425 Jülich, Germany; ²Department of Plant Biology, ³Institute of Genomic Biology,
10 University of Illinois, Urbana-Champaign, Urbana IL 61801; ⁴U.S. Department of Agriculture,
11 Photosynthesis Research Unit, Agricultural Research Service, Urbana IL 61801

12

13

14 *Correspondence:

15 Fluorescence and canopy structure: Uwe Rascher, Institute of Chemistry and Dynamics of the
16 Geosphere ICG-III: Phytosphere, Forschungszentrum Jülich, Leo-Brandt-Straße, 52425 Jülich,
17 Germany. Tel: +49 (2461) 61 2638, Fax: +49 (2461) 61 2492, email: u.rascher@fz-juelich.de.

18 LAI, gas-exchange: Elizabeth Ainsworth, USDA ARS, Photosynthesis Research Unit, 147

19 ERML, 1201 W. Gregory Dr., Urbana IL 61801, USA. Tel: +1 (217) 265-9887, FAX +1 (217)

20 244-4419.

21

1 *E-Mail:*

- 2 U. Rascher: u.rascher@fz-juelich.de
 3 B. Biskup: b.biskup@fz-juelich.de
 4 A.D.B. Leakey: leakey@illinois.edu
 5 J.M. McGrath: jmcgrath@illinois.edu
 6 E.A. Ainsworth: lisa.ainswoth@ars.usda.gov

7

8

9 *Key words:*

- 10 three-dimensional canopy surface, photosynthesis, light reactions, chlorophyll fluorescence,
 11 elevated CO₂, *Glycine max*, structure-function relations

12

13 *Abbreviations:*

- 14 ψ leaf incidence angle, i.e. angle between sun and leaf normal
 15 α leaf absorbance, i.e. proportion of absorbed PPFD
 16 A photosynthetic CO₂ uptake rate ($\mu\text{mol m}^{-2} \text{s}^{-1}$)
 17 ETR photosynthetic electron transport rate ($\mu\text{mol electrons m}^{-2} \text{s}^{-1}$)
 18 ETR_{max} maximum photosynthetic electron transport rate at light saturation ($\mu\text{mol electrons}$
 19 $\text{m}^{-2} \text{s}^{-1}$)
 20 F fluorescence of the light-adapted leaf
 21 F_0 minimum fluorescence of the dark-adapted leaf
 22 F_m maximum fluorescence of the dark-adapted leaf
 23 F_m' maximum fluorescence of the light-adapted leaf

1	F_v/F_m	maximum quantum efficiency of PS II ($F_v = F_m - F_0$)
2	LAI	leaf area index (m^2 of leaf / m^2 of ground)
3	NPQ	non-photochemical quenching (rel.)
4	PPFD	photosynthetic photon flux density ($\lambda = 400 - 700$ nm) ($\mu\text{mol photons } m^{-2} s^{-1}$)
5	PPFD _{dir}	direct photosynthetic photon flux density on a horizontal surface ($\lambda = 400 - 700$ nm)
6		($\mu\text{mol photons } m^{-2} s^{-1}$)
7	PPFD _{diff}	diffuse photosynthetic photon flux density ($\lambda = 400 - 700$ nm) ($\mu\text{mol photons } m^{-2} s^{-1}$)
8	PPFD _{inci}	effective incident photosynthetic photon flux density on the leaf surface ($\lambda = 400 -$
9		700 nm) ($\mu\text{mol photons } m^{-2} s^{-1}$)
10	PS	photosystem
11	$V_{c,max}$	maximum apparent carboxylation capacity of Rubisco ($\mu\text{mol } m^{-2} s^{-1}$)
12	$\Delta F/F_m'$	effective quantum efficiency of PS II ($\Delta F = F_m' - F$) measured at ambient light

1 **ABSTRACT**

2 Previous studies of elevated carbon dioxide concentration ($[\text{CO}_2]$) on crop canopies have found
3 that radiation-use efficiency is increased more than radiation-interception efficiency. It is
4 assumed that increased radiation-use efficiency is due to changes in leaf-level physiology;
5 however, canopy structure can affect radiation-use efficiency if leaves are displayed in a manner
6 that optimizes their physiological capacity, even though the canopy intercepts the same amount
7 of light. Patterns of leaf display have not been examined in soybean in response to elevated
8 $[\text{CO}_2]$. In order to determine the contributions of physiology and canopy structure to radiation-
9 use and radiation-interception efficiency, this study relates leaf-level physiology and leaf display
10 to photosynthetic rate of the outer canopy. We used a new imaging approach that delivers three-
11 dimensional maps of the outer canopy during the growing season. The 3D data were used to
12 model leaf orientation and mean photosynthetic electron transport of the outer canopy, which
13 governs the predominant proportion of photosynthetic light conversion. Leaf orientation changes
14 did not contribute to increased radiation-use; leaves of the outer canopy showed similar diurnal
15 leaf movements and leaf orientation in both treatments. Elevated $[\text{CO}_2]$ resulted in an increased
16 maximum electron transport rate (ETR_{max}) and increased capacity of non-photochemical energy
17 dissipation at high light. Modeling of light interception showed that stimulated leaf-level electron
18 transport at elevated $[\text{CO}_2]$, and not alterations in leaf display, was associated with stimulated
19 radiation-use efficiency and, therefore, increased carbon uptake and biomass production in
20 elevated $[\text{CO}_2]$. This study quantified structure-function relationships in combination, allowing a
21 quantitative estimate of the contribution of both effects to canopy energy conversion under
22 elevated $[\text{CO}_2]$.

1 Introduction

2 The contribution that photosynthetic and leaf area index (LAI) responses make to the
3 stimulation of plant productivity under elevated [CO₂] has been extensively studied (Hirose *et al.*
4 1997, Ainsworth and Long 2005, Norby *et al.* 2005). In forest FACE experiments, the fraction of
5 enhanced NPP at elevated [CO₂] which is attributable to enhanced radiation interception as a
6 function of greater LAI decreases exponentially with increasing stand LAI, approaching zero at a
7 LAI of 7 m² m⁻² (Norby *et al.* 2005). In FACE experiments on C₃ grasses there was no
8 significant stimulation of LAI at elevated [CO₂] (Ainsworth and Long 2005). Therefore, it is
9 generally assumed that leaf-level changes in physiology are the sole driver of enhanced carbon
10 gain by high-LAI canopies at elevated [CO₂] (Ainsworth and Long 2005, Norby *et al.* 2005).
11 These analyses do not consider the possibility that at elevated [CO₂] changes in leaf display
12 could contribute to enhanced productivity. This is despite the fact that variation in leaf display,
13 without any change in LAI, can theoretically alter canopy carbon gain by up to ~40 % as a result
14 of changes in the distribution of photosynthetic photon flux density (PPFD) incident on leaves at
15 different canopy positions and its subsequent impacts on the efficiency with which radiation is
16 converted into photoassimilate (Long *et al.* 2006). The lack of data on leaf display responses to
17 elevated [CO₂] results from the difficulty in collecting such data. Most commonly, information
18 on the distribution and orientation of leaves within a canopy is collected manually with either
19 mathematical instruments (e.g. Pearcy and Yang, 1996) or a three-dimensional digitizer (e.g.
20 Falster and Westoby, 2003). However, considerable time and labor are required for both methods
21 and measurements are very difficult to perform in a closed canopy.

22 A new stereo imaging approach (Biskup *et al.*, 2007) and the Soybean Free-Air CO₂
23 Enrichment (SoyFACE) facility in Champaign, IL. (www.soyface.illinois.edu) provided a unique

1 means to test the contribution of changes in leaf display to stimulated productivity of soybean at
2 elevated [CO₂]. The soybean crop was grown over its entire lifetime at ambient or elevated
3 [CO₂] under open-field conditions, without disturbance of microclimate or growing volume
4 above- or below-ground that could alter patterns of leaf display. In addition, soybean provides a
5 valuable model system because: (1) its paraheliotropic leaf movements over the diurnal period
6 may interact with the effects of elevated [CO₂] and (2) the environmental and genetic
7 homogeneity of this experimental setting provided the ideal setting in which to detect subtle
8 treatment effects.

9 The stereo imaging approach of Biskup et al., (2007) has the advantage of rapidly
10 collecting data on the distribution and orientation of leaves across a relative large area (~1 m²) of
11 a closed canopy. Data collection is limited to leaf surfaces that are directly visible from above
12 and not occluded by the upper layers of leaves. This fails to provide information on the structure
13 and function of the shaded canopy layers. Nonetheless, in short, dense canopies, such as
14 soybean, with high LAI (>6 m² m⁻²; Dermody et al., 2006), the upper sunlit leaves dominate
15 whole canopy carbon uptake as a result of greater incident PPFD, as well as greater stomatal
16 conductance and photosynthetic capacity resulting from their growth environment and relatively
17 young physiological age (Morgan et al., 2004).

18 Previous studies at SoyFACE demonstrated that the 17-18% stimulation of above-ground
19 net primary productivity (NPP; Morgan *et al.* 2005) resulting from growth at elevated [CO₂]
20 (~550 ppm) compared to ambient [CO₂] (~380 ppm) was driven by a 3% stimulation of the
21 efficiency of radiation interception by the canopy and a 12 % stimulation of the efficiency with
22 which intercepted radiation was converted to biomass energy (Dermody *et al.* 2008). The
23 improvement in radiation interception efficiency at elevated [CO₂] was small despite greater

1 peak LAI and leaf area duration, because even under ambient [CO₂] LAI is >6 m² m⁻² and almost
2 all radiation was therefore intercepted (Dermody *et al.* 2006, 2008). Enhanced radiation
3 conversion efficiency was the primary driver of greater NPP at elevated [CO₂] and was assumed
4 to be the result of enhancements in photosynthesis that arise from greater carboxylation and
5 reduced oxygenation by Rubisco (Bernacchi *et al.* 2006). In order to test this assumption and to
6 link leaf distribution and orientation to canopy photosynthesis, calculations of the PPF incident
7 on individual leaves were combined with measurements of leaf-level electron transport rate to
8 model upper canopy radiation interception and upper canopy photosynthetic electron transport.
9 The results are directly relevant to regional biogeochemical land-atmosphere exchanges since
10 soybean production covers more than 60 million hectares, and represents one of the largest land-
11 use types in the Midwest U.S.

12

13 **Material and Methods**

14 ***Study site***

15 The study was conducted in a 16 ha soybean (*Glycine max* variety Pioneer 93B15) field
16 at the Soybean Free Air Concentration Enrichment (SoyFACE) facility in Champaign, Illinois,
17 USA (40°02' N, 88°14' W, 228 m a.s.l.). The facility operation procedures and crop management
18 practices have been described in detail previously (Ainsworth *et al.*, 2004; Leakey *et al.*, 2006;
19 Rogers *et al.*, 2004). Soybean was planted on 25 May 2006 and emerged on 29 May 2006. The
20 CO₂ enrichment systems were installed immediately after planting. CO₂ fumigation began on 30
21 May 2006 and the crop was fumigated until plants were fully mature and leaves had senesced
22 (October 1, 2006). The experiment contained four experimental blocks, each containing one
23 control plot (ambient [CO₂] of 378 ppm) and one elevated [CO₂] treatment plot (550 ppm).

1 Field measurements for this study were taken during the period of maximum
2 photosynthetic uptake by the crops between 26 July and 20 August 2006. In general,
3 meteorological conditions during this 4 week period were close to ideal for plant growth and leaf
4 level rates of photosynthesis were at the upper range of observations over the last 5 years
5 (Bernacchi et al., 2006; Leakey et al., 2009).

6

7 ***Leaf pigments and parameters***

8 Between 11:00 and 13:00 on 31 July 2006, three leaf disks (11.75 mm diameter) per plot
9 were sampled and immediately plunged into liquid nitrogen, before analysis for pigment content.
10 Pigments were extracted from frozen leaf disks ground in 4 ml of 100% chilled methanol (Porra
11 et al., 1989). Following centrifugation (2500 rpm at 4 °C for 10 min.), absorbance of methanol
12 extracts was measured in a 96-well plate reader (HT-Synergy, Bio-Tek, Winooski, VT, USA) at
13 666, 653 and 470 nm. Chlorophyll a, chlorophyll b and total carotenoid content were calculated
14 according to (Lichtenthaler, 1987). In the same sampling period, two leaf disks (20.6 mm
15 diameter) per leaf, from three plants per plot, were sampled before being dried at 70°C to
16 determine mass for calculation of specific leaf weight (g m^{-2}).

17 One terminal leaflet per plot was sampled for absorptance measurements. Leaf
18 reflectance and transmittance from 400 to 700 nm were measured using an integrating sphere (LI
19 1800, LI-COR, Lincoln, NE, USA) and spectroradiometer. Leaf absorbance was calculated as: 1
20 – reflectance – transmittance.

21

1 **Leaf photosynthesis**

2 *Chlorophyll fluorescence*

3 The photosynthetic performance of upper canopy leaves was assessed in terms of the
4 chlorophyll *a* fluorescence parameters $\Delta F/F_m'$ (effective quantum efficiency of light-adapted
5 leaves), ETR (photosynthetic electron transport rate) and NPQ (non-photochemical quenching),
6 using a miniaturized pulse-amplitude modulated fluorescence analyser (Mini-PAM, Walz,
7 Effeltrich, Germany) with a leaf clip holder described by Bilger et al. (1995). $\Delta F/F_m'$ and ETR
8 were measured at incident PPFD between 10:00 and 15:00 h over four consecutive days, for a
9 total of 50 - 80 individual leaves in each plot. F_v/F_m of dark adapted leaves was measured
10 between 23:00 and 01:00 h on the same dates. The high light flash used to measure saturated
11 fluorescence had a PPFD of $4000 \mu\text{mol m}^{-2} \text{s}^{-1}$ and a duration of 800 ms. All chlorophyll
12 fluorescence parameters were calculated as described by Rascher et al. (2004). Spot
13 measurements of photosynthetically active light intensity (PPFD, $\lambda = 380 - 710 \text{ nm}$) were taken
14 inside the measuring field by the micro-quantum sensor of the Mini-PAM. ETR was calculated
15 assuming equal excitation of both photosystems, PS II and PS I, and using the average leaf
16 absorptance of leaves measured in each plot. Throughout all measurements, special care was
17 taken not to change the ambient conditions, e.g., the angle of the leaf or shading, thus light
18 reactions of photosynthesis were in a steady state.

19

20 The measurements of $\Delta F/F_m'$, ETR and NPQ from many leaves and local light
21 environments were used to calculate canopy light-response curves for each experimental plot. In
22 general, measurement of light-response curves in this manner better reflects the average

1 photosynthetic performance of leaves within a plot, as it eliminates influence from momentary
2 ambient light conditions and leaf-to-leaf variability.

3 Maximum apparent electron-transport rate (ETR_{\max}) of the canopy was quantified from
4 the light response curves, as described by (Rascher et al., 2000; Rascher et al., 2004).

5 Maximum electron transport rate (ETR) was fitted according to:

$$6 \quad f(x) = ETR_{\max}(1 - e^{-bx}) \quad (1)$$

7 where ETR_{\max} and b were independent parameters, and x was light intensity. The parameter
8 ETR_{\max} describes the extrapolated maximum electron transport rate at high light intensities.

9 Non-photochemical quenching (NPQ) was fitted with a sigmoidal Hill function:

$$10 \quad f(x) = NPQ_{\min} + \frac{NPQ_{\text{increase}} \cdot x^c}{d^c + x^c} \quad (2)$$

11 where NPQ_{\min} , NPQ_{increase} , c , and d were independent parameters, and x was light intensity. The
12 parameter NPQ_{\min} denotes the minimum NPQ prevailing at low light intensities and NPQ_{increase}
13 describes the increase of NPQ values when leaves were exposed to high light. Therefore,
14 NPQ_{increase} denotes the dynamic capacity of leaves to increase their NPQ in high light conditions.
15 c indicates the steepness of the curve; and d is the light level at the inflection point. The
16 parameters were tested statistically using the Wald Test (Rascher et al. 2000, 2004).

17

18 *Gas Exchange*

19 Photosynthetic gas exchange measurements were taken on 20 August 2006. Two leaves
20 per plot were sampled from the canopy before dawn. Petioles were re-cut under water and leaves
21 were kept at low light until measurement. This procedure avoided transient decreases in water

1 potential, decreased chloroplastic inorganic phosphate concentration, and decreased maximum
2 photosystem II efficiency, which can occur after a few hours of sunlight and alter the A/c_i
3 response. The response of photosynthesis (A) to changes in intercellular $[\text{CO}_2]$ (c_i) was measured
4 with portable, steady-state gas-exchange systems (LI-6400, Li-Cor, Lincoln, NE, USA). A red-
5 blue LED light source provided saturating light ($1750 \mu\text{mol m}^{-2} \text{s}^{-1}$) and measurements were
6 made at a leaf temperature of 25°C . Photosynthesis was initially induced at growth $[\text{CO}_2]$. The
7 $[\text{CO}_2]$ at the leaf surface was reduced stepwise to a lower concentration of $50 \mu\text{mol mol}^{-1}$ and
8 then increased stepwise to an upper concentration of $1100 \mu\text{mol mol}^{-1}$. Ten or eleven points were
9 measured to construct each A/c_i curve. Values for c_i were calculated according to the method of
10 von Caemmerer and Farquhar (1981). Light-saturated photosynthesis (A_{sat}) at growth $[\text{CO}_2]$ was
11 calculated from A/c_i response curves. The response of A to c_i was fit with the model of Farquhar
12 et al. (1980) using maximum likelihood regression to predict the maximum apparent *in vivo*
13 Rubisco activity ($V_{c,\text{max}}$) and maximum apparent electron transport capacity (J_{max}), as described
14 in Long and Bernacchi (2003).

15

16 **Canopy structure**

17 *Leaf Area Index*

18 A leaf canopy analyzer (LAI-2000, Li-Cor, Lincoln, Nebraska, USA) was used to
19 measure leaf area index at four places within the canopy of each plot. For each location within a
20 ring, four below-canopy measurements were coupled with one above-canopy measurement. The
21 usual assumption that leaves are randomly distributed throughout the canopy does not hold for
22 row crops such as soybean. Therefore, a lens cover was used to occlude a portion of the field of
23 view, and separate measurements were taken parallel and perpendicular to the crop rows.

1

2 *Three-dimensional stereo reconstruction of the outer canopy using a stereo imaging system*

3 The outer surface of the soybean canopy was reconstructed in three dimensions using the
4 stereo camera system described in Biskup et al. (2007). Briefly, this system employs a
5 correlation-based correspondence analysis between two images taken from different positions, as
6 well as image segmentation techniques, to compute leaf-level 3D information. Images were
7 taken on 1 - 2 August 2006 between 7:00 h and 20:00 h.

8 The stereo rig was mounted on a 4 m pole, facing in nadir direction. The stereo baseline,
9 i.e. the horizontal distance between the two cameras, was 44.3 ± 2.0 cm, and the cameras
10 converged at an angle of $7.6 \pm 0.5^\circ$. Both cameras covered approximately the same field of view.
11 A horizontal reference plane (105 cm above the ground, horizontally adjusted by a water level
12 that was visible in every image) was attached to the pole and imaged by both cameras (Fig. 1a;
13 canopy height was in the range of 90 - 120 cm). Four stereo image pairs (subsamples) were taken
14 in each of the three replicate plots. Each stereo image covered a canopy section of approx. $170 \times$
15 115 cm. Each image pair was reconstructed and results from the four image pairs per plot were
16 pooled for further analysis, resulting in a sampled area of approx. 4.0 m^2 per plot.
17 Correspondences between left and right images were determined by comparing correlation
18 windows of 17×7 pixels. The 3D models (surface grids; Fig. 1b) and zenith leaf angle
19 distributions were obtained from 3D reconstruction as described in (Biskup et al., 2007).

20

21 *Calculation of leaf angle distribution*

22 Distribution of leaf inclination and azimuth angles were computed from the stereo
23 images. Images were segmented using a semi-autonomous algorithm into regions corresponding

1 to whole leaves or leaf parts (Biskup et al., 2007). Depending on illumination conditions, leaf
2 patches of different sizes were selected and results were dependent on the selection of the
3 comparable size classes. We carefully analyzed the dependency of the results on different size
4 classes. Most robust results were obtained for leaf patches between 100 and 500 mm². For each
5 segment, a plane was fitted to the corresponding part of the 3D model (variance of the fit was set
6 to 2 mm²). In general 858 - 1772 single leaf patches were reconstructed in each plot with the
7 lowest number of successfully reconstructed patches at the 17:00h measurement, which was
8 caused by high contrast shadings in the canopy at this time. The highest number of patches was
9 reconstructed at 20:00 h because of homogenous illumination. To avoid artifacts because of the
10 different numbers of successfully reconstructed leaf patches at different times of the day, we
11 used a Monte Carlo simulation approach and randomly selected leaf patches up to an area of 0.15
12 times the ground area for each time and treatment. The random selection was repeated 10 times.
13 Zenith leaf angle distribution was calculated as the histogram of all observed zenith angles in the
14 interval [0°, 80°], weighted by the 3D area of the surface patch for which the angle was
15 estimated (Biskup et al., 2007). A zenith angle of 0° indicates a leaf surface that is horizontally
16 oriented, i.e. parallel to the ground surface. A zenith angle of 90° indicates a leaf lamina that is
17 vertically oriented (i.e. erect). Azimuth leaf angle distribution was calculated in 10° classes.

18

19 *Determination of intercepted PPFD, integrated PPFD and ETR of sunlit canopy*

20 We aimed to incorporate structural and physiological measurements to derive an
21 integrated PPFD and ETR of the sunlit canopies. Photosynthesis and canopy structure were
22 measured in July and August. Thus, we averaged readings of direct and diffuse PPFD between 1
23 July 1 and 31 August, which yielded average values of direct and diffuse PPFD ($PPFD_{dir}$ and

1 $PPFD_{diff}$) for the measurement times (09:00, 13:00, 17:00 and 20:00h). From leaf azimuth and
 2 inclination and the modeled position of the sun, we calculated leaf incidence angles (ψ) to the
 3 sun for each leaf segment, with an angle of 0° describing a leaf that is perpendicular to the
 4 incoming solar radiation (i.e. receiving maximal radiation). Effective incident PPFD ($PPFD_{inci}$)
 5 was calculated according to eq 3.

6

$$7 \quad PPFD_{inci} = \cos(\Psi) \cdot PPFD_{dir} + PPFD_{diff} \quad (3)$$

8

9 Effective ETR (ETR_{eff}) of the reconstructed leaf patches was calculated using data from the
 10 measured light response curves, according to eq 4:

11

$$12 \quad ETR_{eff} = ETR_{max} \cdot (1 - e^{-b \cdot PPFD_{inci}}) \quad (4)$$

13

14 ETR_{max} and the factor b were taken from light response characteristics for soybean grown at
 15 ambient or elevated $[CO_2]$ (Fig. 2, Table 1).

16 From information on single leaf orientation and the knowledge of the position of the sun
 17 during the course of the day, we calculated integrated intercepted PPFD and integrated ETR of
 18 the outer, visible canopy. For this, we developed a new approach that is based on an equal
 19 distribution of azimuthal orientation of the outer leaves: (1) We randomly picked leaf segments
 20 (Monte Carlo Approach), (2) we calculated $PPFD_{inci}$ and ETR_{eff} of the leaf. (3) We calculated the
 21 casted shadow of the segment on a horizontal plane. The size of the shadow corresponds to the

1 intercepted sun light by the leaf and can be used as a measure of the deeper canopy that becomes
2 shaded. For example, a vertical leaf absorbs a great proportion of the incoming sun-light in the
3 early morning and late evening, while it casts almost no shadow during solar noon (Fig 1). (4)
4 We summed $PPFD_{inci}$ and ETR_{eff} until the shadows of the segments added to a ground area of
5 0.4 m^2 . Ideally we would have summed until the summed shadows reached 1 m^2 , but some of the
6 midday pictures had poor reconstruction because of high contrasts and shadows did not exceed
7 0.7 m^2 . In order to have appropriate random sampling, a cut-off criterion of 0.4 m^2 proved to
8 give the most robust results that were free of sampling bias. This Monte Carlo procedure was
9 repeated 100 times for each plot and values were then normalized to 1 m^2 ground area.

10 With this procedure we selected a representative sample of leaves of the outer canopy
11 that were sun lit and could integrate their $PPFD_{inci}$ and ETR_{eff} . The remaining leaves were
12 shaded and it can be assumed that they only received PPFD well below light saturation. As there
13 were differences for light response characteristics at low PPFD we neglected those leaves for
14 simplicity.

15

16

17 **Results**

18 *Photosynthesis and photosynthetic pigments*

19 *Chlorophyll Fluorescence*

20 Maximum quantum efficiency (F_v/F_m) was high in ambient as well as elevated $[\text{CO}_2]$.
21 Values of 0.80, which were measured 3 hours after sunset, indicate that neither the plants grown
22 in ambient nor those grown in elevated $[\text{CO}_2]$ were photoinhibited.

1 Light response curves of effective quantum efficiency ($\Delta F/F_m'$) showed the characteristic
2 trend with an approximately exponential decay of $\Delta F/F_m'$ with increasing PPFD, that was not
3 significantly different in ambient and elevated $[\text{CO}_2]$ (Fig. 2a). The initial slope of the ETR
4 curves was not affected by the $[\text{CO}_2]$ treatment (Fig. 2b). The maximum values of ETR (ETR_{max})
5 were 12.4% higher under elevated $[\text{CO}_2]$ (Fig. 2b); however, this was not statistically significant
6 (Table 1).

7 Below PPFD of $1000 \mu\text{mol m}^{-2} \text{s}^{-1}$, NPQ was maintained at a baseline level of 0.75 - 1
8 (Fig. 2c). Above $1000 \mu\text{mol m}^{-2} \text{s}^{-1}$, NPQ of plants grown at ambient $[\text{CO}_2]$ increased and
9 saturated at ≈ 2.2 ; NPQ of plants grown at elevated $[\text{CO}_2]$ increased with no indication of
10 saturation (Fig. 2c).

11

12 *A/ci Response Characteristics*

13 The rate of photosynthesis under growth $[\text{CO}_2]$ and saturating light (A_{sat}) was
14 significantly increased by growth at elevated $[\text{CO}_2]$ despite acclimation of photosynthesis,
15 observed as reductions in $V_{\text{c,max}}$ (Table 1). J_{max} was not significantly affected by elevated $[\text{CO}_2]$
16 (Table 1).

17

18 **Leaf pigments and parameters**

19 There were no significant effects of elevated $[\text{CO}_2]$ on chlorophyll *a* content, chlorophyll
20 *b* content, total carotenoid and xanthophyll content or the ratio of chlorophyll *a:b* (Table 1).
21 Mean leaf absorbance in the range of 400 – 700 nm was 0.90 for both treatments, which means
22 that 90 % of the incident photons were absorbed by the leaves of the soybeans.

1

2 **Canopy structure**

3 *Leaf Area Index*

4 Leaf area index (LAI) peaked in the middle of July and then gradually decreased with
5 leaf senescence towards the end of the growing period (Fig. 3). LAI was 0.5 to 1.0 m² m⁻² greater
6 on average at elevated [CO₂] ($F = 11.03, p = 0.014$).

7

8 *Leaf angle distribution*

9 Leaf zenith angle distributions of canopies grown under both treatments showed a diurnal
10 course, with leaves being predominantly horizontal in the morning, became increasingly vertical
11 during midday and horizontal again towards the evening (Fig. 4 left panels). No early morning
12 measurements were available for this study, but visual inspection confirmed that leaf inclination
13 was even more planophile immediately after sunrise (see also Biskup et al. (2007)). In contrast,
14 no clear diurnal course in leaf azimuth orientation was detected (Fig. 4, middle panels). A slight
15 preference for leaf orientation towards the NNE and SSW direction may be visible, which could
16 be an effect of the row planting of the soybeans.

17 Both inclination and azimuth orientations did not differ significantly between ambient
18 and elevated [CO₂] treatment. The ANOVA confirmed the strong effect of time of day ($F = 115,$
19 $p < 0.001$), whereas elevated [CO₂] did not have a significant effect ($F = 0.98, p < 0.38$). Leaf
20 surfaces were most vertically oriented with respect to ground during solar noon, resulting in a
21 relatively low incidence angle (ψ , Fig 4f). In contrast, ψ was higher in the morning and the
22 evening. Again there was no early morning measurement, but we assume that early morning
23 measurements would be similar to the 20:00 h distribution.

1

2 *Integrated incident PPFD and ETR of sun-lit canopy*

3 Using ψ , the light response characteristics of the soybeans (Fig. 1), and the average PPFD from
4 July and August, we modeled the integrated incident PPFD and ETR of the outer canopy,
5 summing up those leaf patches which were representative to the directly sun-exposed part of the
6 canopy (see Material for details on the approach and Fig. 5 for results). We assume that directly
7 illuminated leaves are the main contributors to canopy photosynthesis, as light intensity within
8 the canopy greatly decreases with depth. Integrated incident PPFD was highest during solar noon
9 (Fig. 5a). During the afternoon, integrated incident PPFD was lower than during morning hours
10 with a comparable sun angle (09:00 vs. 17:00 hour measurements). This difference was due to
11 the generally higher cloudiness in the afternoon and the thus reduced incoming radiation. There
12 was no difference in integrated incident PPFD between the canopy grown in ambient or elevated
13 $[\text{CO}_2]$.

14 Integrated ETR was also highest during solar noon and decreased towards the morning
15 and the evening hours (Fig. 5b). A clear difference between the plants grown at ambient and
16 elevated $[\text{CO}_2]$ was observed during midday (13:00 h) with integrated ETR of the elevated $[\text{CO}_2]$
17 treatment being 3.7 % higher. There was also a slightly higher integrated ETR at the 09:00 and
18 17:00 h measurement. As leaf orientation and incident PPFD did not show a difference between
19 the treatments, the difference in integrated ETR can be assumed to be solely due to the higher
20 leaf-level electron transport (Fig. 2).

21

1 Discussion

2 This study used stereo imaging (Biskup et al., 2007) to reveal that there were no significant
3 effects of long-term growth at elevated [CO₂] under field conditions on leaf display in the upper
4 canopy of a soybean crop. This provides unique evidence in support of the commonly accepted,
5 but rarely tested assumption, that changes in leaf-level physiology are the primary driver of
6 enhanced radiation conversion efficiency and, thereby, productivity by high-LAI canopies under
7 elevated [CO₂] (Ainsworth and Long 2005, Norby *et al.* 2005, Dermody *et al.* 2008).

8 The response of photosynthesis is nonlinear and efficiency decreases with increasing light
9 intensity, with many leaves saturating at light concentrations well below full sunlight. This
10 means that an efficient manner of display is for uppermost canopy leaves to have low angles of
11 incidence and lower canopy leaves to have high angles of incidence, such that the maximum
12 possible fraction of the canopy is at or near the light saturation point, but not exceeding it (Long
13 *et al.* 2006). If this can be achieved, it will have a secondary impact of maximizing the
14 enhancement of photosynthesis by elevated [CO₂], which is greater when photosynthesis is
15 Rubisco-limited rather than RuBp regeneration-limited. In soybean grown at elevated [CO₂], the
16 addition of additional nodes (Morgan *et al.* 2005) and changes in the density of the canopy
17 (Dermody *et al.* 2006) create the potential for altered leaf display that could alter the distribution
18 of PPFD incident on leaves to either increase or decrease the stimulation of productivity.
19 However, there were no significant differences in leaf orientation of the outer canopy between
20 soybeans grown at ambient and elevated [CO₂] (Fig. 4). There was also no significant difference
21 in the diurnal leaf movements in the outer, sunlit canopy grown at ambient and elevated [CO₂]
22 (Fig. 4). As a result, the distribution of PPFD incident upon leaves of the outer canopy was not
23 different between ambient and elevated [CO₂] (Fig 5a).

1 There was no effect of growth at elevated $[\text{CO}_2]$ of leaf absorbance, and therefore we
2 conclude that changes in the function of this key portion of the canopy under elevated $[\text{CO}_2]$ are
3 primarily determined by changes in the efficiency with which absorbed radiation is utilized for
4 photosynthetic carbon fixation. As in previous studies at this site (Bernacchi et al., 2006), the
5 average stimulation of ETR ($\sim 5\%$) under elevated $[\text{CO}_2]$ was small. However, because
6 photosynthesis at elevated $[\text{CO}_2]$ in soybean is co-limited by Rubisco carboxylation capacity and
7 the capacity of electron transport to support regeneration of RuBp in the Calvin Cycle, small
8 changes in ETR under elevated $[\text{CO}_2]$ can translate into a large stimulation of total daily A (20-
9 25 %) as a result of improved quantum efficiency of CO_2 fixation (Bernacchi et al., 2006).
10 Growth at elevated $[\text{CO}_2]$ resulted in $\sim 12\%$ greater peak LAI, which takes the form of a more
11 dense canopy (Dermody et al., 2006). However, the increase in canopy carbon gain resulting
12 from additional shaded leaves is probably small, despite their greater ($\sim 13\%$) maximum
13 quantum efficiency of photosynthesis (Dermody et al., 2006). As a consequence, the observed
14 stimulation of above-ground net primary production ($\sim 18\%$, Morgan et al., 2005) seems likely
15 to be primarily determined by the balance of stimulated A (Bernacchi et al 2006) and stimulated
16 night-time respiration (Leakey et al., 2009) of upper canopy leaves at elevated $[\text{CO}_2]$.

17 Producing germplasm which benefits more in terms of yield enhancement at elevated
18 $[\text{CO}_2]$ than current cultivars will be important to meeting growing global food demands under
19 changing climatic and atmospheric conditions this century (Ainsworth, Rogers and Leakey
20 2008). Understanding canopy structure and leaf display is an important step towards increasing
21 crop yields by optimizing the interception and conversion of radiation by the canopy. Soybeans
22 show strong diurnal leaf movements and thus are a good model system to test for the interplay of
23 structural properties with environmental factors. The cultivar used in this study, Pioneer 93B15,

1 showed distinct paraheliotropic leaf movements. The stereo imaging technique was sufficiently
2 sensitive to characterize a clear decrease in solar incidence angle around solar noon for plants
3 grown in both ambient and elevated [CO₂] (Fig. 4), a phenomenon common to other soybean
4 cultivars (Bawhey et al., 2003), which serves to minimize UVB radiation, excessive leaf
5 temperatures and/or photoinhibition (Bawhey et al., 2003; Rosa and Forseth, 1995; Wofford and
6 Allen, 1982). However, different cultivars of soybean have been described by varying strategies
7 of leaf movements (e.g. Wofford and Allen, 1982; Bawhey et al., 2003). For example, in a study
8 focusing on the terminal leaflet, the cultivar Forrest was found to have the steepest leaf
9 inclinations in the morning, whereas the cultivar Cumberland had the steepest inclination around
10 noon (Rosa and Forseth, 1995). This suggests that there is potential to improve soybean yield
11 enhancement by elevated [CO₂] by traditional breeding or biotechnological manipulation to
12 optimize leaf display.

13 While optical LAI measurements provide an integrated value of foliage density (Welles
14 and Norman, 1991), the explicit mapping using the stereo approach (Biskup et al., 2007) allows
15 modeling of effective electron transport with respect to leaf orientation. Due to increased
16 occlusion, only the outer levels (up to a cumulative LAI of approximately 2) are accessible with
17 the stereo approach method. However, since the outer canopy levels are the most responsive to
18 environmental conditions and are hypothesized to govern light interception into the lower strata
19 of the canopy (Ward and Strain, 1999; Morgan et al., 2004), this provides a technique with which
20 to rapidly probe genetic variability in canopy structure and leaf orientation to maximize
21 productivity under global atmospheric change.

22 In summary, our results revealed that there was no significant effect of elevated [CO₂] on
23 leaf display in the upper soybean canopy. Therefore, in this soybean canopy, leaf level changes

1 in physiology, including increased photosynthetic carbon gain (Rogers et al., 2004; Ainsworth et
2 al., 2004; Bernacchi et al., 2006), decreased stomatal conductance (Ainsworth et al., 2004;
3 Bernacchi et al., 2006; Leakey et al., 2006), and stimulated nighttime respiration (Leakey *et al.*
4 2009) drive canopy scale changes in radiation conversion efficiency and net primary
5 productivity.

6 **Acknowledgements**

7 We thank Tim Mies for technical assistance and Steve Long for supporting our research at
8 SoyFACE. SoyFACE was supported by the Illinois Council for Food and Agricultural Research,
9 Archer Daniels Midland Company, the U.S. Department of Agricultural, and the Illinois
10 Agricultural Experiment Station. B. Biskup and U. Rascher were supported by a NSF/DAAD
11 grant (grant PPP D/05/50496). B. Biskup also acknowledges support of his PhD thesis by the
12 Heinrich-Heine University of Düsseldorf, Germany. We thank K.G. Rascher for assistance with
13 the statistical analyses and we thank H. Scharr for supporting the development of the stereo
14 system and the development of the analyses algorithms.

15

1 REFERENCES

- 2 Ainsworth, E.A., Long, S.P., 2005. What have we learned from 15 years of free-air CO₂
3 enrichment (FACE)? A meta-analytic review of the responses of photosynthesis, canopy
4 properties and plant production to rising CO₂. *New Phytol.* 165, 351-372.
- 5 Ainsworth, E.A., Rogers, A., Leakey, A.D.B., Heady, L.E., Gibon, Y., Stitt, M., Schurr U. ,
6 2006. Does elevated atmospheric [CO₂] alter diurnal C uptake and the balance of C and
7 N metabolites in growing and fully expanded soybean leaves? *J. Exp. Bot.* 58, 579-591.
- 8 Ainsworth, E.A., Rogers, A., Nelson, R.L., Long, S.P., 2004. Testing the "source-sink"
9 hypothesis of down-regulation of photosynthesis in elevated [CO₂] in the field with
10 single gene substitutions in *Glycine max*. *Agric. For. Meteorol.* 122, 85-94.
- 11 Bawhey, C.I. , R.H. Grant, Gao, W., 2003. Digital measurement of heliotropic leaf response in
12 soybean cultivars and leaf exposure to solar UVB radiation. *Agric. For. Meteorol.* 120,
13 161-176.
- 14 Bernacchi, C.J., Leakey, A.D.B., Heady L.E., Morgan, P.B., Dohleman, F.G., McGrath, J.M.,
15 Gillespie, K.M., Wittig, V.E., Rogers, A., Long, S.P., Ort, D.R., 2006. Hourly and
16 seasonal variation in photosynthesis and stomatal conductance of soybean grown at
17 future CO₂ and ozone concentrations for 3 years under fully open-air field conditions.
18 *Plant Cell Environ.* 29, 2077-2090.
- 19 Bilger, W., Björkman, O., 1990. Role of the xanthophyll cycle in photoprotection elucidated by
20 measurements of light-induced absorbance changes, fluorescence and photosynthesis in
21 leaves of *Hedera canariensis*. *Photosynth. Res.* 25, 173-185.
- 22 Bilger, W., Schreiber, U., Bock, M., 1995. Determination of the quantum efficiency of
23 photosystem II and of non-photochemical quenching of chlorophyll fluorescence in the
24 field. *Oecologia* 102, 425-432.
- 25 Biskup B., Scharr, H., Schurr, U., Rascher, U., 2007. A stereo imaging system for measuring
26 structural parameters of plant canopies. *Plant Cell Environ.* 30, 1299-1308.
- 27 Blackman, V.H., 1919. The compound interest law and plant growth. *Ann. Bot.* 33, 353-360.

- 1 Caemmerer S von, Farquhar, G.D., 1981. Some relationships between the biochemistry of
2 photosynthesis and the gas exchange of leaves. *Planta* 153, 376-387.
- 3 Campbell, G.S., Norman, J.M., 1989. The description and measurement of plant canopy
4 structure. In: Russell, G., Marshall, B., Jarvis, P.G. (Eds.), *Plant Canopies: Their*
5 *Growth, Form, and Function* , pp. 1 – 19. Cambridge University Press, Cambridge, UK.
- 6 Cousins, A.B., Adam, N.R., Wall, G.W., Kimball, B.A., Pinter, P.J., Ottman, M.J., Leavitt, S.W.,
7 Webber, A.N., 2002. Photosystem II energy use, non-photochemical quenching and the
8 xanthophyll cycle in *Sorghum bicolor* grown under drought and free-air CO₂
9 enrichment (FACE) conditions. *Plant Cell Environ.* 25, 1551-1559.
- 10 Dermody, O.; Long, S.P.; DeLucia, E.H., 2006. How does elevated CO₂ or ozone affect the leaf-
11 area index of soybean when applied independently? *New Phytol.* 169, 145-155.
- 12 Dermody, O., Long, S.P., McConnaughay, K., DeLucia, E.H., 2008. How do elevated CO₂ and
13 O₃ affect the interception and utilization of radiation by a soybean canopy? *Global*
14 *Change Biol.* 14, 556-564.
- 15 Duvick, D.N., Cassman, K.G., 1999. Post-green revolution trends in yield potential of temperate
16 maize in the north-central United States. *Crop Sci.* 39, 1622-1630.
- 17 Ehleringer, J., 1981. Leaf Absorptances of Mohave and Sonoran Desert Plants. *Oecologia* 49,
18 366-370.
- 19 Falster, D.S., Westoby, M., 2003. Leaf size and angle vary widely across species: what
20 consequences for light interception? *New Phytol.* 158, 509-525.
- 21 Farquhar, G.D., von Caemmerer, S., Berry, J.A., 1980. A biochemical model of photosynthetic
22 CO₂ assimilation in leaves of C3 species. *Planta* 149, 78-90.
- 23 Ford, E.D., Cocks, A., Horton, L., Fellner, M., Van Volkenburgh, E., 2008. Estimation, variation
24 and importance of leaf curvature in *Zea mays* hybrids. *Agric. Forest Meteorol.* 148,
25 1598-1610.
- 26 Genty, B., Briantais, J.-M., Baker, N.R., 1989. The relationship between the quantum yield of
27 photosynthetic electron transport and quenching of chlorophyll fluorescence. *Biochim.*
28 *Biophys. Acta* 990, 87-92.

- 1 Guo, J., Trotter, C.M., Newton, P.C.D., 2006. Initial observations of increased requirements for
2 light-energy dissipation in ryegrass (*Lolium perenne*) when source / sink ratios become
3 high at a naturally grazed free air CO₂ enrichment (FACE) site. *Funct. Plant Biol.* 33,
4 1045–1053.
- 5 Hirose, T., Ackerly, D.D., Traw, M.B., Ramseier, D., Bazzaz, F.A., 1997. CO₂ elevation, canopy
6 photosynthesis and optimal leaf area index. *Ecology* 78, 2339-2350.
- 7 Kammann, C., Grunhage, L., Gruters, U., Janze, S., Jager, H.J., 2005. Response of aboveground
8 grassland biomass and soil moisture to moderate long-term CO₂ enrichment. *Basic*
9 *Appl. Ecol.* 6, 351-365.
- 10 Leakey, A.D.B., Ort, D.R., Long, S.P., 2006. Long-term growth of soybean at elevated [CO₂]
11 does not cause acclimation of stomatal conductance under fully open-air conditions.
12 *Plant Cell Environ.* 29, 1794-1800.
- 13 Leakey, A.D.B., Xu, F., Gillespie, K.M., McGrath, J.M., Ainsworth, E.A., Ort, D.R. 2009.
14 Genomic basis for stimulated respiration by plants growing under elevated carbon
15 dioxide. *Proc. Nat. Acad. Sci.* 106, 3597-3602.
- 16 Lichtenthaler, H.K., 1987. Chlorophylls and carotenoids - Pigments of photosynthetic
17 biomembranes. *Method. Enzymol.* 148, 350-382.
- 18 Liberloo, M., Dillen, S.Y., Calfapietra, C., Marinari S., Bin Luo, Z., De Angelis, P., Ceulemans,
19 R., 2005. Elevated CO₂ concentration, fertilization and their interaction: growth
20 stimulation in a short-rotation poplar coppice (EUROFACE). *Tree Physiol.* 25, 179-189.
- 21 Long, S.P., Zhu, X.-G., Naidu, S.L., Ort, D.R., 2006. Can improvement in photosynthesis
22 increase crop yield? *Plant Cell Environ.* 29, 315–330.
- 23 Long, S.P., Bernacchi, C.J., 2003. Gas exchange measurements, what can they tell us about the
24 underlying limitations to photosynthesis? Procedures and sources of error. *J. Exp. Bot.*
25 54, 2393-2401.
- 26 Long, S.P., Zhu, X.-G., Naidu, S.L., Ort, D.R., 2006. Can improvement in photosynthesis
27 increase crop yield? *Plant Cell Environ.* 29, 315–330.

- 1 Luo, Y., Medlyn, B., Hui, D., Ellsworth, D., Reynolds, J., Katul, G., 2001. Gross primary
2 productivity in Duke Forest: Modeling synthesis of CO₂ experiment and eddy-flux data.
3 *Ecol. Appl.* 11, 239-252.
- 4 Maddonni, G.A., Otegui, M. E., 1996. Leaf area, light interception, and crop development in
5 maize. *Field Crops Res.* 48, 81-87.
- 6 Morgan, P.B., Bernacchi, C.J., Ort, D.R., Long, S.P., 2004. An in vivo analysis of the effect of
7 season-long open-air elevation of ozone to anticipated 2050 levels on photosynthesis in
8 soybean. *Plant Physiol.* 135, 2348-2357.
- 9 Morgan, P.B.; Bollero, G.A.; Nelson, R.L.; Dohleman, F.G.; Long, S.P., 2005. Smaller than
10 predicted increase in aboveground net primary production and yield of field-grown
11 soybean under fully open-air [CO₂] elevation. *Glob. Change Biol.* 11, 1856-1865
- 12 Norby, R.J., Delucia, E.H., Gielen, B., Calfapietra, C., Giardina, C.P., King, J.S., Ledford, J.,
13 McCarthy, H.R., Moore, D.J.P., Ceulemans, R., De Angelis, P., Finzi, A.C., Karnosky,
14 D.F., Kubiske, M.E., Lukac, M., Pregitzer, K.S., Scarascia-Mugnozza, G., Schlesinger,
15 W.H., Oren, R., (2005) Forest response to elevated CO₂ is conserved across a broad
16 range of productivity. *Proc. Natl. Acad. Sci.* 102, 18052-18056.
- 17 Norby, R.J., Sholtis, J.D., Gunderson, C.A., Jawdy, S.S., 2003. Leaf dynamics of a deciduous
18 forest canopy: no response to elevated CO₂. *Oecologia* 136, 574-584.
- 19 Norby, R.J., Wullschleger, S.D., Gunderson, C.A., 1996. Tree responses to elevated CO₂ and
20 implications for forests. pp 1-22 in *Carbon dioxide and terrestrial ecosystems* editors
21 Koch, G.W. & Mooney, H.A. Academic Press. San Diego.
- 22 Nowak R.S., Ellsworth, D.S., Smith, S.D., 2004. Functional responses of plants to elevated
23 atmospheric CO₂ - do photosynthetic and productivity data from FACE experiments
24 support early predictions? *New Phytol.* 162, 253-280.
- 25 Ort, D.R., Long, S.P., 2003. Converting Solar Energy into Crop Production. In: Chrispeels, M.J.,
26 Saehle, H. (Eds.), *Converting Solar Energy Into Crop Production*, pp. 240-269.
27 American Society of Plant Biologists, Jones and Bartlett, Boston, MA, USA.
- 28 Percy R.W., Yang, W.M., 1996. A three-dimensional crown architecture model for assessment
29 of light capture and carbon gain by understory plants. *Oecologia* 108, 1-12.

- 1 Porra, R.J., Thompson, W.A., Kriedemann, P.E., 1989. Determination of accurate extinction
2 coefficients and simultaneous equations for assaying chlorophylls a and b extracted with
3 four different solvents: verification of the concentration of chlorophyll standards by
4 atomic absorption spectroscopy. *Biochim. Biophys. Acta* 975, 384-394.
- 5 Rascher, U., Bobich, E.G., Lin, G.H., Walter, A., Morris, T., Naumann, M., Nichol, C.J., Pierce,
6 D., Bil, K., Kudeyarov, V., Berry, J.A., 2004. Functional diversity of photosynthesis
7 during drought in a model tropical rainforest - the contributions of leaf area,
8 photosynthetic electron transport and stomatal conductance to reduction in net
9 ecosystem carbon exchange. *Plant Cell Environ.* 27, 1239-1256.
- 10 Rascher, U., Liebigh, M., Lüttge, U., 2000. Evaluation of instant light-response curves of
11 chlorophyll-fluorescence parameters obtained with a portable chlorophyll fluorometer
12 on site in the field. *Plant Cell Environ.* 23, 1397-1405.
- 13 Rogers, A., Allen, D.J., Davey, P.A., Morgan, P.B., Ainsworth, E.A., Bernacchi, C.J., Cornic,
14 G., Dermody, O., Heaton, E.A., Mahoney, J., Zhu, X., Delucia, E.H., Ort, D.R., Long,
15 S.P., 2004. Leaf photosynthesis and carbohydrate dynamics of soybeans grown
16 throughout their life-cycle under Free-Air Carbon dioxide Enrichment. *Plant Cell*
17 *Environ.* 27, 449-458.
- 18 Rosa, L.M., Forseth, I.N., 1995. Diurnal patterns of soybean leaf inclination angles and
19 azimuthal orientation under different levels of UVB radiation. *Agric. For. Meteorol.* 78,
20 107-119.
- 21 Schreiber, U., Bilger, W., 1993. Progress in chlorophyll fluorescence research: major
22 developments during the past years in retrospect. *Progress in Botany*. Springer Verlag
23 Berlin, Heidelberg 53, 151-173.
- 24 Springer, C.J., Thomas, R.B., 2007. Photosynthetic responses of forest understory tree species to
25 long-term exposure to elevated carbon dioxide concentration at the Duke Forest FACE
26 experiment. *Tree Physiol.* 27, 25-32.
- 27 Ward J.K., Strain, B.R., 1999. Elevated CO₂ studies: past, present and future. *Tree Physiol.* 19,
28 211-220. Welles, J.M., Norman, J.M., 1991. Instrument for indirect measurement of
29 canopy architecture. *Agron. J.* 83, 818-825.

- 1 Wofford, T.J., Allen, F.L., 1982. Variation in leaflet orientation among soybean cultivars. *Crop*
- 2 *Sci.* 22, 999.

3

1 **Table 1** Leaf characteristics and photosynthetic properties of soybean (cv. Pioneer 93B15)
 2 exposed to ambient and elevated [CO₂]. Data show mean values ± standard error. Statistical
 3 differences between treatments were tested with a one-way analysis of variance, with [CO₂] as a
 4 fixed effect and block as a random factor. Variables with significantly different values are in
 5 boldface.

6

	Ambient [CO ₂]	Elevated [CO ₂]	F, <i>p</i>
Chlorophyll a (mg m ⁻²)	486.0 ± 32.5	490.0 ± 17.0	0.04, 0.8590
Chlorophyll b (mg m ⁻²)	189.3 ± 3.7	208.6 ± 26.7	0.58, 0.5268
Chlorophyll a: Chlorophyll b	2.6 ± 0.2	2.4 ± 0.3	0.78, 0.4708
Carotenoids (mg m ⁻²)	108.4 ± 13.8	99.0 ± 17.7	5.48, 0.1442
Absorbance α (400 - 700 nm)	0.903 ± 0.001	0.904 ± 0.001	0.18, 0.6977
Fv/Fm	0.81 ± 0.003	0.80 ± 0.003	0.50, 0.5185
ETR _{max} (μmol m ⁻² s ⁻¹)	247.8 ± 9.1	278.6 ± 11.4	6.96, 0.1186
A _{sat} (μmol m ⁻² s ⁻¹)	26.8 ± 0.6	31.5 ± 1.6	7.74, 0.0319
V _{c,max} (μmol m ⁻² s ⁻¹)	123.9 ± 3.3	106.8 ± 3.0	14.58, 0.0088
J _{max} (μmol m ⁻² s ⁻¹)	221.8 ± 6.3	218.0 ± 12.1	0.08, 0.7883

7

1 **Fig. 1** Good example of the soybean canopy that was imaged by the stereo system (a) and 3D
2 surface plot obtained from the stereo image (b). The example was acquired at 17:00h (Results
3 differed and in the worst case only 15% of the area have been reconstructed). The image covers a
4 canopy area of approx. 1.02 m². 4 such images from 3 plots each were used to calculate the
5 distribution of leaf orientation (Fig. 4). Stereo images were taken from nadir orientation 4 meters
6 above canopy. A horizontal plane (lower right corner of image) served as a reference for nadir
7 and compass north. Pixels at which no reconstruction was possible were masked out (black
8 areas) and not used for analyses. The scale bar indicates the depth range from 83 (dark) to 113
9 cm (light) above ground. Minor ticks indicate increments of 2 cm. Horizontal length bar: 10 cm
10 at height of reference plane. E.g. the almost vertical leaves above the compass will cast a large
11 shadow in the morning or evening if the sun is low and coming from the East or West; however,
12 the shadow will be minimal if the sun is in zenith or coming from the North or South. Using the
13 3-D information of each leaf segment we analytically calculated integrated canopy PPFD and
14 ETR (Fig 5).

15

16

17 **Fig. 2** Light response curves of light reactions quantified using chlorophyll fluorescence
18 techniques. Measurements were made in the field under ambient light conditions. Effective
19 quantum efficiency of photosystem II ($\Delta F/F_m'$) was measured directly, electron transport rate
20 (ETR) was calculated using the $\Delta F/F_m'$ values and PPFD readings. Non-photochemical
21 quenching was calculated with the average dark-adapted F_m value for each cultivar and treatment
22 and the F_m' value of each individual leaf in the light. \circ are measurements under ambient
23 atmospheric conditions, \bullet are measured under elevated [CO₂]. Data were mathematically fitted
24 and lines represent the best fit (dashed lines: ambient atmospheric conditions, solid lines:
25 elevated [CO₂]). ETR_{max} values given in Table 1 are derived from these fitted curves.

26

27

1 **Fig. 3** Leaf area index (LAI) of Pioneer cultivars quantified from above the canopy throughout
2 the year using the LAI-2000. ○ are measurements under ambient atmospheric conditions, ● are
3 measured under elevated [CO₂].

4

5

6 **Fig. 4** Left and middle panels: Zenith (a,d,g,j) and azimuth (b,e,h,k) leaf angle distributions at
7 different times of day. Right panels: Incidence angle of the leaves to the sun (c, f, i, l). ○ are
8 measurements under ambient conditions, ● are measured under elevated [CO₂]. Error bars
9 indicate 95% confidence interval around mean ($n = 3$ replicate plots). Leaf angle classes were
10 10° wide (zenith) and 30° wide (azimuth). Zenith angle measurements above 80° were discarded.
11 No difference was made between adaxial and abaxial leaf surfaces, i.e. the range of angles is
12 [0°;90°] and 0 denotes orthogonal orientation of the leaf to the sun. Leaf angle distributions were
13 normalized to 1. Only surface patches with a zenith angle between 10° and 80° were used for
14 estimation of azimuth angles.

15

16

17 **Fig. 5** Integrated leaf incidence angle (a) and integrated effective ETR (b) of leaves that are
18 representative for the outer, sun-lit layer of the upper canopy. ○ are measurements under ambient
19 conditions, ● are measurements under elevated [CO₂]. Integrated leaf incidence angle and
20 effective ETR were summed until the shadow of the leaves cumulated to 0.4 m² ground area,
21 which was a robust cut-off criterion to randomly select representative leaves. Values were than
22 extrapolated for 1 m² ground area.

23

Figures

Fig. 1

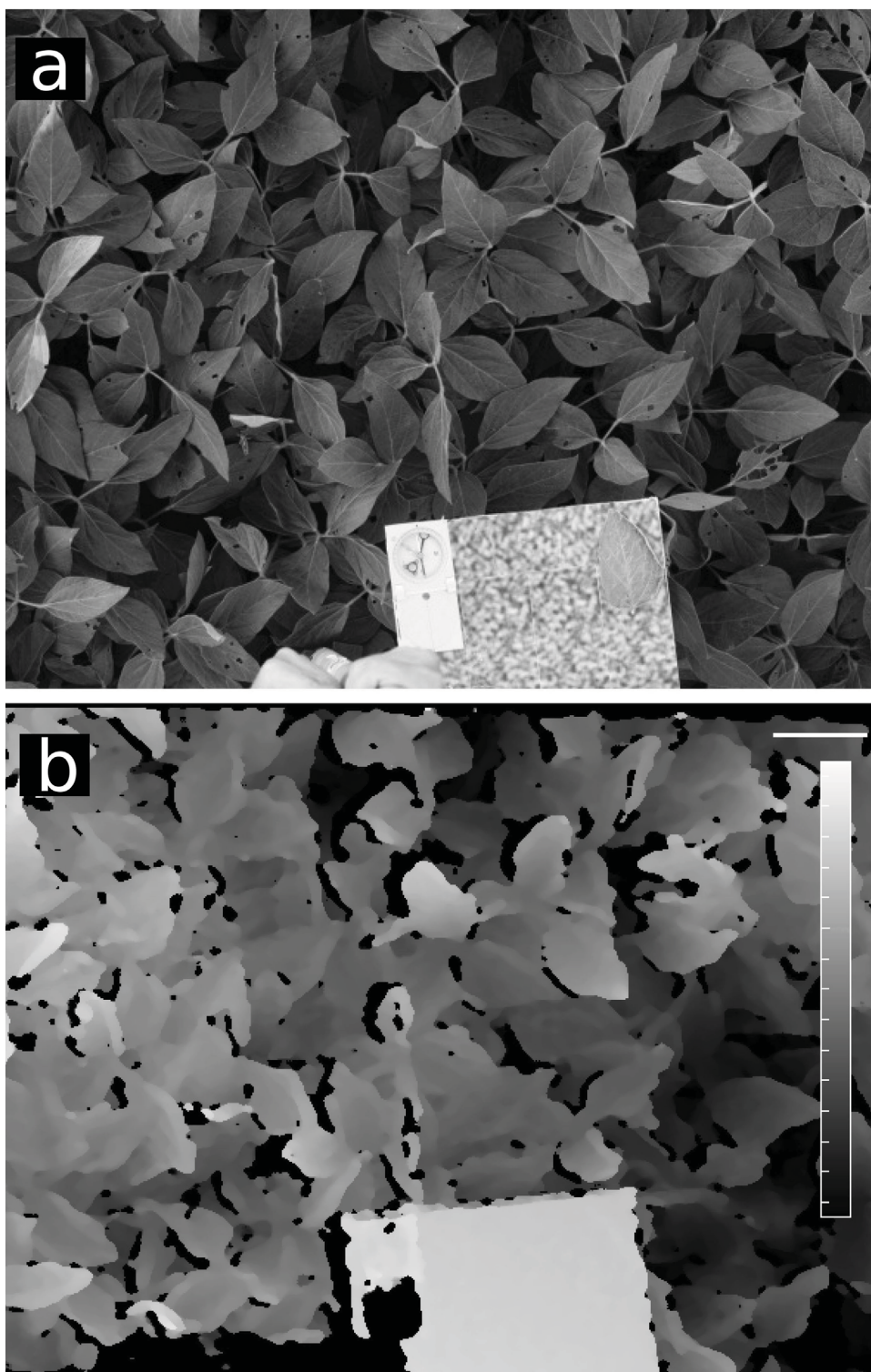


Fig. 2

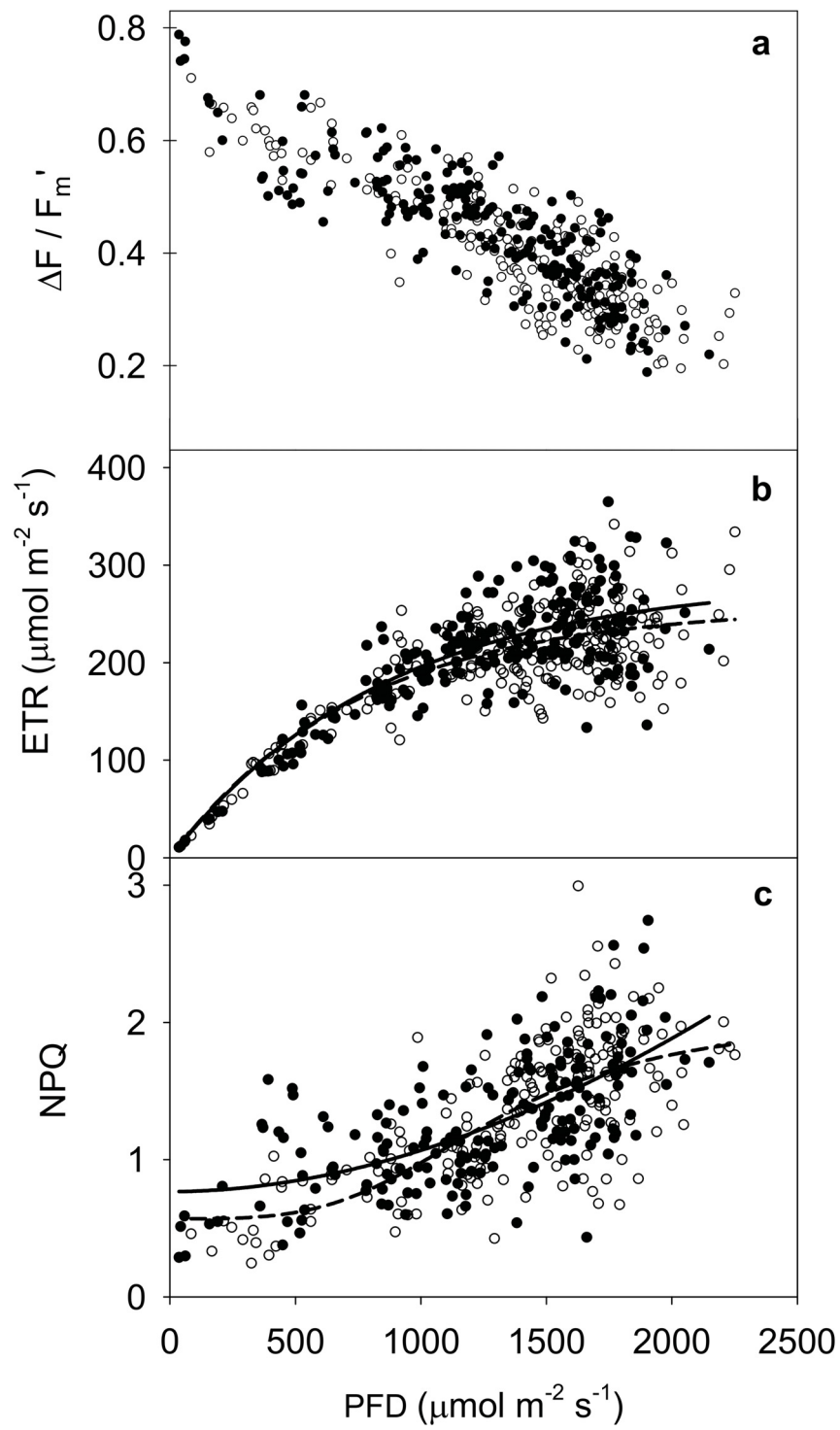


Fig. 3

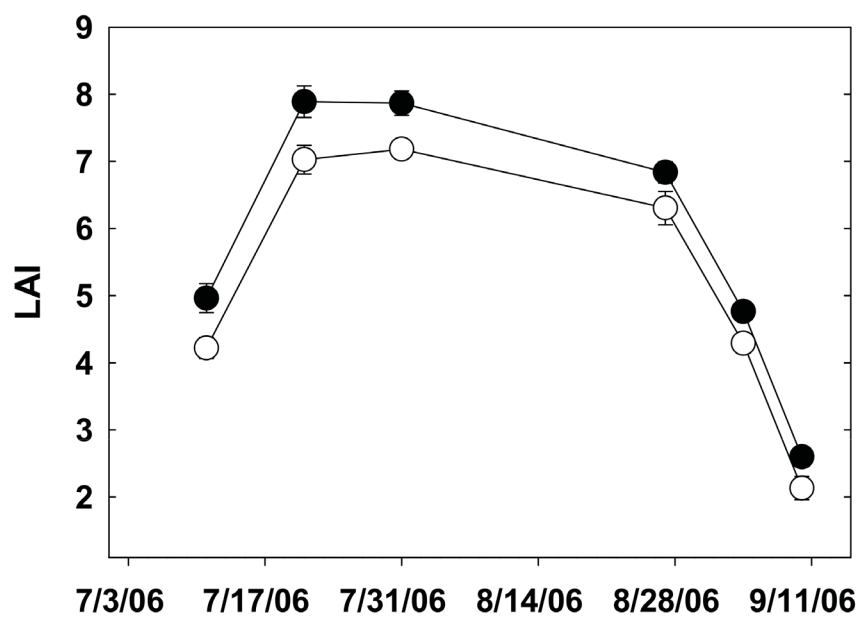


Fig. 4

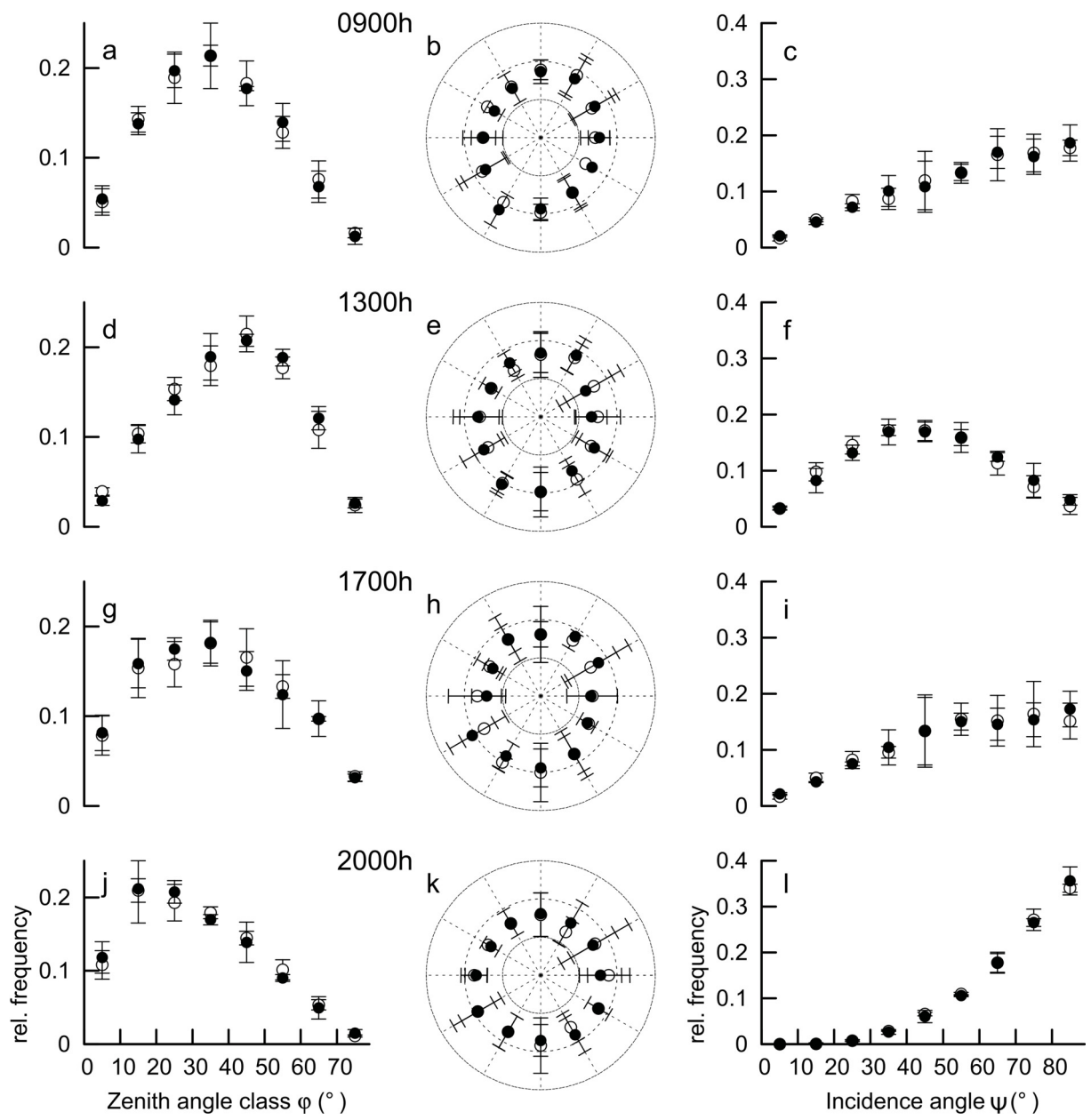
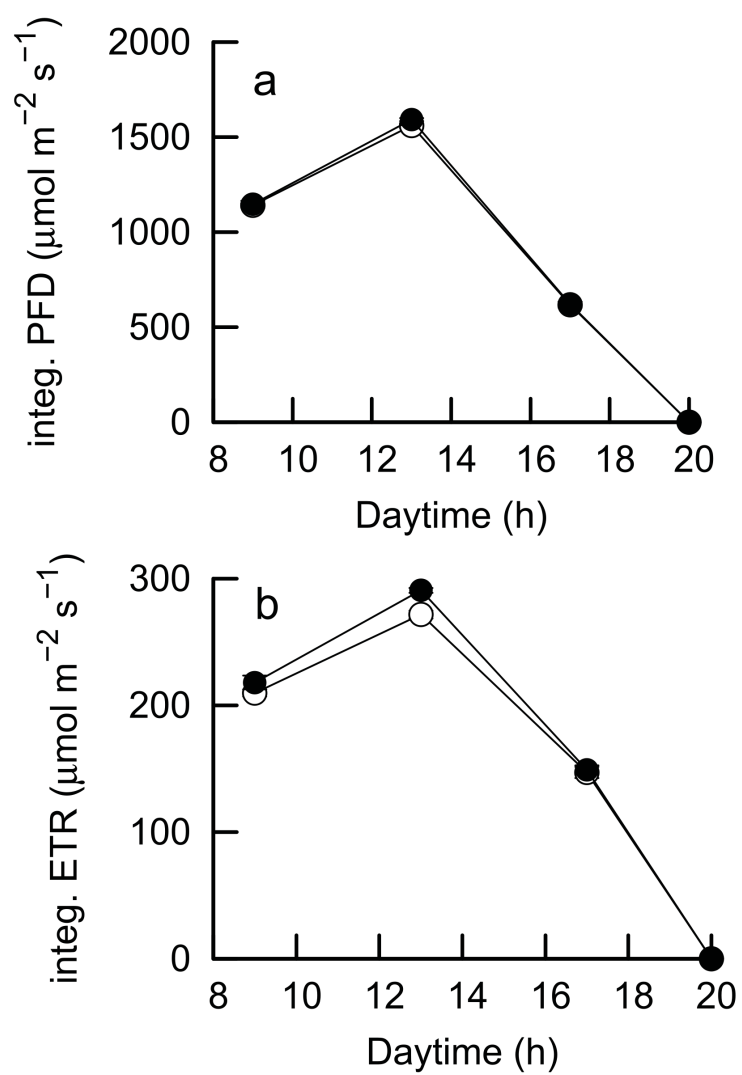


Fig. 5



5.4 Fourth publication: Diel growth cycle of isolated leaf discs analyzed with a novel, high-throughput 3D-imaging method is identical to that of intact leaves

Status: **Published** (March 1, 2009)

Biskup B., Scharr H., Fischbach A., Wiese-Klinkenberg A., Schurr U. & Walter A. (2009) Diel growth cycle of isolated leaf discs analyzed with a novel, high-throughput three-dimensional imaging method is identical to that of intact leaves. *Plant Physiology* **149**, 1452–1461.

Own contribution

- Design and implementation of database and system architecture
- Design and implementation of framework and processing steps
- Validation
- Screening experiments
- Comparison of growth dynamics obtained by DISP and by GROWSCREEN 3D
- Data analysis and interpretation
- Preparation of essential parts of manuscript

Diel Growth Cycle of Isolated Leaf Discs Analyzed with a Novel, High-Throughput Three-Dimensional Imaging Method Is Identical to That of Intact Leaves^{1[W]}

Bernhard Biskup, Hanno Scharr, Andreas Fischbach, Anika Wiese-Klinkenberg, Ulrich Schurr, and Achim Walter*

Institute of Chemistry and Dynamics of the Geosphere ICG-3 (Phytosphere), Forschungszentrum Jülich GmbH, 52425 Jülich, Germany

Dicot leaves grow with pronounced diel (24-h) cycles that are controlled by a complex network of factors. It is an open question to what extent leaf growth dynamics are controlled by long-range or by local signals. To address this question, we established a stereoscopic imaging system, GROWSCREEN 3D, which quantifies surface growth of isolated leaf discs floating on nutrient solution in wells of microtiter plates. A total of 458 leaf discs of tobacco (*Nicotiana tabacum*) were cut at different developmental stages, incubated, and analyzed for their relative growth rates. The camera system was automatically displaced across the array of leaf discs; visualization and camera displacement took about 12 s for each leaf disc, resulting in a time interval of 1.5 h for consecutive size analyses. Leaf discs showed a comparable diel leaf growth cycle as intact leaves but weaker peak growth activity. Hence, it can be concluded that the timing of leaf growth is regulated by local rather than by systemic control processes. This conclusion was supported by results from leaf discs of *Arabidopsis thaliana* Landsberg *erecta* wild-type plants and *starch-free1* mutants. At night, utilization of transitory starch leads to increased growth of Landsberg *erecta* wild-type discs compared with *starch-free1* discs. Moreover, the decrease of leaf disc growth when exposed to different concentrations of glyphosate showed an immediate dose-dependent response. Our results demonstrate that a dynamic leaf disc growth analysis as we present it here is a promising approach to uncover the effects of internal and external cues on dicot leaf development.

Leaf growth occurs in an ever-changing environment, to which especially the growing leaves of dicot plants are exposed. While growth zones of monocot plants are protected from direct exposure to the environment by being ensheathed by older leaves, dicot leaf growth zones have to cope with temperature and light regimes that fluctuate strongly throughout 24 h (diel cycle). Dicot leaf growth is intimately connected to light quality and quantity perceived by the organ (Dale, 1988; Van Volkenburgh, 1999), and growth intensity fluctuates characteristically throughout the diel cycle. As leaf growth is an integrating behavior that is controlled by a wide range of interconnected regulatory systems, its regulation will only be understood on the basis of a combination of appropriate analysis methods and experimental approaches addressing relevant parts of the control network. Recently, an important aspect of the connection between growth, the circadian clock, and diurnally fluctuating light intensity was

revealed in *Arabidopsis thaliana* hypocotyls (Nozue et al., 2007). During the day, light inhibits growth by inactivating the growth-promoting transcription factors phytochrome-interacting factor 4 and 5. During the first half of the night, these factors are further repressed by the circadian clock, but toward dawn, this repression finally ceases, allowing an increase of growth. All factors involved in this specific regulatory chain act locally, implying that diel growth patterns controlled by this system do not depend on an intact, systemic exchange between sink and source tissue with long-range transport of phytohormones or key metabolites.

In both hypocotyls (Nozue et al., 2007) and leaves (Wiese et al., 2007) of *Arabidopsis*, highest relative growth rate (RGR) is reached in the early morning. This is comparable to the diel growth cycle in tobacco (*Nicotiana tabacum*; Walter and Schurr, 2000), while other species may show RGR maxima at other times of the day (Dale, 1988; Matsubara and Walter, 2006). We raise the hypothesis that the diel growth cycle of leaves of *Arabidopsis* and tobacco is controlled by locally acting processes that do not strongly depend on the provision of systemically distributed substances.

Leaf disc assays have been successfully used in growth measurements (Powell and Griffith, 1960; Stiles and Van Volkenburgh, 2004; Kovács et al., 2007) and in the assessment of the effects of agrochemicals (Gibon et al., 1997; Barbagallo et al., 2003) before. It has been shown that leaf discs can grow as rapidly as intact

¹ This work was supported by Forschungszentrum Jülich GmbH. B.B. acknowledges support of his Ph.D. thesis by the Heinrich-Heine University of Düsseldorf, Germany.

* Corresponding author; e-mail a.walter@fz-juelich.de.

The author responsible for distribution of materials integral to the findings presented in this article in accordance with the policy described in the Instructions for Authors (www.plantphysiol.org) is: Hanno Scharr (h.scharr@fz-juelich.de).

^[W] The online version of this article contains Web-only data.

www.plantphysiol.org/cgi/doi/10.1104/pp.108.134486

leaf tissue (Dale, 1967) and that they can react strongly upon alterations of external cues (Stahlberg and Van Volkenburgh, 1999). Leaf disc assays have a number of advantages over whole plant assays. Leaf discs require little space, allowing higher numbers of replicates. Application of treatments such as nutrient solutions or phytohormones is simple, as they do not have to be taken up by the root and be transported to the leaves. Instead, leaf discs can float on solutions of active ingredients that are presented, for example, on microtiter plates (Barbagallo et al., 2003). Finally, image-based phenotyping techniques benefit from the simple shape of leaf discs, as they allow an unoccluded view of the entire area.

Yet, the use of leaf disc assays to decipher the control of leaf growth dynamics has been limited, since precise, automatic detection of leaf disc area is difficult. Automated analysis of the projected, two-dimensional (2D) area (A_{2D}), seen from a single point above the object, should be feasible with simple camera systems but has several shortcomings. The most important one is that

A_{2D} depends on leaf disc inclination. Growth rates of leaf discs that are tilted (e.g. because they adhere to the wall of the vessel they reside in) or strongly curved (e.g. due to epinastic or hyponastic growth) can only be estimated with substantial errors. Moreover, when the liquid level decreases in the course of an experiment, A_{2D} decreases solely because the object distance increases. In this case, the imaging system measures the actual growth superimposed by an apparent shrinking. While the (temperature-dependent) evaporation rate across the surface of the liquid could be determined by measuring A_{2D} of nongrowing, synthetic objects, the transpiration rate of the leaf discs may differ and thus affect water loss rate.

Hence, the aim of this study was to analyze the growth of the three-dimensional (3D) surface area (A_{3D}) of leaf discs via a stereoscopic approach (called GROWSCREEN 3D; Fig. 1) to test the hypothesis that diel leaf growth cycles of the model species tobacco and *Arabidopsis* are controlled locally.

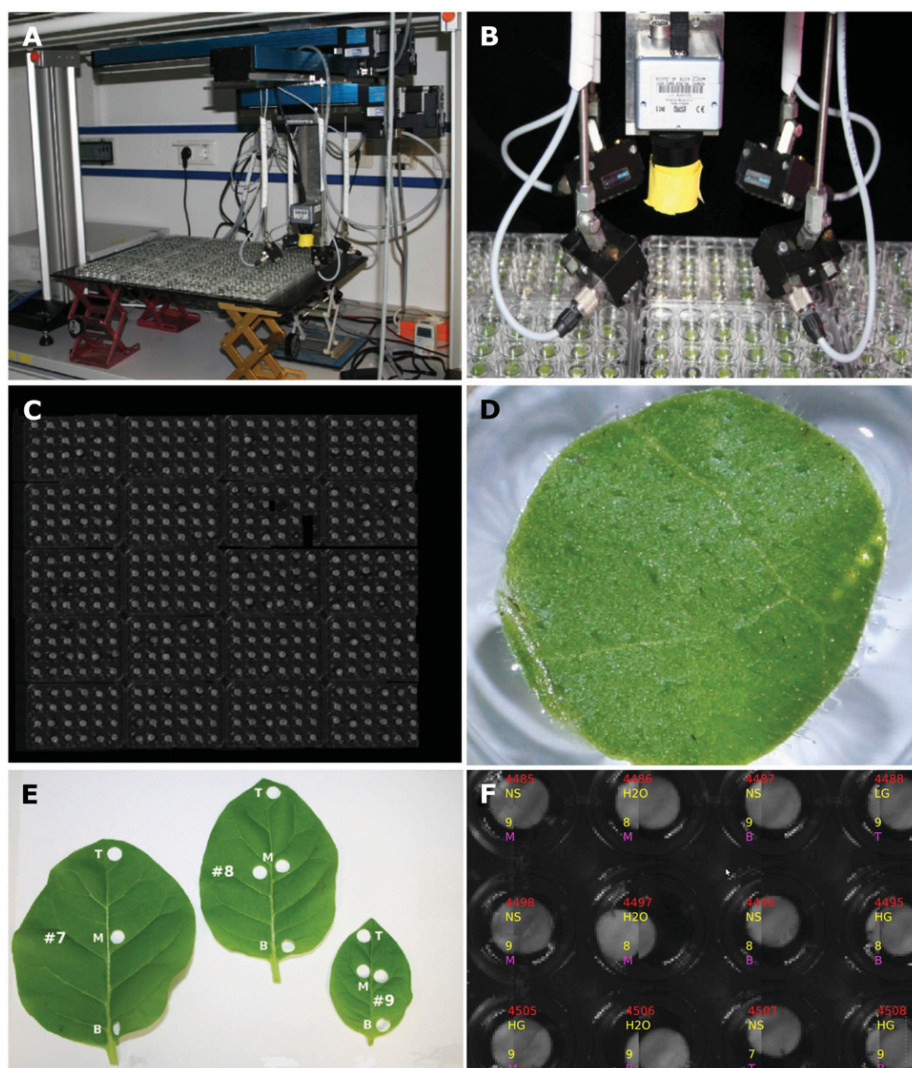


Figure 1. GROWSCREEN 3D. A, Scaffold with acquisition system. The X displacement stage is mounted to the scaffold and carries the Y and X₂ displacement stages. B, Camera surrounded by near-infrared light-emitting diode arrays. C, Overview image composed from 395 single images taken under near-infrared illumination. Some leaf discs are smaller or missing because of insufficient leaf area. D, Typical leaf disc floating in solution inside the well. The surface is slightly bent. E, Leaf numbers (counting from base, including cotyledons) and locations along the lamina (B, base; M, middle; T, tip) at which leaf discs were excised. F, Client application with superimposed information about leaf discs (plant identification number, treatment, leaf number, and location along lamina).

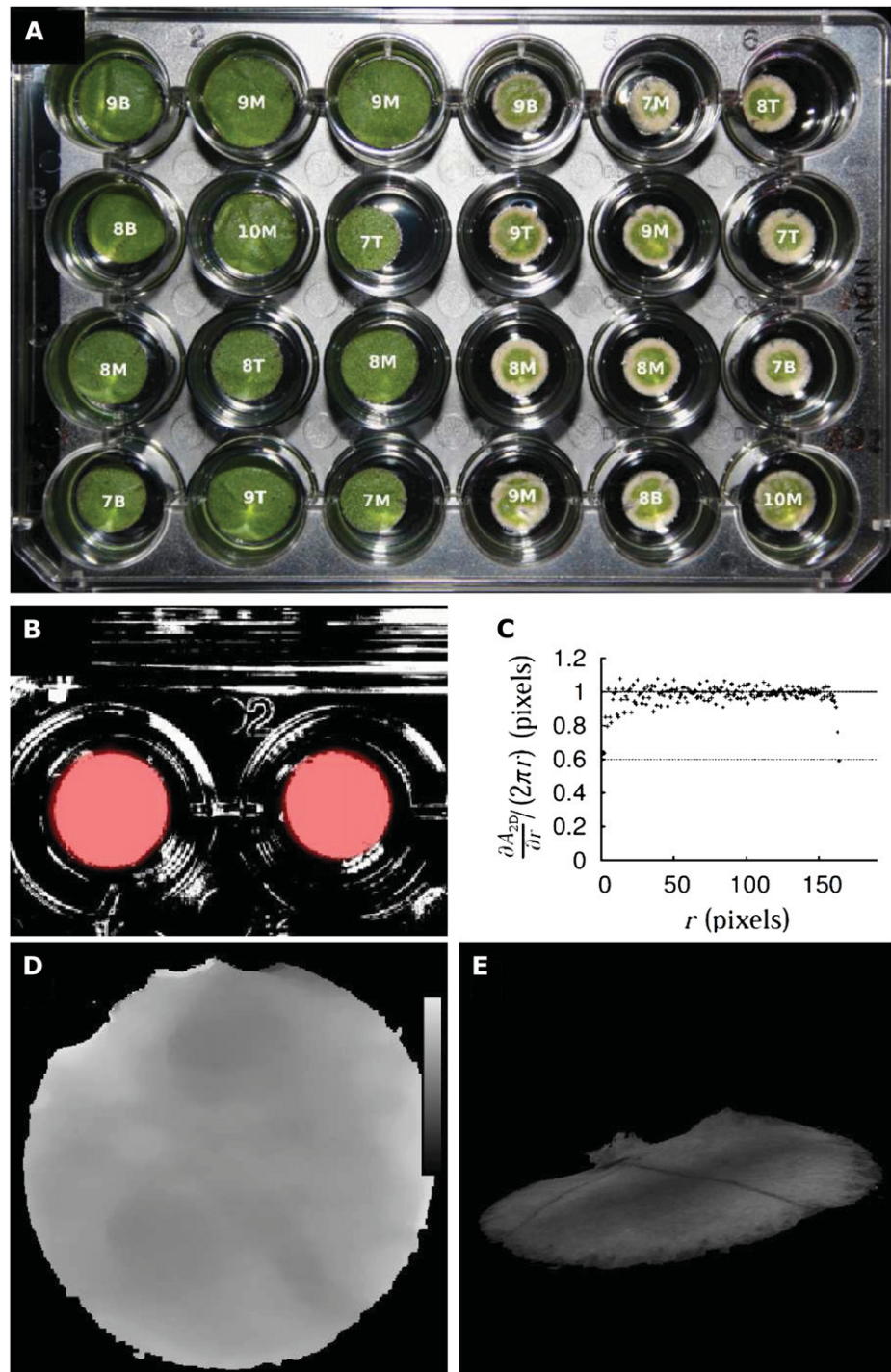
RESULTS

Technical Specification of the Setup

A total of 458 tobacco leaf discs, exposed to different conditions, were used for a case study of leaf growth measurements (Figs. 1 and 2). Running image acquisition at the highest possible rate, each individual leaf disc was visited approximately every 1.5 h. This corre-

sponds to an average acquisition job duration of 11.8 s per disc, including positioning. The experiment was terminated after 72 h. With two images taken at every time point and leaf disc position, approximately 22,000 images were produced during the experiment. 3D area reconstruction was performed with very high precision by the system (Figs. 2 and 3), as described more extensively in "Materials and Methods." Further technical

Figure 2. Examples of resulting images. A (left), Leaf discs treated with NS (nutrient solution). A (right), Leaf discs treated with HG (glyphosate at high concentration). Images were taken 72 h after the beginning of treatment. B, Binary mask M_t obtained by gray level segmentation (white, foreground; black, background); superimposed (red) are leaf disc circles as detected by computing $\partial A_{2D}/\partial r$. The final segmentation mask M_s contained those pixels of M_t closer than r to the centroid of the detected leaf disc and that had the value 1 in M_t . C, $\partial A_{2D}/\partial r$ versus r . Points show measured increase; the dashed line shows theoretical increase, $2\pi r$. D, Regularized and masked disparity map; the bar indicates the disparity range: 610 to 620 pixels. E, 3D view of a leaf disc. All depicted leaf discs are from tobacco.



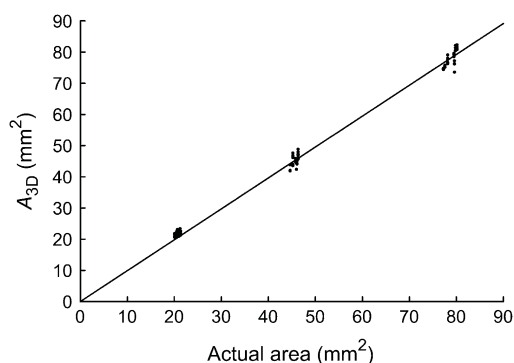


Figure 3. Accuracy of GROWSCREEN 3D determined by imaging of synthetic objects of known size. The *x* axis shows the area of paper discs determined by weighing the paper discs; the *y* axis shows A_{3D} determined using GROWSCREEN 3D. The line gives the linear fit through all data points ($y = ax$; $a = 0.991$; $R^2 = 0.9952$).

details concerning the setup and software are contained in Supplemental Appendix S1.

Base Tip Gradient and Spatial Heterogeneity of Growth

In a preliminary experiment, growth of tobacco leaf discs sampled from different leaves (leaves 7, 8, and 9) and locations along the lamina (B [base], M [middle], and T [tip]) were measured ($n = 40$) to assess the variability of growth in different regions of the plant (Walter and Schurr, 1999). This was done to determine the most suitable sampling region within the leaf canopy to test the central hypothesis on local control of leaf growth in the central experiment. Supplemental Figure S1 shows the variability of A_{3D} measured on different leaves and different locations along the lamina for the nutrient solution (NS) treatment. For locations T and B, the oldest leaves (position 7) consistently exhibited the smallest coefficients of variation [CV (A_{3D})]; younger leaves showed markedly higher CV (A_{3D}). CV (A_{3D}) in location M was similar in leaves from all positions, slowly increasing from approximately 0.025 to approximately 0.05 in the course of the experiment.

In leaves 7 and 8, a pronounced base tip gradient of growth occurred (Fig. 4). Discs cut from the base expanded more strongly than discs from the leaf tip. In leaf 9, no clear base tip gradient was found, but RGR_{3D} was higher than in leaves 7 and 8.

Since leaf 9 showed the strongest growth and since location M showed the least variability among the different leaf positions, we chose the subset of leaf discs of leaf 9, location M for detailed analysis comparing all treatments. For each replicate, A_{3D} of two subsamples (i.e. two leaf discs sampled on the same leaf; Fig. 1E) was averaged.

Growth Effects of the Incubation Solution

Leaf discs were subjected to four different treatments (Fig. 5): (1) NS; (2) water; and (3 and 4) two concentra-

tions of the herbicide glyphosate (LG, low glyphosate; HG, high glyphosate), an inhibitor of the shikimate pathway (Steinrücken and Amrhein, 1980). The treatment effect on leaf 9, location M was tested using one-way ANOVA. Variances were homogeneous according to Levene's test ($F = 2.68$, $P = 0.06$). Treatments had a significant effect on RGR_{3D} within 24 h ($F = 93.6$, $P < 0.001$). This time interval was chosen because it integrates one full diel cycle of growth. All comparisons between treatments except for LG versus HG resulted in significant differences ($P < 0.0001$). Leaf discs from NS showed highest RGR_{3D} , whereas LG-treated leaf discs grew more slowly than leaf discs incubated in water. HG-treated leaf discs showed negative growth rates, clearly indicating senescence.

Diel Growth Cycle

NS-treated leaf discs showed characteristic diel growth variations that are clearly visible in A_{2D} , A_{3D} , and RGR_{3D} (Fig. 6). The maximum diel growth rate ($RGR_{3D,max}$) occurred at approximately 8:00 AM, reaching a peak of almost $3\% h^{-1}$ on the first two mornings; the increase coincided with the onset of illumination. During the day, RGR_{3D} decreased, becoming even slower at 8:00 PM, when the light was switched off. On the third morning, $RGR_{3D,max}$ was only about $1.5\% h^{-1}$. The total increase of A_{3D} within 36 h was about 91%. In contrast, A_{2D} increased by only 81%.

The diel growth pattern was much less pronounced in water-treated leaf discs (Fig. 6F). Moreover, RGR_{3D} decayed strongly after the first 24 h, changing toward a monotonous increase superimposed by oscillations in the range of $1\% h^{-1}$. The 8:00 AM peak on the second morning reached only $1\% h^{-1}$. The total increase within 36 h was 32% for A_{3D} but only 17.4% for A_{2D} . Both glyphosate treatments caused inwardly progressing chlorosis of leaf disc borders (Fig. 2A, right), a well-known effect of glyphosate (Uotila et al., 1980; Plin-Srnic, 2005). The effect was stronger in treatment HG compared with treatment LG. Under infrared illumination, the gray values of green versus chlorotic (white) tissue did not differ; hence, area estimation was not influenced by discoloration. For LG-treated leaf discs, A_{2D} stagnated during the first hours of the experiment

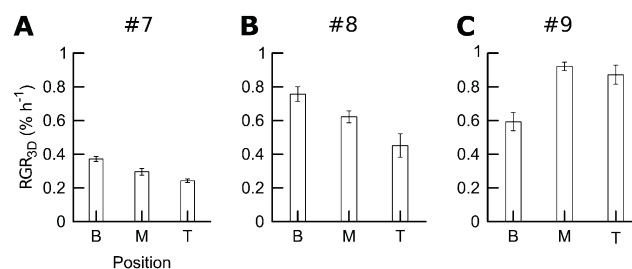


Figure 4. Base tip gradient of leaf growth in tobacco. A, Leaf 7. B, Leaf 8. C, Leaf 9. Leaf positions are as follows: B, base; M, middle; T, tip. Error bars indicate SE ($n \geq 6$). RGR_{3D} was computed between $t_1 = 0$ h and $t_2 = 48$ h.

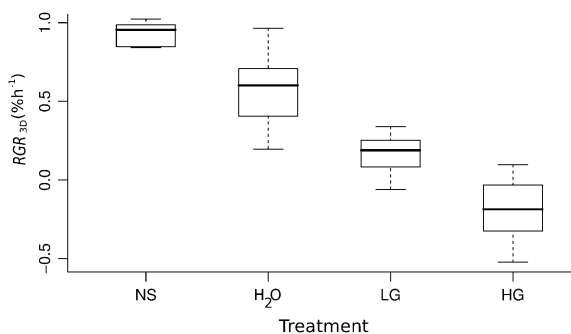


Figure 5. RGR_{3D} of leaf 9. The box plot shows the RGR_{3D} of leaf 9 between 0 h and 24 h after the beginning of the experiment, grouped by treatment ($n \geq 10$). Treatments are as follows: NS, nutrient solution; H_2O , tap water (control); LG and HG, glyphosate at low and high concentration, respectively.

and then decreased (Fig. 6G), whereas A_{3D} increased for the first hours and stagnated thereafter (Fig. 6H). Accordingly, the net change of A_{2D} over 36 h was -9.2% , while A_{3D} increased by 5.1% . $RGR_{3D,max}$ on the first morning was only $0.8\% h^{-1}$. Later on, oscillations of RGR_{3D} were much weaker compared with other treatments. Leaf discs of both glyphosate treatments did not grow any more at the end of the experiment. HG-treated leaf discs showed a net decrease of A_{2D} as well as A_{3D} . A_{2D} decreased almost linearly over 36 h, resulting in a net loss of 12.9% . A_{3D} first increased by about 2% and finally decreased by 3.3% with respect to the initial area. Although there was a weak RGR_{3D} peak in the morning ($0.3\% h^{-1}$), RGR_{3D} was very low from the beginning on.

Growth of Leaf Discs of Arabidopsis (*Landsberg erecta* versus *starch-free1*)

By analogy with the tobacco experiment, leaf discs were taken from different leaves of Arabidopsis. Discs from leaf 12 showed little growth variation and were thus chosen to determine the diel growth cycle in terms of RGR_{3D} (Fig. 7). As in tobacco, Arabidopsis leaf discs of both lines (*Landsberg erecta* [*Ler*] and *starch-free1* [*stf1*]) exhibited a growth maximum in the morning. The minimum growth rate occurred approximately 3 h after the light was switched off. During most of the night and in the early morning, RGR_{3D} was substantially higher in *Ler* than in *stf1*. In contrast, during the second half of the day, RGR_{3D} of *stf1* plants was higher than RGR_{3D} of *Ler*. The onset of RGR_{3D} increase in the morning was delayed in *stf1* in comparison with *Ler*. During the night, RGR_{3D} of *Ler* increased to more than $1\% h^{-1}$, whereas RGR_{3D} of *stf1* remained around $0.5\% h^{-1}$. RGR_{3D} amplitudes decayed over the observed time period. This effect was more pronounced in *Ler*, for which $RGR_{3D,max}$ on the second morning was only 63% of $RGR_{3D,max}$ on the first morning. In contrast, $RGR_{3D,max}$ of the *stf1* mutant only decreased to 87% compared with the value obtained on the first morning.

Growth of Leaves on Intact Plants of Arabidopsis and Tobacco

For intact plants of Arabidopsis and tobacco, similar diel cycles of leaf growth activity as reported in the literature before were observed in the conditions of this study (Fig. 8). Peak values of RGR were obtained early in the morning, and RGR decreased almost to zero during the night. Peak values were higher in intact leaves compared with leaf discs. Growth phasing in Arabidopsis *Ler* and *stf1* differed in the same way as described above for the leaf discs: *stf1* grew more slowly than *Ler* during the night and in the first half of the day, but it was able to catch up during the second half of the day.

DISCUSSION

Performance and Possible Improvements of GROWSCREEN 3D

The performance of the distributed computer system is sufficient for high-throughput screening. Computation of RGR_{3D} time series while an experiment is running ("real-time" evaluation) saves time by providing quick feedback. Depending on the hypothesis to be tested, data can be integrated in different ways (e.g. allowing one to investigate even higher numbers of leaf discs with a smaller temporal resolution or vice versa).

In future analyses, the determination of A_{3D} would benefit from improved image segmentation. This could be achieved by (1) more homogeneous illumination, (2) backlight illumination, which would provide better contrast because of vascular tissue, and (3) using a more refined segmentation algorithm (e.g. using a contour model; Kass et al., 1987; Osher and Sethian, 1988). An automated plate positioning system (e.g. a conveyor belt) could increase throughput, especially for scenarios in which only a few stereo images per leaf disc and per day are needed. Acquisition time per leaf disc could be decreased by using two or more cameras simultaneously. Depending on the optical system and working distance, these cameras might need to be mounted convergently to obtain sufficiently overlapping fields of view. Possible limitations of input/output rates could be alleviated by using multiple file servers and by balancing job result directories over these, possibly via separate network connections.

Diel Growth Cycle and Base Tip Gradient in Tobacco

Timing of the diel distribution of growth activity coincides well with the diurnal growth cycle of intact tobacco leaves (Walter and Schurr, 2000). This indicates clearly that the timing of the diel growth cycle is controlled by local regulatory mechanisms, such as the interplay between the phytochrome system and the circadian clock (Nozue et al., 2007) or light-induced elicitation of ion fluxes and alteration of membrane potential (Van Volkenburgh, 1999) rather than by long-

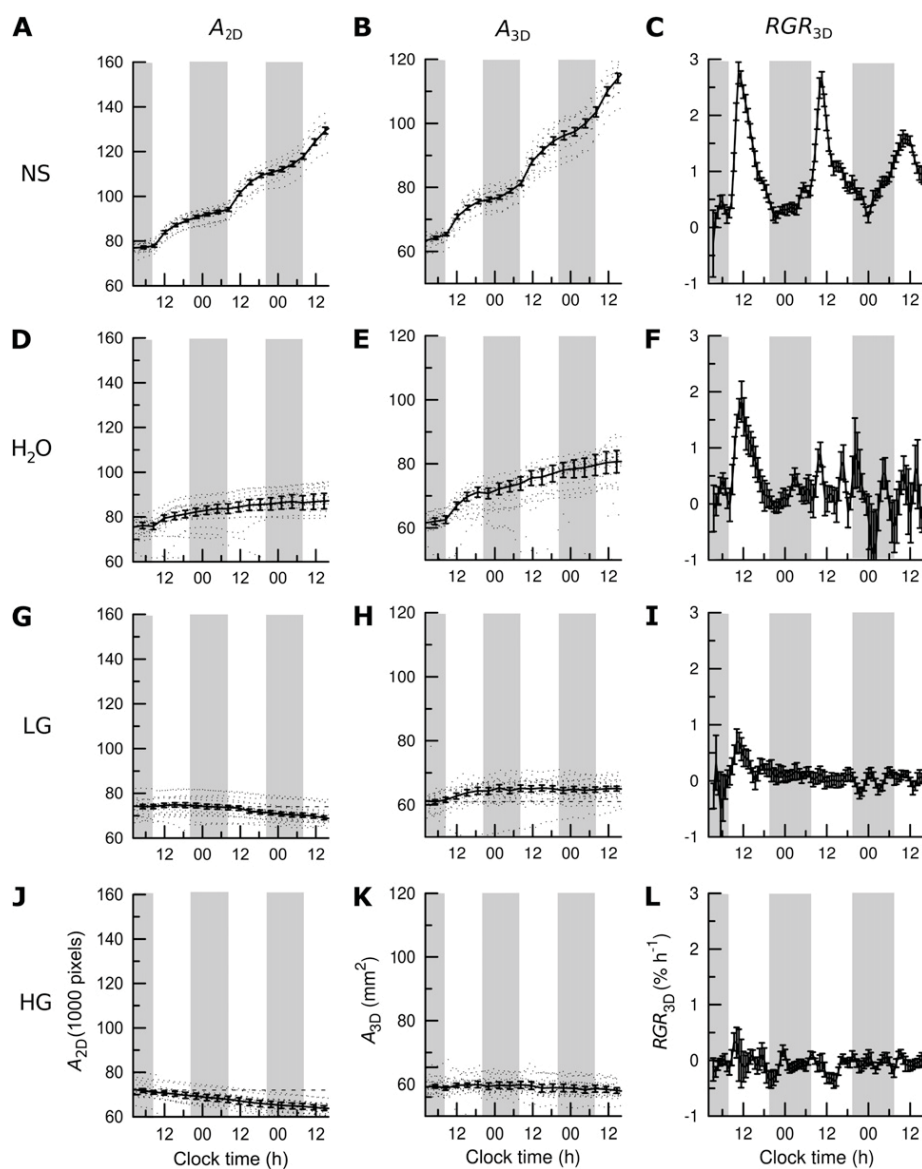


Figure 6. Time course of leaf disc area development of tobacco in A_{2D} (left panels), A_{3D} (middle panels), and RGR_{3D} (right panels). Time courses were measured on leaf 9, middle location. A to C, Treatment NS (nutrient solution). D to F, Treatment H_2O (tap water control). G to I, Treatment LG (low glyphosate concentration). J to L, Treatment HG (high glyphosate concentration). Dot traces indicate time course of areas of individual leaf discs. Solid curves show median \pm SE (HG, $n = 9$; LG, $n = 9$; NS, $n = 8$; H_2O , $n = 9$). Dotted curves show A_{3D} of individual leaf discs (including outliers). Dashed horizontal lines in LG and HG indicate areas at the beginning of measurement to illustrate the net effect of superimposed growth and the perceived shrinking due to decreasing water level. RGR_{3D} was calculated from the time course of A_{3D} (mean \pm SE). Shaded vertical bars in the background of each panel indicate night.

distance signaling via import of hormones (Rahayu et al., 2005) or carbohydrates from source leaves. The necessity of an intact local metabolism for undisturbed diel growth performance is demonstrated by the vanishing diel growth cycle in leaf discs treated with glyphosate (Fig. 5, I and L). Glyphosate is known to primarily inhibit the shikimate pathway (Steinrücken and Amrhein, 1980) and subsequently affects general metabolic processes, such as protein synthesis, photosynthesis, and carbon metabolism (Geiger et al., 1986, 1987; de María et al., 2005). Lower peak growth rates of leaf discs compared with leaves from intact plants (compare Figs. 6, 7, and 8) might be caused by missing carbohydrate import from source tissue. Although it is known from short-term experiments with excised leaf tissue that intact photosynthesis is not a prerequisite for short-term growth reactions (Dale, 1988; Van Volkenburgh, 1999),

a coordinated supply with carbohydrates for cell wall assembly and other purposes, from storage pools, source tissue, or local photosynthesis, is essential to sustain the timing of diel growth cycles for days. In addition to an undisturbed timing of carbohydrate availability, sufficient external supply of mineral nutrients is required for coordinated diel growth activity lasting several days in isolated leaf discs (Figs. 5 and 6C).

The base tip gradient in leaves 7 and 8 (Fig. 4, A and B) is in accordance with the relations in intact, growing leaves and results from the delayed initiation of the tissue at leaf emergence (Walter and Schurr, 1999). Cell expansion rate reduces with age, which is reflected by the highest RGR at the base and the lowest RGR at the tip, where cell expansion has proceeded for a longer time. In the developmental stage, at which samples were taken from leaves 7 and 8, cell divisions have

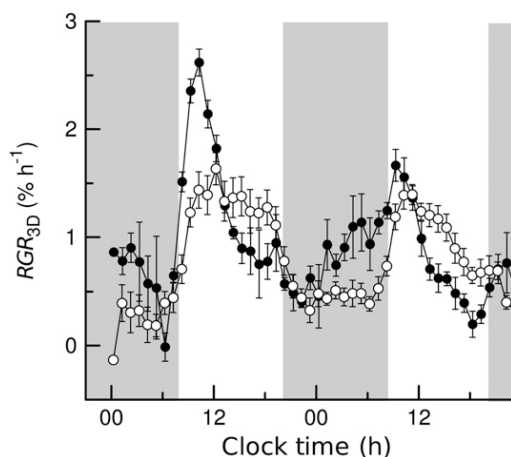


Figure 7. Diel growth cycles of leaf discs of two genotypes of *Arabidopsis*. Leaf discs of *Ler* (black circles) and *stf1* (white circles) were grown in NS. Individual area measurements were smoothed using a 2.5-h running average filter. Shaded vertical bars in the background indicate night. RGR_{3D} values are given $\pm SE$ ($n \geq 3$).

ceased at both the leaf tip and the base (Walter et al., 2003). The reversed base tip gradient in leaf 9 (Fig. 4C) might be due to cell division activity that can still be found in the leaf base of this developmental stage and with the slower rate of cell expansion in dividing cells. For undisturbed expansion of this tissue, long-distance signals might still be crucial.

For two reasons, the quality of the results increases markedly when 3D information (A_{3D}) instead of 2D information (A_{2D}) is used (Fig. 6). The first reason is that evaporation and transpiration cause the water level to decrease during a screening experiment. Using A_{3D} instead of A_{2D} allows compensating for the perceived area decrease in perspective projection. This effect may be negligible in the presence of pronounced positive RGR (e.g. under NS treatment); however, to correctly measure weaker growth rates, the compensation is clearly necessary, as it may even cause a sign reversal of RGR (apparent shrinking of leaf discs; e.g. HG treatment; Fig. 6J). The second reason is the distortion of the leaf discs during the experiment (Fig. 2): most leaf discs develop from flat discs into buckling ovate sheets, making it necessary to follow the topography of the object in three dimensions to capture its surface area correctly.

Altered Diel Growth Cycle of an *Arabidopsis* Mutant

Diel growth cycles of the *Ler* wild type and the *stf1* mutant of *Arabidopsis* were measured using GROWSCREEN 3D. The observed patterns are in good agreement with previous observations by Wiese et al. (2007). There, the growth cycles of the two lines were characterized in leaves of intact plants by means of a well-established, noninvasive digital image sequence processing (DISP) technique, along with measurements of diel carbohydrate metabolism. Yet, the

DISP technique has two major shortcomings. On the one hand, leaves need to be mechanically constrained in the focal plane of the camera, as nyctinastic movements of the entire plant would make quantitative analyses impossible. On the other hand, only small replicate numbers are possible with this technique, as one camera can only visualize the growth of one leaf. The different growth kinematics of *Ler* and *stf1* can be explained by the way that the *stf1* mutation affects the diel carbohydrate availability (Kofler et al., 2000). In the daytime, the inability to synthesize starch causes an excess of hexoses to be available; thus, higher RGR in comparison with *Ler* can be maintained by *stf1* mutants. In contrast, in the nighttime, the lack of mobilizable starch reduces *stf1* RGR. This explains the overall weaker growth in *stf1*, which has been observed by other authors for starch-free mutants before (Caspar et al., 1985; Huber and Hanson, 1992). The similarities between DISP and GROWSCREEN 3D analyses are striking, given that the growth phenotypes were observed in completely different systems (leaf discs versus intact plants). The difference between *Ler* and *stf1* indicates clearly that even transitory starch produced in the growing leaf, and not in fully developed source leaves, is sufficient to drive the coordinated growth activity of the leaf tissue. Again, this underlines the

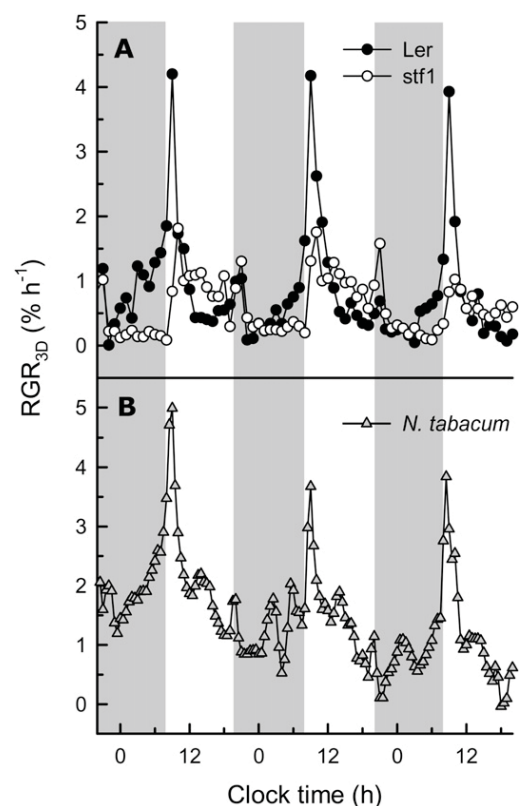


Figure 8. Leaf growth dynamics of individual intact leaves as determined by the DISP method. A, *Arabidopsis*. B, *Tobacco*. Shaded vertical bars in the background indicate night.

importance of local regulatory mechanisms controlling the diel expansion of leaf tissue.

CONCLUSION

This study introduced an image-based phenotyping system for leaf discs that uses 3D information to compensate for tissue surface deformations and sinking water levels, overcoming major disadvantages of leaf discs for growth analyses. The system has the potential for high-throughput growth assays and is capable of resolving detrimental and beneficial effects of substances added to the incubation solution. Due to the high precision of the system, characteristic features of the diel growth activity of *Arabidopsis* and tobacco leaf discs were obtained. Diel growth cycles of leaf discs resembled those of intact leaves attached to the plant very closely, demonstrating the importance of local control mechanisms on the timing of dicot leaf expansion.

MATERIALS AND METHODS

Imaging System of GROWSCREEN 3D

A brief description of the system and image-processing procedures is given below; for a more detailed description of the hardware and software (including sources of supply), refer to the Supplemental Appendix S1. GROWSCREEN 3D (Fig. 1) is based on the mechanical design of the 2D screening setup GROWSCREEN (Walter et al., 2007). Two moving stages (Fig. 1A; X and Y) are used to move a 2-megapixel camera in the horizontal plane. A third moving stage (X_2) facilitates horizontal displacement for acquiring stereo image pairs. The camera is directed downward and equipped with an infrared long-pass filter. The scene is illuminated by four near-infrared light-emitting diode arrays (Fig. 1B; wavelength, 880 nm), because near-infrared illumination is physiologically inactive. Leaf discs under investigation are kept on 24-well Microtiter plates (Fig. 5A; well volume, 2.5 mL). Lids are removed for the duration of the experiment to ensure gas exchange and to avoid fogging, which would hamper imaging. At each camera position (X and Y), two images are taken, using a stereo baseline (displacement of moving stage X_2) of $b = 20$ mm.

Image Segmentation

The purpose of image segmentation is to separate leaf discs from background. A clean segmentation is a prerequisite to precise area measurements. Because images are acquired in near-infrared light, only grayscale images are available. This allows image acquisition throughout day and night but makes segmentation more challenging in comparison with color images (Russ, 2002; Walter et al., 2007). Therefore, the following segmentation procedure is applied (Fig. 2). (1) Images are corrected for illumination uniformity. (2) Gray level thresholding is applied to remove most of the background. (3) Morphological erosion is applied to clean up the segmentation mask. (4) Leaf disc borders are detected. (5) Candidate leaf discs from both images of a pair are matched. (6) For a newly detected leaf disc, a unique identification number is assigned. (7) The projected area A_{2D} is computed for each leaf disc.

Stereo Matching and 3D Reconstruction

To measure A_{3D} and ultimately RGR_{3D} , surface models at different time points are required. Using leaf discs detected by image segmentation, 3D surface models are obtained as follows. (1) Image distortions are removed and images are rectified such that corresponding features share the same y coordinate in both images of a pair. (2) A stereo matching algorithm (Faugeras et al., 1993) is applied to compute a disparity map (a map of displacements;

Fig. 2D). (3) Outliers are removed. (4) 3D coordinates are recovered by stereo triangulation. (5) The surface model is smoothed. (6) The leaf disc surface area A_{3D} is computed (Fig. 2E).

Setup Calibration

Measurement accuracy is affected by a multitude of parameters: quality of camera and stereo calibration, position of an object in the images, object shape, object distance, object inclination, object size, color, texture, reflections, and stereo baseline, to name only some. We chose to limit our accuracy considerations to the following parameters that are most relevant to the presented study: leaf disc size (varying because of growth), object distance (varying because of sinking water level), curvature (varying because of increased bending of leaf discs during the experiment), and inclination, which changes, for example, when floating leaf discs begin to adhere to the vessel wall.

For each of these four parameters, two to three values spanning the range of expected values were selected and several replicate calibration targets were produced. This resulted in a total number of 96 calibration measurements. As calibration targets, circular paper discs with nominal diameters of 5, 7.5, and 10 mm and with leaf-like texture were printed on laser printer paper (80 g m^{-2}) and cut out. In order to determine their actual area, the discs were weighed using a laboratory scale (accuracy, 0.01 mg). Eight paper discs of each nominal diameter were glued to the round wall of a black, horizontal cylinder (diameter, 16.5 mm). Half of the discs of one diameter touched the cylinder along their entire surface, thus having the same curvature as the cylinder. The other half were connected to the cylinder only in the middle and were therefore planar. The planar discs were mounted exactly on top of the cylinder. The curved discs were mounted off-center, covering an inclination range from -36° to $+36^\circ$ around the center. Synthetic leaf discs were imaged at distances of 107, 112, 117, and 122 mm from the image plane, covering the object distances realized in the experiments.

Figure 3 shows the depiction of A_{3D} versus the area determined by weighing the paper discs. For the other three parameters tested in this calibration procedure (disc curvature, distance, and inclination), no systematic effect on A_{3D} was determined; each calibration measurement is included as a data point in Figure 3. The slight deviation of the inclination of the fit line from unity results from the weight of the laser toner printed on the calibration targets. The results demonstrate that the accuracy of GROWSCREEN 3D is sufficient for measuring leaf disc areas and consequently RGR of leaf discs in ranges encountered in typical measurement configurations. It should be noted that RGR computation does not even require absolute area measurements, because only area ratios are used.

DISP Leaf Growth Analysis in Intact Plants

Leaves were mechanically constrained to the focal plane of a camera and analyzed for RGR by a procedure described in more detail elsewhere (Walter and Schurr, 2000; Wiese et al., 2007). In short, images of flat leaves were illuminated in the near-infrared wavelength range (880 nm), ensuring image acquisition at constant brightness throughout day and night. Structural elements of the leaves, such as trichomes and vein intersections, are followed throughout parts of an image sequence, and the divergence of structural elements with time renders the relative growth rate of the tissue between structural elements. Plants were exposed to the same environmental conditions as for the leaf disc experiments.

Plant Material and Cultivation Procedures

Seeds of tobacco (*Nicotiana tabacum* 'Samsun') were germinated on well-watered soil ED73 (Einheitserde, Balster Einheitserdewerk; approximately 250 mg L^{-1} nitrogen, approximately $300 \text{ mg L}^{-1} \text{ P}_2\text{O}_5$, and approximately $400 \text{ mg L}^{-1} \text{ K}_2\text{O}$). Prior to experiments, plants were cultivated in a greenhouse in winter with a photoperiod of 12 h/12 h of light/dark. Plants were acclimated to laboratory conditions ($50 \mu\text{mol m}^{-2} \text{ s}^{-1}$ photosynthetically active radiation; same photoperiod; peak day temperature, 24.9°C ; night temperature, 22.9°C ; oscillations due to change in illumination) 24 h before the experiment began. Plants were 31 d old and vegetative at the beginning of the experiment.

Leaf discs were excised using a cork borer (9 mm i.d.) from defined locations along the lamina at the base (B), middle (M), and tip (T) of still expanding leaves 7, 8, and 9 (counting from bottom to top, including cotyledons; Fig. 1, D and E). Leaf discs were immediately transferred to their respective treatment solution, floating adaxial (top) side up.

Biskup et al.

Arabidopsis (*Arabidopsis thaliana*) plants were grown in soil in a growth chamber ($125 \mu\text{mol m}^{-2} \text{s}^{-1}$ photosynthetically active radiation with a 12-h/12-h light/dark period; temperature, 23°C during the day, 18°C at night; relative humidity, 60% during the day, 65% at night). The starch-free mutant *stf1* (Kofler et al., 2000) carries a 55-bp deletion in the plastidic phosphoglucomutase gene in the background of the *Ler* ecotype. Seeds for *stf1* were obtained from Dr. H. Kofler (University of Cologne). *Arabidopsis* plants were 32 d old and vegetative at the beginning of the experiment.

Leaf discs were excised using a cork borer (5 mm i.d.) from the middle of leaf 12, excluding the midvein.

Treatments

Tobacco leaf discs were subjected to four different treatments: (1) NS (1:10 Hakaphos nutrient solution; Hakaphos Blau) full-strength solution was prepared according to the manufacturer's specification for young flowering plants and contained 15% (w/w) nitrogen, 10% (w/w) P_2O_5 , 15% (w/w) K_2O , 2% (w/w) MgO, 0.01% (w/w) boron, 0.02% (w/w) copper, 0.05% (w/w) iron, 0.05% (w/w) manganese, 0.001% (w/w) molybdenum, and 0.015% (w/w) zinc (Ca^{2+} and SO_4^{2-} were contained in tap water); (2) tap water; (3) LG, low concentration of glyphosate ($0.74 \mu\text{mol L}^{-1}$; N-(phosphonomethyl)Gly; Clinic Nufarm); (4) HG, high concentration of glyphosate ($74 \mu\text{mol L}^{-1}$). Treatments were applied on 24-well Microtiter plates in 2 mL of liquid volume per leaf disc. The typical time until total evaporation was approximately 7 d. Leaf discs of both *Arabidopsis* lines were only subjected to treatment NS (see above).

Due to evaporation and water/nutrient uptake by the growing leaf disc, nutrient concentrations can decrease or increase during the experiment, depending on RGR and evaporative demand. pH of the nutrient solution is buffered to values between 5 and 6, depending on the strength of the solution.

Growth Rates

Assuming exponential growth of the form $A(t_2) = A(t_1) e^{\text{RGR}(t_2-t_1)}$, RGRs of leaf tissue are determined as

$$\text{RGR}[\%/d] = \frac{100}{t_2 - t_1} \ln \frac{A(t_2)}{A(t_1)}$$

where $A(t_2)$ and $A(t_1)$ are projected or actual 3D areas at two time points, t_1 and t_2 (Walter and Schurr, 1999).

Statistics

All statistical computations were carried out using the R statistics package (R Foundation). A_{3D} values more distant from the group median than ± 2 sds were considered outliers and discarded. Treatments were compared using one-way ANOVA (Faraway, 2005). Homogeneity of variances was tested using Levene's test (Levene, 1960). Pairwise comparisons of treatments were done with a pairwise *t* test, adjusting *P* values using Holm's correction (Holm, 1979).

Supplemental Data

The following materials are available in the online version of this article.

Supplemental Figure S1. Variability of area measurements.

Supplemental Figure S2. Deployment of the GROWSCREEN 3D system.

Supplemental Figure S3. Database scheme.

Supplemental Figure S4. Activity diagram of essential workflow steps.

Supplemental Figure S5. Scalability of job execution.

Supplemental Table S1. Most important database tables.

Supplemental Table S2. Third-party software.

Supplemental Table S3. Artificial job types for scalability measurements.

Supplemental Appendix S1. Technical details of GROWSCREEN 3D.

ACKNOWLEDGMENTS

We are grateful to S. Briem and G. Dreissen, who developed parts of the client software of our screening system; to A. Aversch, who maintained the network infrastructure; and to B. Uhlig for plant cultivation. M.M. Christ kindly conducted preliminary experiments on leaf discs, and H. Kofler provided seeds of the *Arabidopsis stf1* mutant.

Received December 17, 2008; accepted January 12, 2009; published January 23, 2009.

LITERATURE CITED

- Barbagallo RP, Oxborough K, Pallett KE, Baker NR** (2003) Rapid, noninvasive screening for perturbations of metabolism and plant growth using chlorophyll fluorescence imaging. *Plant Physiol* **132**: 483–493
- Caspar T, Huber SC, Somerville C** (1985) Alterations in growth, photosynthesis, and respiration in a starchless mutant of *Arabidopsis thaliana* (L.) deficient in chloroplast phosphoglucomutase activity. *Plant Physiol* **79**: 11–17
- Dale JE** (1967) Growth changes in disks cut from young leaves of Phaseolus. *J Exp Bot* **18**: 660–671
- Dale JE** (1988) The control of leaf expansion. *Annu Rev Plant Physiol Plant Mol Biol* **39**: 267–295
- de María N, de Felipe MR, Fernández-Pascual M** (2005) Alterations induced by glyphosate on lupin photosynthetic apparatus and nodule ultrastructure and some oxygen diffusion related proteins. *Plant Physiol Biochem* **43**: 985–996
- Faraway JJ** (2005) Linear Models with R. Texts in Statistical Science, Vol 63. CRC Press, Boca Raton, FL, pp 179–186
- Faugeras O, Hotz B, Mathieu H, Viéville T, Zhang Z, Fua P, Théron E, Moll L, Berry G, Vuillemin J, et al** (1993) Real Time Correlation Based Stereo: Algorithm Implementations and Applications. Technical Report 2013. INRIA Sophia Antipolis, Sophia Antipolis, France, pp 4–12
- Geiger DR, Kapitan SW, Tucci M** (1986) Glyphosate inhibits photosynthesis and allocation of carbon to starch in sugar beet leaves. *Plant Physiol* **82**: 468–472
- Geiger DR, Tucci MA, Serviates JC** (1987) Glyphosate effects on carbon assimilation and gas exchange in sugar beet leaves. *Plant Physiol* **85**: 365–369
- Gibon Y, Bessières MA, Larher F** (1997) Is glycine betaine a non-compatible solute in higher plants that do not accumulate it? *Plant Cell Environ* **20**: 329–340
- Holm S** (1979) A simple sequentially rejective multiple test procedure. *Scand J Stat* **6**: 65–70
- Huber SC, Hanson KR** (1992) Carbon partitioning and growth of a starchless mutant of *Nicotiana sylvestris*. *Plant Physiol* **99**: 1449–1454
- Kass M, Witkin A, Terzopoulos D** (1987) Snakes: active contour models. *Int J Comput Vis* **1**: 321–331
- Kofler H, Häusler RE, Schulz B, Gröner F, Flügge UI, Weber A** (2000) Molecular characterisation of a new mutant allele of the plastid phosphoglucomutase in *Arabidopsis*, and complementation of the mutant with the wild-type cDNA. *Mol Gen Genet* **263**: 978–986
- Kovács E, Sárvári E, Nyitrai P, Darók J, Cseh E, Láng F, Keresztes A** (2007) Structural-functional changes in detached cucumber leaves, and modelling these by hormone-treated leaf discs. *Plant Biol* **9**: 85–92
- Levene H** (1960) Robust tests for equality of variances. *In Contributions to Probability and Statistics*. Stanford University Press, Stanford, CA, pp 278–292
- Matsubara S, Walter A** (2006) Living in day-night cycles: specific diel leaf growth patterns and the circadian control of photomorphogenesis. *Prog Bot* **68**: 288–314
- Nozue K, Covington MF, Duek PD, Lorrain S, Fankhauser C, Harmer SL, Maloof JN** (2007) Rhythmic growth explained by coincidence between internal and external cues. *Nature* **448**: 358–363
- Osher S, Sethian JA** (1988) Fronts propagating with curvature dependent speed: algorithms based on Hamilton-Jacobi formulation. *J Comput Phys* **79**: 12–49
- Pline-Smic W** (2005) Technical performance of some commercial glyphosate-resistant crops. *Pest Manag Sci* **61**: 225–234
- Powell R, Griffith M** (1960) Some anatomical effects of kinetin and red light on disks of bean leaves. *Plant Physiol* **35**: 273–275

- Rahayu YS, Walch-Liu P, Neumann G, Römheld V, von Wiren N, Bangerth F (2005) Root-derived cytokinins as long-distance signals for NO₃-induced stimulation of leaf growth. *J Exp Bot* **56**: 1143–1152
- Russ JC (2002) *The Image Processing Handbook*, Ed 5. CRC Press, Boca Raton, FL, pp 408–412
- Stahlberg R, Van Volkenburgh E (1999) The effect of light on membrane potential, apoplastic pH and cell expansion in leaves of *Pisum sativum* L. var. *Argenteum*. *Planta* **208**: 188–195
- Steinrücken HC, Amrhein N (1980) The herbicide glyphosate is a potent inhibitor of 5-enol pyruvyl-shikimic acid-3-phosphate synthase. *Biochem Biophys Res Commun* **94**: 1207–1212
- Stiles KA, Van Volkenburgh E (2004) Role of K⁺ in leaf growth: K⁺ uptake is required for light-stimulated H⁺ efflux but not solute accumulation. *Plant Cell Environ* **27**: 315–325
- Uotila M, Evjen K, Iversen TH (1980) The effects of glyphosate on the development and cell infrastructure of white mustard (*Sinapis alba* L.) seedlings. *Weed Res* **20**: 153–158
- Van Volkenburgh E (1999) Leaf expansion: an integrating plant behaviour. *Plant Cell Environ* **22**: 1463–1473
- Walter A, Roggatz U, Schurr U (2003) Expansion kinematics are an intrinsic property of leaf development and are scaled from cell to leaf level at different nutrient availability. *Plant Biol* **5**: 642–650
- Walter A, Scharr H, Gilmer F, Zierer R, Nagel KA, Ernst M, Wiese A, Virnich O, Christ MM, Uhlig B, et al (2007) Dynamics of seedling growth acclimation towards altered light conditions can be quantified via GROWSCREEN: a setup and procedure designed for rapid optical phenotyping of different plant species. *New Phytol* **174**: 447–455
- Walter A, Schurr U (1999) The modular character of growth in *Nicotiana tabacum* plants under steady-state nutrition. *J Exp Bot* **50**: 1169–1177
- Walter A, Schurr U (2000) Spatio-temporal variation of leaf growth, development and function. In B Marshall, J Roberts, eds, *Leaf Development and Canopy Growth*. Sheffield Academic Press, Sheffield, UK, pp 96–118
- Wiese A, Christ MM, Virnich O, Schurr U, Walter A (2007) Spatio-temporal leaf growth patterns of *Arabidopsis thaliana* and evidence for sugar control of the diel leaf growth cycle. *New Phytol* **174**: 752–761

1 **SUPPLEMENTAL DATA**

2 **SUPPLEMENTAL APPENDIX 1: TECHNICAL DETAILS OF** 3 **GROWSCREEN 3D**

4 ***Key Requirements***

5 The following key requirements had to be met by the technical system to
6 achieve a high-resolution time-series analysis of leaf disc growth: (1) Full
7 automation: once acquisition and evaluation parameters are set, the system
8 must be able to run unattended, typically for days. (2) Extensibility of the
9 concept: Other screening systems, such as different imaging systems or
10 systems supporting alternative types of evaluation, should be easy to implement
11 with the same infrastructure. (3) Scalability: The system should be largely
12 independent of the size of the objects. (4) Enabling 'real-time' screening:
13 Evaluation of images should keep up with image acquisition at moderately high
14 throughput. (5) Well-structured access to result data: It should be easy to
15 implement evaluation modules or client software. (6) Image acquisition in the
16 near infrared range to allow for continuous recording during day and night.

17 ***Imaging System***

18 The hardware setup (Fig. 1A,B) is based on the design of the 2D screening
19 setup GROWSCREEN (Walter et al., 2007). It covers a rectangular area of
20 58 cm × 58 cm. Images are acquired using a Point Grey Scorpion SCOR-
21 20SOM 2 Megapixels (1600 × 1200 pixels) camera with FireWire 400
22 (IEEE 1394a; max. transfer rate: 400 MBit s) connector (Point Grey Research,
23 Vancouver, BC, Canada). A 15 mm C-mount objective lens (Rodenstock,
24 München, Germany) is mounted to the camera. The camera is directed vertically
25 downward; it carries an infra-red (IR) long pass filter (Model 27 093; Schneider-
26 Kreuznach, Bad-Kreuznach, Germany) transmissible only for wavelengths > 800
27 nm. The scene is illuminated by four IR LED arrays, each containing 18 LEDs
28 ($\lambda_{\text{max}} = 880 \text{ nm}$; Conrad Electronic, Hirschau, Germany). IR illumination is

1 physiologically inactive and has the additional advantage of enhancing contrast
2 of plant tissue. The LED arrays stay on during the entire experiment to reduce
3 temperature-dependent intensity drift which was observed to settle to within 1%
4 of the steady state value only after >20 min. Five images are averaged per
5 position to decrease noise. Images are acquired at a resolution of 1280 × 960
6 pixels and stored in TIFF format (using lossless PackBits compression).

7 The camera and IR illumination unit are moved in the horizontal plane by two
8 highly precise displacement stages ('X' and 'Y'; Pico-Maxi, Type FMD-
9 LPT80.550.1205-SM, Laser 2000 GmbH, München, Germany). The
10 displacement stages are equipped with microstepping motors (MDrive 23 Plus;
11 Intelligent Motion Systems, Marlborough, USA). A third displacement stage ('X₂')
12 is used to move the camera in X direction when taking stereo images, while
13 keeping the IR illumination in constant position. This is necessary because
14 stereo matching requires constant illumination (see below). The positioning
15 system is mounted on a solid stand built of X-95 profile elements (Linos
16 Photonics, Göttingen, Germany).

17 Leaf discs under investigation are kept in 24-well Microtiter plates (Fig. 6A;
18 Nunc, Roskilde Denmark). The 24 wells are equally spaced and have a volume
19 of 2.5 ml each. Lids are removed for the duration of the experiment to ensure
20 gas exchange and to avoid fogging which would hamper imaging. The plates
21 rested on a platform that is adjustable for height at the corners (Swiss BOY 110,
22 Rudolf Grauer AG, Degersheim, Switzerland). A water level is used to ensure
23 the platform is aligned parallel to the XY plane of the acquisition system to avoid
24 depth-of-field and perspective problems. The platform is covered with smooth
25 black plastic tarp which reflected little IR radiation, providing a suitable
26 background for image segmentation.

1 **Computers**

2 Fig S2 schematically shows the hardware components of GROWSCREEN 3D
3 and the software components running on each computer. The image acquisition
4 is done on a personal computer (called MASTER in the following; (Intel®
5 Pentium® 4 DualCore, 2 GB DDR400 RAM (Intel, Santa Clara, USA), SuSE
6 Linux 10.2; SuSE, 2006), which also hosts a multi-user database (see below).

7 In addition, several Linux computers are available to process the acquired
8 images. Five Intel® Pentium® 4 DualCore computers (cluster nodes) equipped
9 with 1 GB DDR 400 RAM each, running SuSE Linux 10.2 (Novell, Provo, USA)
10 are dedicated to the screening system. In addition, several other Linux
11 workstations running either SuSE 10.2 (32 or 64-bit) or Ubuntu Linux 7.04
12 (Canonical, Douglas, UK) are temporarily available. These computers are
13 shared with other users; on these machines, the priority of screening processes
14 is usually reduced to consume only excess CPU time. The number of nodes is
15 higher than would be required for 'real-time' processing to allow timely re-
16 computation in case parameters need to be modified.

17 All participating computers are connected via a fast Gigabit network, which is
18 crucial to avoid bottlenecks when running multiple simultaneous evaluations.

19 **Data management**

20 Data management is achieved via a MySQL database (MySQL AB, Uppsala,
21 Sweden) in conjunction with a file server. Stock and dynamic data of the
22 screening system get stored in the database and are accessible via the network.
23 The database forms the basis of communication between the core components
24 and cluster nodes.

25 Images and other bulk data are stored on a file server that is accessible from
26 each node as a common Internet file system (CIFS) share. Files stored on this
27 server are referenced by their path; the database stores metadata (e.g. type,
28 origin, creation date) along with each result path.

29 Supplemental Table S1 shows the main database tables of GROWSCREEN
30 3D. The conceptual database scheme is depicted in Supplemental Fig. S5. The

1 scheme is partitioned in tables related to configuration, job handling, workflow
2 and plant information.

3 ***Parallelization and workflow concept***

4 The processing of acquired images was implemented using the workflow
5 paradigm (Ellis, 1999), breaking down the complete task in a series of distinct
6 workflow steps. This way, (1) processing steps can be re-used in other
7 workflows, (2) the evaluation is easily parallelizable, and (3) intermediate results
8 can be resorted to if a particular workflow step is to be re-executed with different
9 settings. Supplemental Fig. S4 shows the steps involved in computing the
10 3D area of leaf discs from the originally acquired images.

11 ***Camera and stereo calibration***

12 Before doing experiments, the camera is calibrated using a well-established
13 method based on Zhang (1999, 2000): a minimum of 30 images is acquired of a
14 chessboard pattern positioned in arbitrary orientations, spanning the working
15 volume (10–15 cm from the camera center). Intrinsic parameters (focal length,
16 principal point, skew coefficient, radial and tangential distortion) are estimated
17 using the OpenCV implementation of J. Y. Bouguet's camera calibration toolbox
18 (Bouguet, 2005; Intel, Santa Clara, CA, USA).

19 Stereo calibration, i.e. the determination of extrinsic parameters (rotation and
20 translation of camera reference frames with respect to each other), is achieved
21 by two means: since highly precise displacement stages are used for camera
22 translation, the stereo baseline is known precisely, and there is no rotation
23 between camera axes. However, due to a possible slight rotation of the CCD
24 sensor in the XY plane, the direction of camera motion may deviate from the
25 orientation of scan lines on the sensor. Since the rotation angle is fixed, the
26 vertical deviation is linearly dependent on the length of the stereo baseline. To
27 compensate for this effect, which can degrade the quality of 3D reconstruction
28 and consequently of area measurements, the positions of approx. 40 landmark
29 points in the image are determined using the panorama stitching software Hugin
30 (D'Angelo, 2007) to compute the average rotation angle for later rectification.

1 This procedure needs to be carried out only once after mounting the camera.

2

3 ***Image acquisition***

4 Predefined acquisition positions (Fig. 1F) are visited in optimal order as
5 determined using Dijkstra's algorithm (Dijkstra, 1959) to minimize positioning
6 time. At each such position p_{acq} , two images are acquired with a stereo baseline
7 $b = 20$ mm. It is desirable to use a large baseline, because larger disparities
8 mean better depth resolution; however, the value was chosen such that the leaf
9 discs are completely visible in both images of a stereo pair during the entire
10 experiment.

11

12 ***Image segmentation***

13 The necessity of using IR illumination instead of visible light makes
14 segmentation more challenging: with color images, segmentation of green plant
15 tissue would be straightforward (Russ, 2002; Walter et al., 2007). However,
16 given the limited spectrum of the IR illumination and IR blocking filter, only
17 grayscale images are available. Using black plastic tarp as background
18 facilitates threshold-based segmentation, but the walls of the wells of the
19 microtiter plates cannot be separated from leaf discs by gray level alone.
20 Therefore, the following segmentation procedure is applied: (1) Acquisition
21 images I_{acq} are corrected for intensity variations (due to inhomogeneous
22 illumination) in the XY plane using reference (background) images (Jähne,
23 2002). (2) Binary masks, \mathbf{M}_t , are created from the acquired images using
24 minimum and maximum intensity thresholds, and (8-bit) gray values. These
25 values separate leaf discs and background well. (3) Mask borders are
26 morphologically eroded by thresholding the distance transform of \mathbf{M}_t , discarding
27 mask pixels with a distance below 10 pixels to the border. This value removes
28 irregularities at the border of leaf discs. Then, the centroid \mathbf{c}_i of each candidate
29 leaf disc is determined from the remaining pixels. (4) The increase of the
30 number of pixels (pixel area) with increasing distance r from \mathbf{c}_i , $\partial A_{2D} / \partial r$, is used

1 to determine the bounds of a leaf disc: The radius r_{\max} at which $\partial A_{2D} / \partial r$ falls
2 short of 0.6 times the theoretical increase of a solid disk, $2\pi r$, is used as a bound
3 for the segmentation of the leaf disc (Fig. 6B and C), yielding the final
4 segmentation mask \mathbf{M}_s . (5) Candidate leaf discs from both images of a stereo
5 pair are matched using the expected horizontal disparity of their centroids, $d_c =$
6 650 ± 100 pixels. If no candidate leaf discs are present in an image, the job is
7 flagged as *INVALID* to avoid downstream processing. (6) If no plant tissue has
8 previously been detected in the position of a leaf disc in the proximity of
9 360 pixels, a new unique identifier (`plant_id`) is created; otherwise, an existing
10 `plant_id` is assigned to the leaf disc to allow later retrieval of observations by leaf
11 disc. (7) The projected leaf disc area A_{2D} is measured as the total number of
12 non-zero pixels in \mathbf{M}_s of the first image (of a stereo pair) at a given position.
13 (8) To reduce data volume, bounding box regions of interest (ROI) containing
14 the detected leaf discs and segmentation masks are cut from \mathbf{I}_{acq} and stored on
15 the file server along with the ROI geometry for later reconstruction.

16

17 ***Stereo matching and 3D reconstruction***

18 Leaf disc image pairs created in the previous steps are used to create a
19 depth map using 2-view stereo.

20 (1) Images are rectified to align the CCD sensor scan lines with the direction
21 of camera motion by applying a rotation of -0.09° around the center of \mathbf{I}_{acq}
22 (determined with the software program Hugin (D'Angelo, 2007); see above) to
23 both images. Rotated images are resampled using bilinear interpolation. (2) A
24 correlation-based stereo algorithm (Faugeras et al., 1993; Biskup et al., 2007) is
25 applied to the rectified images. In short, this algorithm attempts to find the
26 disparity (i.e. shift of image features between images taken at different camera
27 positions) for each pixel in the first input image. A correlation function (C_2 in
28 Faugeras et al. (1993)) is used to compare rectangular image regions
29 (correspondence search). Because of the camera pose and the rectification
30 done in step (1), disparities can only be in horizontal direction, thus

1 correspondence search only needs to be done in 1D rather than in 2D (Hartley
 2 and Zisserman, 2004; Trucco and Verri, 1998). Stereo matching was carried out
 3 with the predetermined disparity range [620;680] (correlation mask size:
 4 35×15), producing a disparity image \mathbf{D} (Fig. 6D). (3) Outliers in \mathbf{D} are removed
 5 by applying a disc median filter (radius: 25 pixels). Since the objective is to
 6 measure the surface area of the entire leaf disc, a closed surface is needed.
 7 Therefore, points for which no matches could be obtained (Faugeras et al.,
 8 1993) are interpolated from surrounding matches using normalized convolution
 9 (Knutson and Westin, 1993), yielding a regularized disparity image, \mathbf{D}_{reg} . (4) The
 10 intrinsic calibration parameters, along with the known extrinsic parameters, are
 11 used to triangulate the 3D position of each point in \mathbf{D}_{reg} , resulting in the
 12 Euclidean coordinates image \mathbf{W} , storing the coordinates X , Y and Z in slices.
 13 (5) The depth Z of the 3D point cloud of the previous step is smoothed with a
 14 disc average filter (radius: 15 pixels) to ensure the subsequent area
 15 measurement will only reflect large scale surface structure, omitting unevenness
 16 due to quantization noise. (6) The 3D surface area of the leaf disc is measured
 17 using the knowledge of point proximity relationships on subsampled grid \mathbf{W}
 18 containing only every 7th vertex in X and Y direction, Triangular areas of 3
 19 neighboring points are added to obtain the total area

$$A_{3D} = \sum_{y=1}^h \sum_{x=1}^w A_{\Delta}(\mathbf{W}_{x,y}, \mathbf{W}_{x-1,y}, \mathbf{W}_{x-1,y-1})$$

20

21

22

23

24 where w and h are the width and height of \mathbf{W} , respectively and A_{Δ} is the area
 25 of a triangle specified by three 3-vectors.

26 **Software architecture**

27 GROWSCREEN 3D mostly relies on Open Source software. Supplemental

1 Supplemental Table S2 lists third-party software components used for building
2 the system.

3 The client software (program `client`) was implemented in C++/Qt (Trolltech,
4 Oslo, Norway). Its main purposes are (1) to parameterize new campaigns
5 (measurement intervals, etc.); (2) to allow adjusting camera and displacement
6 stage settings; (3) to create an overview image of the whole working area
7 (Fig. 1C) and to allow selection of positions at which images are to be acquired
8 (Fig. 1F); (4) to allow monitoring the running system by providing runtime
9 statistics such as average execution time of jobs, or system load. The program
10 runs on Linux and Win32 platforms.

11 **Performance**

12 To measure the performance of the distributed computer system, the average
13 execution time of different artificial job types was analyzed (Supplemental
14 Table S3). The measurements were repeated with different numbers of nodes
15 active to determine scalability. The distributed system used for the performance
16 test consisted of one 64-bit 2.6 GHz DualCore computer hosting the database
17 and acquisition software, and five 32-bit Intel® Pentium® 4 DualCore computers
18 for job processing (*nodes*). In the maximum configuration of the performance
19 test, two `consumer` processes were started on each node. Supplemental Fig. S3
20 shows scalability under different artificial job scenarios. `EMPTY` and
21 `CPU_BOUND` jobs have very similar characteristics, scaling almost linearly over
22 the range of 1-10 CPUs. `IO_BOUND` jobs show little scalability, with throughput
23 increasing to only 300%. Typical real jobs behave more like `CPU_BOUND` jobs,
24 in particular because only input/output destined to or from the file server, and not
25 local input/output, impedes execution speed of other nodes.

26 **Server programs**

27 Server programs were implemented using the Python programming language
28 (Van Rossum, 2006) and using the SWIG wrapper generator (Beazley, 1996) to
29 create bindings to performance-critical and low-level C++ code. The program
30 workflow periodically checks the database table *job* for jobs that have timed out

1 or reached state ERROR and re-schedules such jobs. Moreover, workflow rules
2 are applied, possibly resulting in the creation of new jobs. The program
3 consumer (running on each node) executes jobs in state NEW. The program is
4 started twice on each dual processor machine. The program watchdog
5 periodically checked the database and the file system for problematic conditions,
6 e.g. job backlog or insufficient disk space, and warns the administrator via e-
7 mail.

8

9 LITERATURE CITED

- 10 **Beazley DM** (1996) SWIG: an easy to use tool for integrating scripting
11 languages with C and C++. In: TCLTK'96: Proceedings of the 4th conference
12 on USENIX Tcl/TkWorkshop, 1996, Berkeley, CA. USENIX Association, pp.
13 15–15
- 14 **Biskup B, Scharr H, Schurr U, Rascher U** (2007) A stereo imaging system for
15 measuring structural parameters of plant canopies. *Plant, Cell Environ* **30**:
16 1299 – 1308
- 17 **Bouquet, J-Y** (2005) Calibration toolbox for Matlab.
18 http://www.vision.caltech.edu/bouquet/calib_doc/
- 19 **D'Angelo P** (2007) Image Stitching Software, version 0.7 beta 4
- 20 **Dijkstra EW** (1959) A note on two problems in connexion with graphs. *Numer*
21 *Math* **1**: 269–271
- 22 **Ellis CA** (1999) Workflow technology. In: Beaudouin-Lafon, M. (Ed.), *Computer*
23 *Supported Co-operative Work*, volume 7 of *Trends in Software*, pp. 29–54.
24 John Wiley & Sons Ltd., Chichester, UK
- 25 **Faugeras O, Hotz B, Mathieu H, Viéville T, Zhang Z, Fua P, Théron E, Moll**
26 **L, Berry G, Vuillemin J, Bertin P, Proy C** (1993) Real time correlation
27 based stereo: algorithm implementations and applications. Technical Report
28 2013, INRIA Sophia Antipolis
- 29 **Hartley RI, Zisserman A** (2004) *Multiple View Geometry in Computer Vision*.

-
- 1 Cambridge University Press, Cambridge, UK, second edition
- 2 **Jähne B** (2002) Digital Image Processing (3rd ed.): Concepts, Algorithms, and
3 Scientific Applications. Springer-Verlag, London, UK
- 4 **Knutsson H and Westin CF** (1993) Normalized and differential convolution. In:
5 IEEE Computer Vision and Pattern Recognition or CVPR. pp. 515–523
- 6 **Russ JC** (2002) The image processing handbook. CRC Press, Inc., Boca
7 Raton, FL
- 8 **Trucco E, Verri A** (1998) Introductory Techniques for 3–D Computer Vision.
9 Prentice Hall PTR, Upper Saddle River
- 10 **Van Rossum G** (2006) Python programming language, version 2.5.1
- 11 **Walter A, Scharr H, Gilmer F, Zierler R, Nagel KA, Ernst M, Wiese A, Virnich
12 O, Christ MM, Uhlig B, Jünger S, Schurr U** (2007) Dynamics of seedling
13 growth acclimation towards altered light conditions can be quantified via
14 GROWSCREEN: a setup and procedure designed for rapid optical
15 phenotyping of different plant species. *New Phytol* **174**: 447–455
- 16 **Zhang Z** (1999) Flexible camera calibration by viewing a plane from unknown
17 orientations. In: *Int J Comput Vision* pp. 666 – 673
- 18 **Zhang Z** (2000) A flexible new technique for camera calibration. *IEEE T Pattern
19 Anal* **22**: 1330-1334
- 20

1 TABLES

2

Table S1. Most important database tables. The total number of database tables is 23. Database tables are arranged according to functional groups.

Group	Table name	Description	Cardinality
Configuration	<i>config_spec</i>	Specification of configuration parameters (type, cardinality, etc).	≈ 100 entries
	<i>campaign</i>	Campaign (experiment) data, e.g. cycle time, start & end date, etc.	One entry per campaign
	<i>config</i>	Default configuration settings	Same number of entries as <i>config_spec</i>
	<i>campaign_config</i>	Configuration parameters for a particular campaign	Same number of entries as <i>config</i> , for each campaign
Workflow	<i>rules</i>	Workflow rules	≈ 10 for a typical workflow
	<i>job</i>	Smallest unit of processing	Several thousand, depending on length and frequency of campaign
	<i>result</i>	One entry for each result	dto.
	<i>observation</i>	One entry for each observation	dto.
	<i>nodes</i>	List of available cluster nodes	Typically 5-10
Analysis	<i>plant</i>	Unique identifiers (<i>plant_id</i>) for leaf discs, along with position information	One entry for each leaf disc
	<i>plant_observations</i>	One leaf disc may have <i>n</i> observations, e.g. .	
Miscellaneous	<i>logging</i>	Log messages from all nodes	Few hundred to several thousand per campaign; depending on log

<i>core_state</i>	Current state of acquisition mode; activation state of job processing	level. One entry per acquisition system
<i>local_cache</i>	Administrative table to handle local caching of acquired images	One (temporary) entry for each acquisition result

1

2

Table S2. Third-party software

Software package	Version	Description	Reference
geomview	1.8.1	Viewer for 3D models	Amenta <i>et al.</i> (2005)
hugin	0.6.1	Panorama stitching software	P. D'Angelo (2006)
ImageMagick	6.2.4.5	Image processing library, especially for conversions	ImageMagick Studio
MySQL	5.0.45	MySQL database	MySQL AB, Uppsala, Sweden
OpenCV	1.0	Image processing library	Intel, Santa Clara, USA
Python	2.5	Programming language	Van Rossum (2006)
Qt	3.4	Class library	Trolltech, Oslo, Norway
R	2.4.1	Statistics package	R Foundation
scipy	0.5.2	Scientific Python, incorporating Lapack and BLAS	Jones <i>et al.</i> (2007)
SuSE Linux	10.2 OSS	Operating system	Novell, Provo, USA
SWIG	1.3.31	Interface wrapper generator; used to create interface from C++ to Python	Beazley (1996)
Ubuntu Linux	7.04 Feisty Fawn	Operating system (used on some nodes)	Canonical, Douglas, UK
vigra	1.5.0	Image processing library	Köthe (2000); Jähne (1999)
xampp	1.6.3b	Apache (2.0) web server, MySQL (5.0.45), phpMyAdmin (2.9.1) administration tool for MySQL	Apache Friends

2

3

Table S3. Artificial job types for scalability measurements

Job type	Description	Average duration in sequential mode (s)
EMPTY	Pure overhead; no computation	0.02
CPUBOUND	Computation	46
MIXED	Computation: 10 the computation ; generation of 10 MB file	14
IOBOUND	Generates a 10 MB file (typical output size of a real job)	3

1

2

3

1 FIGURES

2 **Figure S1.** Variability (coefficient of variation, CV) of A_{3D} under NS treatment.
3 Open squares: leaf #7; closed squares: leaf #8; open circles: leaf #9.

4

5 **Figure S2.** Deployment of GROWSCREEN 3D. A Gigabit network connects
6 MASTER (hosting image acquisition, database and workflow engine), client
7 computer, file server, backup system, Linux cluster and additional computers
8 used for evaluation. Rectangular boxes indicate screening programs.

9

10 **Figure S3.** Conceptual database scheme (simplified). The scheme depicts
11 relations of important tables with selected fields. Open diamond: 1:1
12 relationship; half-open diamond: 1:n relationship).

13

14 **Figure S4.** Activity diagram of essential workflow steps (in Unified Modeling
15 Language (UML) notation). Workflow rules are stored in the database table rules
16 (Table S1). There are two kinds of workflow rules: (1) state-based rules that
17 trigger for a particular combination of workflow step and state (e.g. OK or
18 ERROR); an example would be the creation of a leaf disc segmentation job for
19 each acquisition job. (2) code-based rules, that execute a piece of code,
20 typically involving SQL statements to decide whether new jobs need to be
21 created. An example of the latter would be the creation of overview images once
22 all images for a cycle have been completed.

23

24 **Figure S5.** Scalability of job execution. Open squares: EMPTY job; open circles:
25 CPUBOUND jobs; closed squares: IO BOUND jobs; closed circles: MIXED jobs.

26 For comparison, the throughput of each job type has been normalized to

27 sequential execution speed. Error bars indicate standard errors (SEM; $n = 3$).

Supplemental figures

Fig. S1

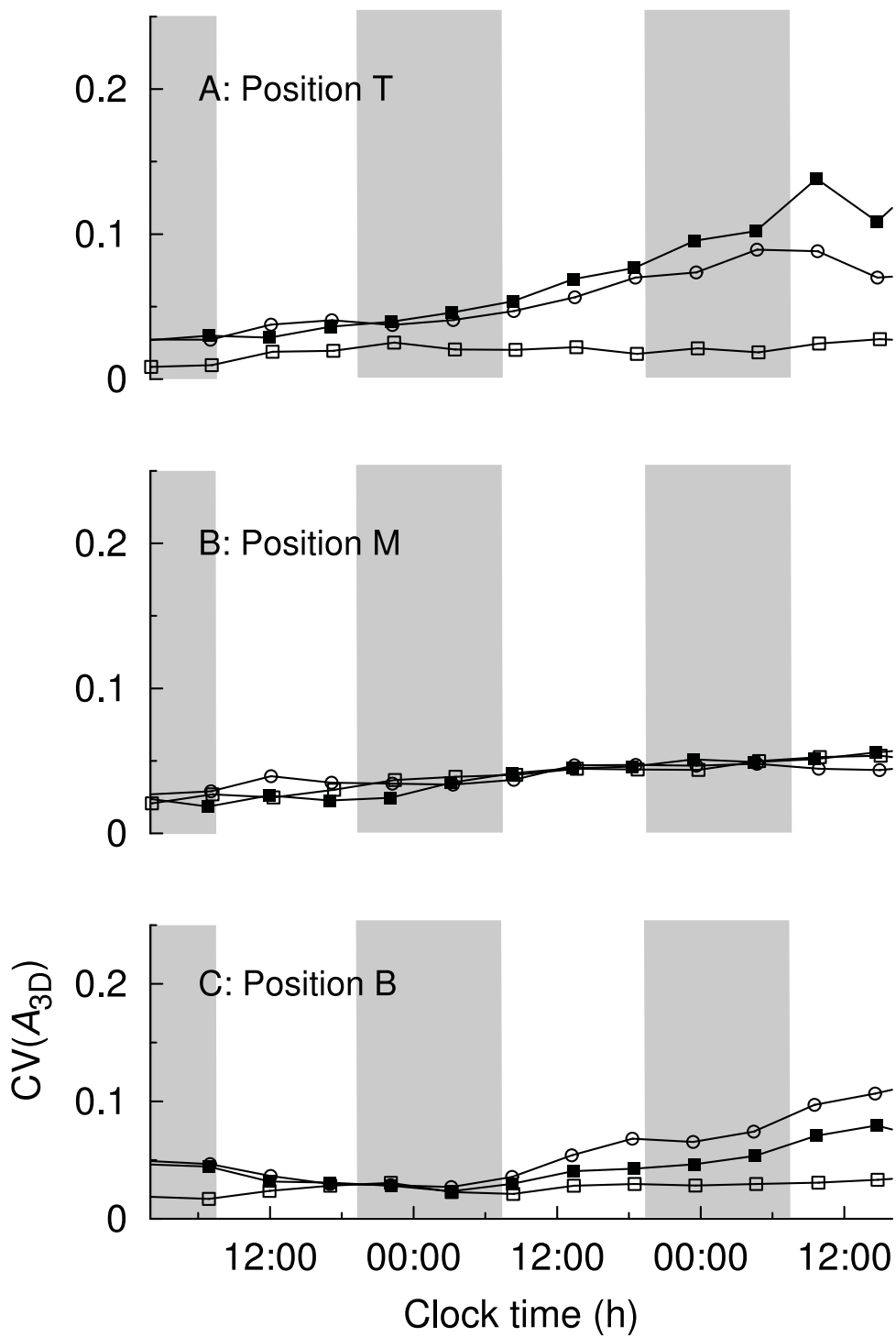


Fig. S2

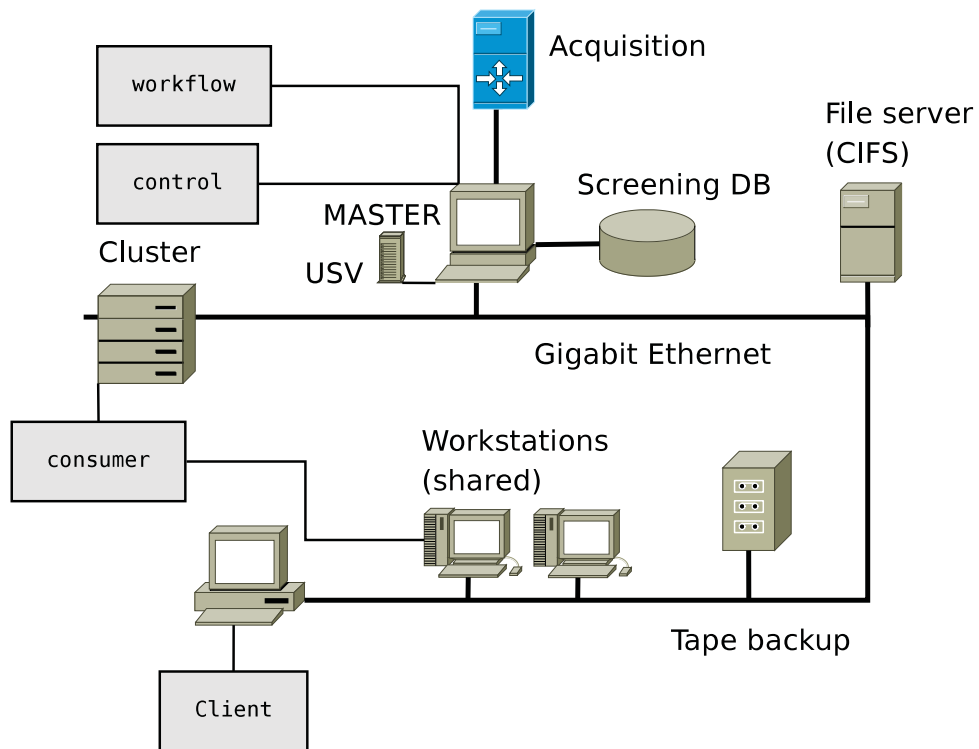


Fig. S3

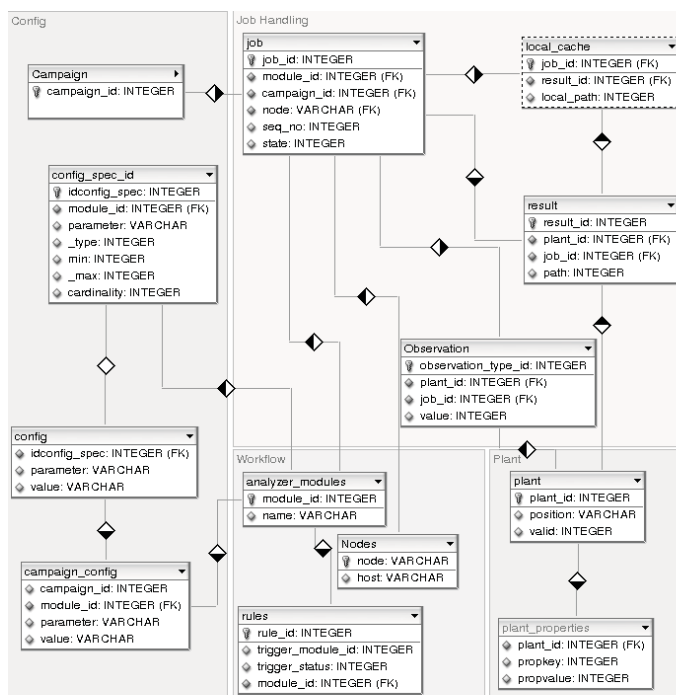


Fig. S4

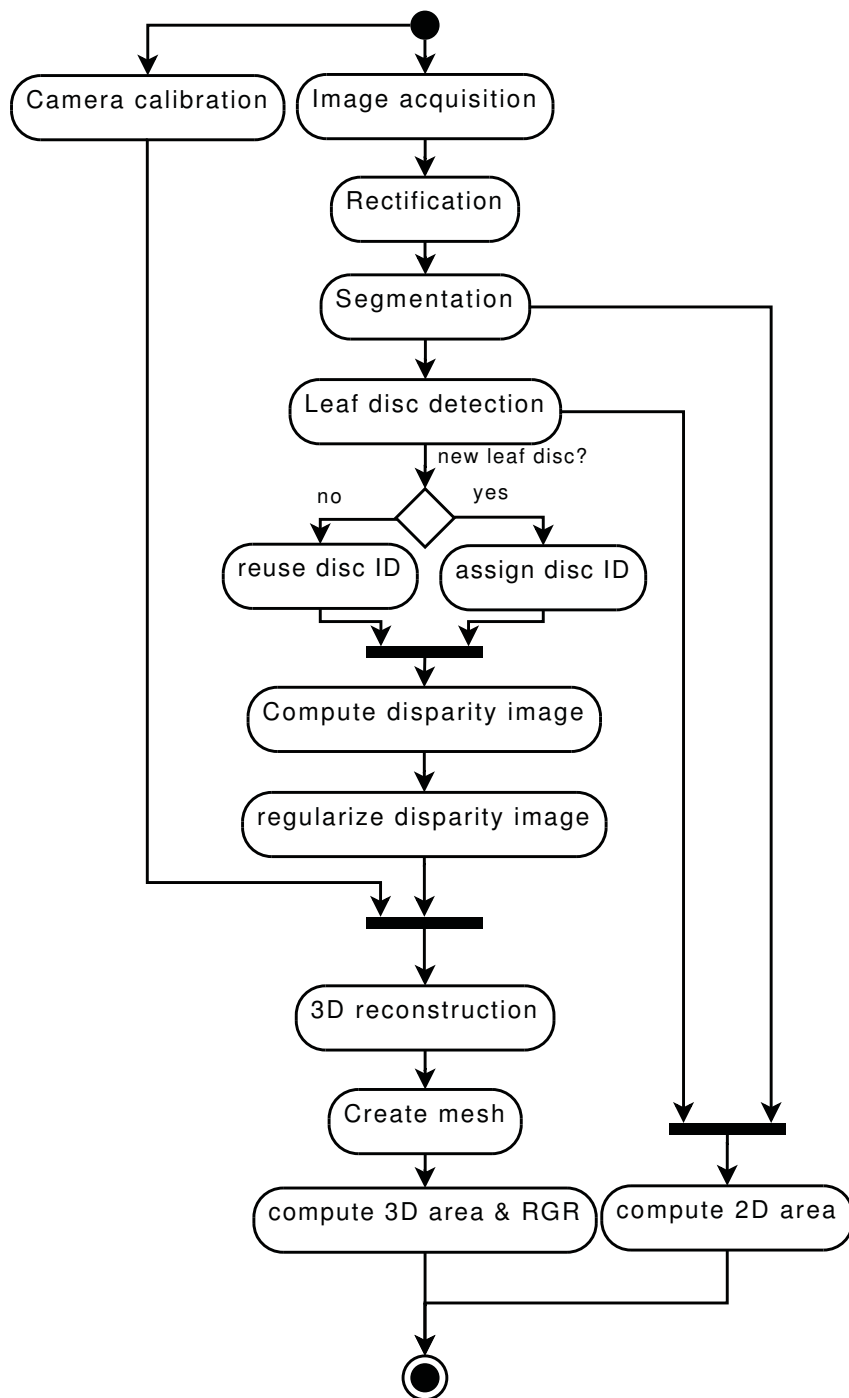
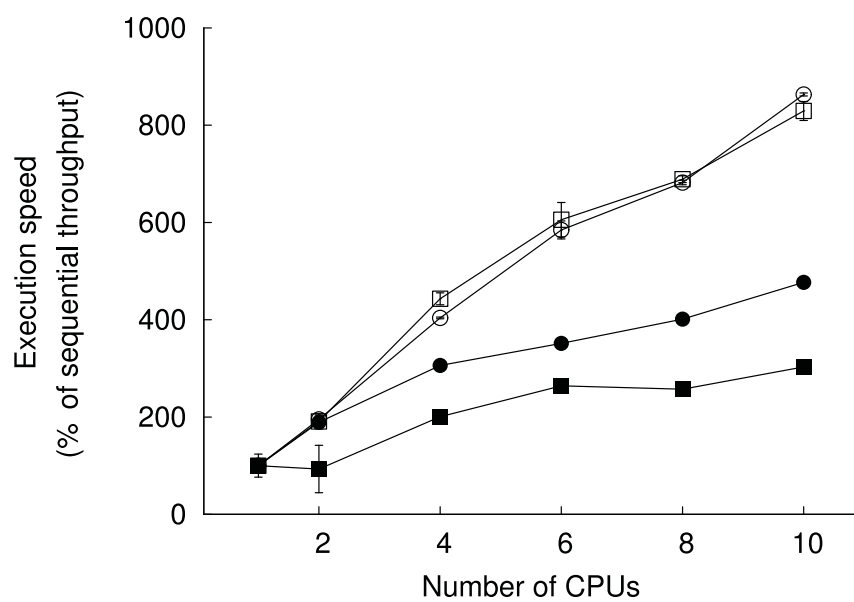


Fig. S5



6 Acknowledgements

I would not have been able to complete my dissertation without the direct or indirect involvement of the following people, to whom I would like to express my sincere gratitude:

- Prof. Elizabeth van Volkenburgh, Prof. Lisa Ainsworth, Prof. Andrew Leakey, Dr. Ladislav Nedbal, Dr. Maja M. Christ, PD Dr. Heike Schneider, Dr. Andrés Chavarría-Krauser and Tobias Schuchert for helpful and stimulating discussion on growth measurements on leaf discs and on leaf movement.
 - Dr. Ralf Küsters, my 'predecessor', for introducing me to 3D growth measurements.
 - Jaromir Borzuchowski, Dr. Andreas Ulbrich, Anna Schochow, Karin Pietzsch, Georg Dreissen and Jessica Stroka for using the 3D reconstruction software (Biskup *et al.* 2007) and for making suggestions to improve software and documentation.
 - Michael Frank for conducting joint measurement campaigns at SoyFACE, Urbana-Champaign, USA.
 - Monika Wessing, Dr. Anika Wiese-Klinkenberg and Anup Karwa for providing useful feedback as users of GROWSCREEN 3D.
 - Andreas Fischbach, Sabine Briem, Georg Dreissen, André Erler and Torge Herber for software development.
 - Beate Uhlig on behalf of the entire greenhouse staff at ICG-3, for plant cultivation and guidance about cultivation procedures.
 - Prof. Dr. Gerhard Thiel for supporting my plans to pursue a PhD project.
 - Prof. Dr. Ulrich Schurr for giving me the opportunity to work on a very interesting and timely topic for a PhD project, for his scientific guidance and for providing financial support.
- Dr. Uwe Rascher, Dr. Achim Walter and Dr. Hanno Scharr for continuous supervision, guidance and support in pursuing my PhD project.
- Our Au-pair Elena Buzalskova and our babysitters Natasza Niedziolka, Dorota Swedzka and Ludmilla Semmenikova for reliably and fondly taking care of our daughters.
 - My mother-in-law Eleonore Reher, for the many time she took care of our sick kids.
 - My parents, for all kinds of valuable support and encouragement during the past years.
 - My wife Jutta Biskup, for her love and support.
 - My daughters Annika and Lilith, who beared my absence and absent-mindedness and who always cheer me up.

Curriculum Vitae

Bernhard Biskup

* 21/01/1971, Bergisch Gladbach, Germany

Nationality: German

married; two daughters

Professional Life

01/2009 – present	Scientific assistant/postgraduate , Institute of Chemistry and Dynamics of the Geosphere – Phytosphere (ICG-3), Forschungszentrum Jülich GmbH, Jülich, Germany: Spin-off evaluation project funded by Helmholtz Enterprise Fonds
06/2008 – 12/2008	Freelance software developer , Köln, Germany
10/2004 – 05/2008	Scientific assistant/postgraduate , Forschungszentrum Jülich GmbH
10/2002 – 09/2004	Software developer , Bardenheuer Software GmbH, Köln, Germany
10/1999 – 09/2002	Freelance software developer , Darmstadt, Germany
03/1999 – 09/1999	Software developer/consultant , Grosch & Link GmbH, Frankfurt am Main, Germany
03/1998 – 02/1999	Scientific assistant/postgraduate , Albrecht-von-Haller-Institut für Pflanzenwissenschaften, University of Göttingen, Germany
25/02/1998	Diplom Title of thesis: ‘Characterization of transient Cl ⁻ channel activity during action potential in <i>Chara corallina</i> ’
1990-1991	Community service , Lazarus Hilfsdienst e. V., Leverkusen

Studies

10/1994 – 02/1998	Advanced study period (<i>Hauptstudium</i> biology; major: Plant biology; minors: tropical & subtropical plant production, physics), University of Göttingen
09/1993 – 05/1994	Exchange student (Biology, Environmental Studies) Wilfrid Laurier University and University of Waterloo, Waterloo, Canada
12/07/1993	Vordiplom University of Marburg, Germany
10/1991 – 07/1993	Basic studies (<i>Grundstudium</i> , biology), University of Marburg

School

25/05/1990	Abitur Lise-Meitner-Schule, Leverkusen, Germany
1981 – 1990	Grammar school (<i>Gymnasium</i>), Lise-Meitner-Schule
1977 – 1981	Elementary school , Köln